

California State University, San Bernardino

CSUSB ScholarWorks

Theses Digitization Project

John M. Pfau Library

2008

Comparative osteohistology of hyperelongate neural spines in basal synapsids (Vertebrata, Amniota): Growth and mechanical considerations

Adam Keith Huttenlocker

Follow this and additional works at: <https://scholarworks.lib.csusb.edu/etd-project>



Part of the [Ecology and Evolutionary Biology Commons](#), and the [Paleontology Commons](#)

Recommended Citation

Huttenlocker, Adam Keith, "Comparative osteohistology of hyperelongate neural spines in basal synapsids (Vertebrata, Amniota): Growth and mechanical considerations" (2008). *Theses Digitization Project*. 3560. <https://scholarworks.lib.csusb.edu/etd-project/3560>

This Thesis is brought to you for free and open access by the John M. Pfau Library at CSUSB ScholarWorks. It has been accepted for inclusion in Theses Digitization Project by an authorized administrator of CSUSB ScholarWorks. For more information, please contact scholarworks@csusb.edu.

COMPARATIVE OSTEOHISTOLOGY OF HYPERELONGATE NEURAL
SPINES IN BASAL SYNAPSIDS (VERTEBRATA, AMNIOTA):
GROWTH AND MECHANICAL CONSIDERATIONS

A Thesis
Presented to the
Faculty of
California State University,
San Bernardino

In Partial Fulfillment
of the Requirements for the Degree
Master of Science
in
Biology

by
Adam Keith Huttenlocker

June 2008

COMPARATIVE OSTEOHISTOLOGY OF HYPERELONGATE NEURAL
SPINES IN BASAL SYNAPSIDS (VERTEBRATA, AMNIOTA):
GROWTH AND MECHANICAL CONSIDERATIONS

A Thesis
Presented to the
Faculty of
California State University,
San Bernardino


by
Adam Keith Huttenlocker

June 2008


Approved by:


Stuart Sumida, Chair, Biology

5 June 2008
Date


Anthony Maccalf


David Polcyn


Kevin Middleton

ABSTRACT

Osteohistological investigation of neural spine microanatomy in "sail-backed" synapsids is performed to elucidate previously unknown aspects of dorsal sail form and function. Histovariability is assessed by examining multiple regions along the lengths of hyperelongate neural spines in Edaphosauridae and Sphenacodontidae (Synapsida: Eupelycosauria), and implications for soft-tissue correlates, growth, mechanics, and phylogenetic systematics are considered.

In sphenacodontids, histovariability within the neural spine appears to record the transition from the proximal (epaxial-embedded) to the distally protruding portion of the spine. These observations and independent pathological evidence support the existence of a short dorsal crest in *Sphenacodon* and possibly other basal sphenacodontids.

Comparisons between sphenacodontids and edaphosaurids reveal family and genus-level distinctions in microstructural properties. Gross morphological comparisons and histomorphometric properties (including the presence of an incipient central cavity) indicate that *Lupeosaurus* is a basal edaphosaurid. Phylogenetic analysis corroborates the current consensus of basal synapsid

phylogeny and additionally demonstrates that *Ctenorhachis* is a basal sphenacodontid.

Statistical analyses indicate weak phylogenetic signal in some histomorphometric characters and slightly stronger correlations with phylogenetically-independent variables (e.g., cross-sectional bone mass, relative spine height). Assumptions of the "thermoregulatory hypothesis" are rejected in both families, and developmental and mechanical components of bone microstructure are emphasized. Quantitative results corroborate hypothesized disparity in neural spine mechanics between edaphosaurids and derived sphenacodontids.

ACKNOWLEDGMENTS

I would like to acknowledge my thesis chair, Dr. Stuart S. Sumida, and committee members Drs. Anthony Metcalf, David Polcyn, and Kevin Middleton for their enthusiastic review of this thesis. I would also like to thank Dr. Elizabeth Rega for useful discussions on normal and pathological osteohistology, bone growth and mechanics, and access to thin-sectioning equipment and facilities.

Specimen donations were made by the Field Museum in Chicago, William May of OMNH, Bryan Small and Dr. Kenneth Carpenter of DMNH, Drs. David Berman and Amy Henrici of CM, and Dr. Robert Reisz and David Mazierski of University of Toronto. I also thank Dr. Kevin Padian and Patricia Holroyd of UCMP and Rich Cifelli and Jeff Person of OMNH for access to comparative material.

I thank Dr. Erik Melchiorre in CSUSB's Geology Department for access to facilities and microscope equipment and Glenn Drewes for his mentorship and assistance in the casting of some specimens.

For their varying degrees of involvement I express immense gratitude to Drs. Andrew Lee and Kenneth Angielczyk, Kim and Eric Scott, Jason Pardo, Ali Jaffri, Toni Culver, and Jeffry Armada.

Funding for materials was principally provided through the laboratories of Drs. Sumida and Rega. Additional funding was provided by the Associated Students Incorporated Research and Travel Fund and the Sally Casanova Predoctoral Scholarship Program of California State University.

This thesis is dedicated to the loving memory of Dr. Sumida's 1992 Isuzu Rodeo.

TABLE OF CONTENTS

ABSTRACT	iii
ACKNOWLEDGMENTS	v
LIST OF TABLES	x
LIST OF FIGURES	xi
CHAPTER ONE: INTRODUCTION	
Background	1
Statement of the Problem	9
Goals and Application of Histological Techniques	19
Materials and Methods	24
CHAPTER TWO: COMPARATIVE ANATOMY AND OSTEOHISTOLOGY OF HYPERELONGATE NEURAL SPINES IN SPHENACODONTIDAE	
Introduction	33
Materials and Methods	44
Results	50
Discussion	72
Conclusions	78
CHAPTER THREE: COMPARATIVE OSTEOHISTOLOGY OF HYPERELONGATE NEURAL SPINES IN EDAPHOSAURIDAE	
Introduction	81
Materials and Methods	88
Results	94

Discussion	114
Conclusions	122
CHAPTER FOUR: PHYLOGENETIC SIGNAL AND PHYLOGENETICALLY- INDEPENDENT CORRELATES: THE MECHANICAL EVOLUTION OF HYPERELONGATE NEURAL SPINES	
Introduction	127
Methods	132
Results	142
Discussion	156
Conclusions	170
APPENDIX A: LIST OF ABBREVIATIONS	176
APPENDIX B: SPECIMEN/LOCALITY DATA	178
APPENDIX C: MORPHOLOGICAL COMPARISONS	181
APPENDIX D: HISTOMORPHOMETRIC DATA	185
APPENDIX E: LIST OF PHYLOGENETICALLY INFORMATIVE CHARACTERS	187
APPENDIX F: CHARACTER MATRIX	194
APPENDIX G: MEAN PAIRWISE DISSIMILARITY BASED ON DISTANCE ANALYSIS OF CHARACTER DATA	197
APPENDIX H: BENDING RIGIDITY DISSIMILARITY	199
APPENDIX I: BONE DENSITY DISSIMILARITY	201
APPENDIX J: CORTICAL POROSITY DISSIMILARITY	203
APPENDIX K: RELATIVE BONE WALL THICKNESS (RBT) DISSIMILARITY	205
APPENDIX L: PARSIMONY ANALYSIS INPUT FILE	207

APPENDIX M: PARSIMONY ANALYSIS OUTPUT FILE (WITH SPINE DATA)	210
APPENDIX N: PARSIMONY ANALYSIS OUTPUT FILE (WITHOUT SPINE DATA)	217
APPENDIX O: BAYESIAN ANALYSIS INPUT FILE	226
APPENDIX P: BAYESIAN ANALYSIS OUTPUT (4 TAXA)	229
APPENDIX Q: BAYESIAN ANALYSIS OUTPUT (5 TAXA)	231
REFERENCES	233

LIST OF TABLES

Table 1.	Selected fossil tetrapods with hyperelongate dorsal neural spines hypothesized to be associated with a dorsal crest or sail . . .	7
Table 2.	Taxonomy of Sphenacodontidae	35
Table 3.	Taxonomy of Edaphosauridae	87
Table 4.	New list of synapomorphies supporting a taxonomic placement of <i>Lupeosaurus</i> within Edaphosauridae	116
Table 5.	Characteristics of the histological profiles of sphenacodontid and edaphosaurid neural spines	128
Table 6.	Phylogenetic correlations of histomorphometric dissimilarity	152
Table 7.	Phylogenetically-independent contrasts of histomorphometric data	153

LIST OF FIGURES

Figure 1.	Current consensus of early amniote phylogeny	2
Figure 2.	Skeletal reconstructions of selected Permian-Carboniferous synapsids in left lateral view	4
Figure 3.	Morphological diversity of hyperelongate neural spines	11
Figure 4.	Preliminary reanalysis of the data presented by Bailey (1997), incorporating additional taxa	17
Figure 5.	Transverse sections through neural spines of selected synapsids	23
Figure 6.	Illustration of a dorsal vertebra indicating the locations along the neural spine where sections were cut for histological analysis	30
Figure 7.	Gross morphology of the neural spine in the genus <i>Dimetrodon</i>	38
Figure 8.	Proximal region of dorsal neural spine of <i>Dimetrodon giganhomogenes</i> (FMNH UC 1134)	52
Figure 9.	Distal region of dorsal neural spine of <i>Dimetrodon giganhomogenes</i> (FMNH UC 1134)	58
Figure 10.	Distal region of mid-dorsal neural spines of <i>Dimetrodon</i> cf. <i>D. giganhomogenes</i> (DMNH 30597) and cf. <i>D. grandis</i> (DMNH 16131) viewed with non-polarized light	60
Figure 11.	Transverse sections through proximal region of dorsal neural spines of <i>Sphenacodon ferox</i>	63

Figure 12.	Distal region of dorsal neural spine of <i>Sphenacodon ferox</i> (UCLA VP uncatalogued)	66
Figure 13.	Healing calluses in dorsal neural spines of <i>Sphenacodon</i>	69
Figure 14.	Transverse section through healing callus of <i>Sphenacodon</i> cf. <i>S. ferocior</i> (CM 73367) viewed with polarized light	71
Figure 15.	Restoration of short segmental epaxial musculature (sensu Olson, 1936) in the genus <i>Sphenacodon</i>	76
Figure 16.	Edaphosauridae postcranial reconstructions and neural spine anatomy	83
Figure 17.	Transverse sections through mid-dorsal neural spine of <i>Lupeosaurus</i> cf. <i>L. kayi</i> (UCLA VP 1651) viewed with polarized light	96
Figure 18.	Sections through mid-dorsal (A, B) and posterior (C) neural spines of <i>Ianthasaurus hardestiorum</i>	100
Figure 19.	Proximal region of the neural spine of <i>Edaphosaurus</i> spp.	106
Figure 20.	Distal region of the neural spine of <i>Edaphosaurus</i> spp.	108
Figure 21.	Tip of the neural spine of <i>Edaphosaurus</i> spp.	110
Figure 22.	Lateral tubercle of the neural spine of <i>Edaphosaurus</i> spp. (OMNH 73802)	112
Figure 23.	Comparison of cross-sectional bone mass distribution and vascularity of mid-dorsal hyperelongate neural spines in selected eupelycosaurs	130

Figure 24. Comparison of (A) distance tree with branch lengths determined from character data and (B) 50% majority-rule consensus of two MPTs reconstructed against stratigraphy 146

Figure 25. Phylogenetic character mapping of selected neural spine characters from Appendices E and F onto 50% majority rule consensus of two MPTs 149

CHAPTER ONE

INTRODUCTION

Background

Basal synapsids (often referred to as "mammal-like reptiles") comprise one of the best represented groups of early tetrapods and demonstrate a classic example of a macroevolutionary transition (Romer and Price, 1940; Reisz, 1986). The basal synapsid fossil record is of significant interest to paleontologists because it presents an excellent opportunity for studying the evolution of vertebrate morphology. First, synapsid fossils are relatively well-documented through geologic time (Sidor and Hopson, 1998; Rubidge and Sidor, 2001). Second, a general consensus regarding their phylogenetic relationships has emerged over the last two decades (Reisz, 1986; Hopson, 1991; Laurin, 1993; Modesto, 1994; Laurin and Reisz, 1995). Finally, their evolutionary history holds clues to the origins of Mammalia (Hopson, 1991; Sidor and Hopson, 1998; Rubidge and Sidor, 2001).

Modern reptilian-grade amniotes (e.g., snakes, lizards, crocodylians) and mammals share an ancient common ancestry, diverging more than 325 million years ago,

probably during the Mississippian Period. Among amniotes, basal synapsids are more closely related to mammals than to modern reptiles (Figure 1A). Two major morphological grades of nonmammalian synapsids are typically distinguished by vertebrate paleontologists: basal pelycosaurian-grade synapsids and the therapsids (which include mammals). Of these early amniotes, the pelycosaurian-grade synapsids (Figures 1B, 2), made famous by certain "sail-backed" genera characterized by hyperelongate neural spines, reached the peak of their diversity during the Early Permian Period (approximately

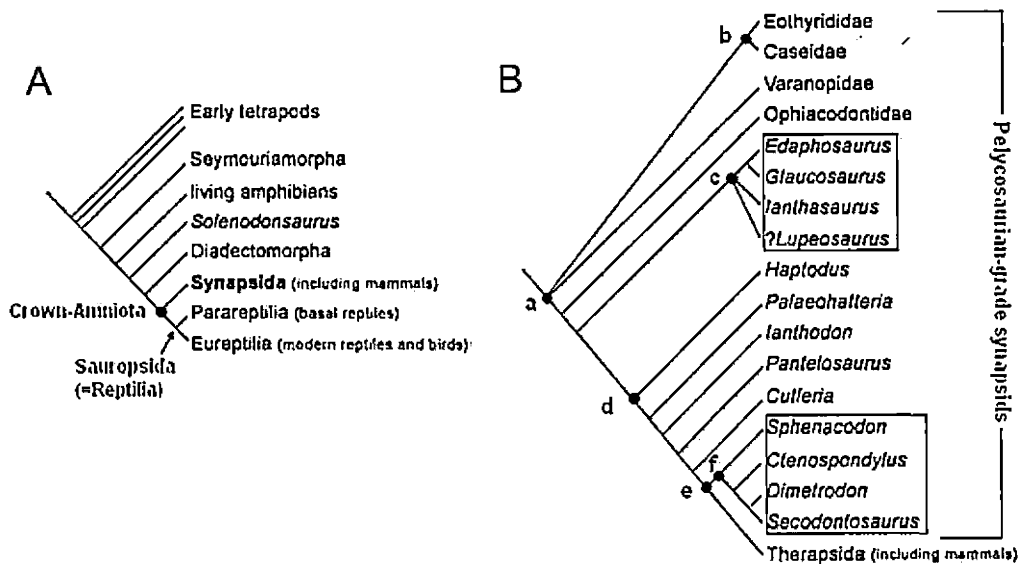


Figure 1. Current consensus of early amniote phylogeny (Reisz, 1986; Reisz et al., 1992; Laurin, 1993; Modesto, 1994; Laurin and Reisz, 1995; Kissel and Reisz, 2004).

A), Relationships of the major amniote clades (including Synapsida); B), Composite cladogram demonstrating synapsid phylogeny: Node-a, Synapsida; Node-b, Caseasauria; Node-c, Edaphosauridae; Node-d, Sphenacodontia; Node-e, Sphenacodontoidea (*sensu* Hopson, 1991; Reisz et al., 1992); Node-f, Sphenacodontidae. Boxes indicate clades (c,f) in which dorsal sails are known to have existed.

299-269 million years ago). By that time, at least six well known families were established (Figure 1B), a few of which had a virtually world-wide distribution with fossils known from North and South America, Europe, and Africa (Romer and Price, 1940; Reisz, 1986; Piñeiro et al., 2003). Some small sphenacodontian specimens from Late Paleozoic deposits of North America, the "haptodonts," form a paraphyletic assemblage demonstrating phylogenetic trends toward the sphenacodontid-therapsid condition (Laurin, 1993; Kissel and Reisz, 2004), and their lack of hyperelongate neural spines further supports the hypothesis that the dorsal sail of basal synapsids evolved more than once (see below). Kemp (1982, 2005) and Reisz (1986) have provided comprehensive summaries of early synapsid evolution and gross osteology.

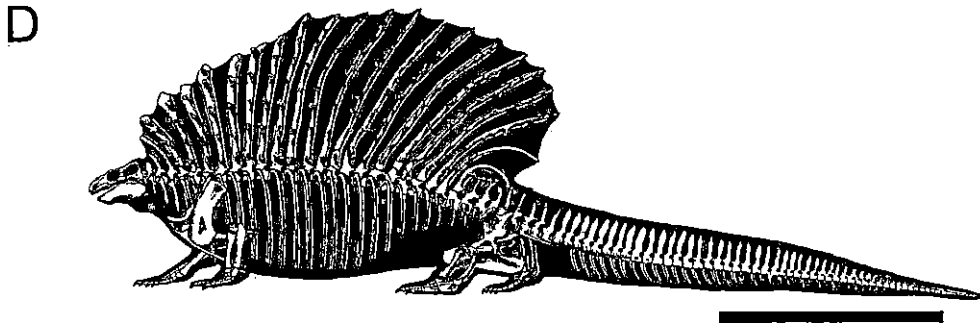
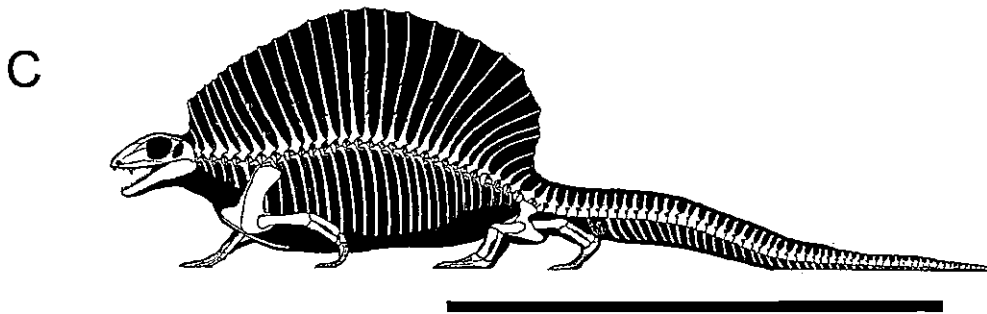
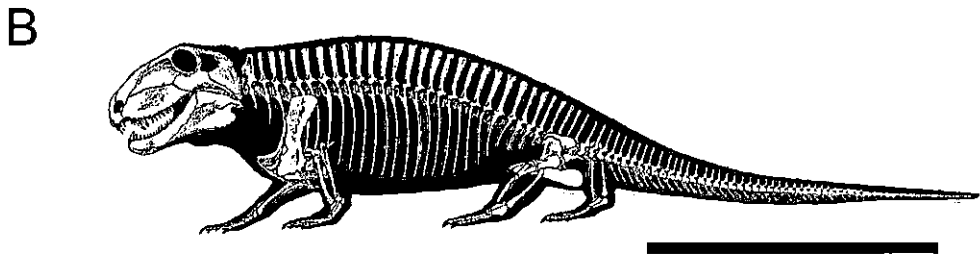
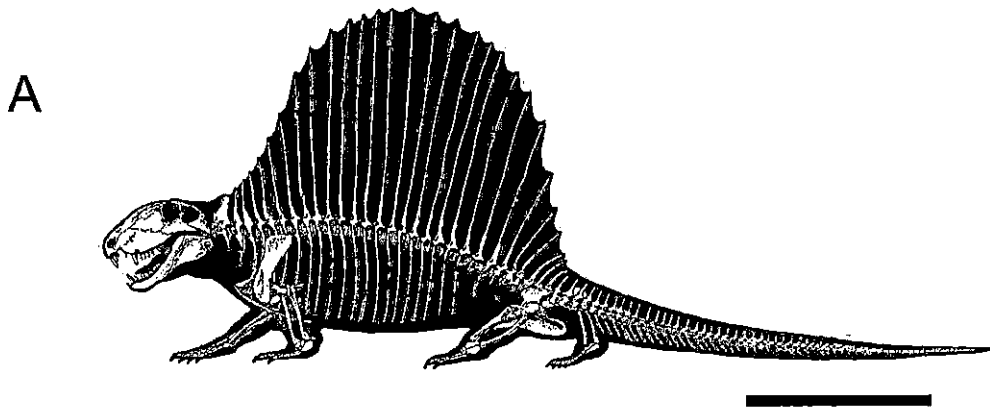


Figure 2. Skeletal reconstructions of selected Permo-Carboniferous synapsids in left lateral view. A), sphenacodontid *Dimetrodon limbatus*; B), sphenacodontid *Sphenacodon ferox*; C), basal edaphosaurid *Ianthasaurus*

hardestiorum; D), derived edaphosaurid *Edaphosaurus pogonias*. All reconstructions modified from Romer and Price (1940) except 'C' (modified from Modesto and Reisz, 1990). Scale bars ~ 0.5 meters.

History of the Dorsal Sail

Although recent studies of early synapsid evolution have helped to clarify their phylogenetic relationships, much less is known about their ontogenetic development and certain aspects of their functional anatomy. Hyperelongation of the vertebral spinous processes or "neural spines" in some basal synapsids is one area that merits further attention (Sumida et al., 2005). These tall processes, which are three to four or more times the height of the vertebral centrum, are believed to have formed an immense sail-like structure spanning the trunk region in some taxa (e.g., *Dimetrodon* and *Edaphosaurus*; see Figure 2) and represent one of the most widely recognized features of pelycosaurian-grade synapsid fossils. Similar structures have been identified in other groups of extinct tetrapods, including dissorophid amphibians, basal archosauromorphs, all ctenosauriscid archosaurs, and some dinosaurs (Table 1). Had these structures evolved in a single taxon with no apparent function, their maintenance might easily be

explained as a developmental anomaly with little or no cost to the fitness of the individuals producing them. In fact, that it arose more than once in pelycosaurian-grade synapsids suggests that there was significant potential to evolve this feature. Moreover, such elaborate modifications of the dorsal vertebrae must have provided some benefit to these organisms as hyperelongate neural spines are present in at least eight well-known synapsid genera (Table 1) and evolved at least twice during early synapsid evolution, first in the Edaphosauridae and later in the Sphenacodontidae (Figure 1B). A few other long-spined synapsids have been described in the literature (e.g., *Echinerpeton* and *Xyrospondylus*; Reisz, 1972; Reisz et al., 1982; Sumida and Berman, 1993) but are not considered in detail here, because they are based on isolated specimens and their anatomy is poorly known.

Primarily, research of the dorsal sail has focused on its potential adaptive utility, which has been the subject of much speculation since its initial discovery in the late 1800s (Cope, 1878; Case, 1907). Numerous hypotheses have been presented to explain dorsal sail function, a few of which include navigation, defense/intimidation, camouflage,

Table 1. Selected fossil tetrapods with hyperelongate dorsal neural spines hypothesized to be associated with a dorsal crest or sail.

AMPHIBIA	AMNIOTA (cont.)
Temnospondyli	Archosauromorpha
Dissorophoidea	Trilophosauridae
<i>Astreptorhachis ohioensis</i>	<i>Spinosuchus caseanus</i>
<i>Platyhystrix rugosus</i>	Rauisuchia: Ctenosauriscidae
	<i>Ctenosauriscus koeneni</i>
	<i>Lotosaurus adentus</i>
AMNIOTA	<i>Arizonasaurus babbitti</i>
Synapsida	<i>Bromsgroveia walkeri</i>
Edaphosauridae	" <i>Hypselorhachis</i> "
<i>Lupeosaurus kayi</i> *	Dinosauria
<i>Ianthasaurus hardestiorum</i> *	Ornithopoda
<i>Edaphosaurus</i> (numerous species)*	<i>Ouranosaurus nigeriensis</i>
? <i>Xyrospondylus eordi</i>	Sauropoda
Sphenacodontidae	<i>Rebbachisaurus</i>
<i>Ctenorhachis jacksoni</i>	<i>Amargasaurus cazau</i>
<i>Sphenacodon ferox</i> *	Theropoda
<i>Sphenacodon ferocior</i> *	<i>Acrocanthosaurus</i>
<i>Ctenospondylus casei</i>	<i>Spinosaurus aegypticus</i>
<i>Ctenospondylus ninevehensis</i>	<i>Suchomimus tenerensis</i>
<i>Dimetrodon</i> (numerous species)*	
<i>Secodontosaurus obtusidens</i>	
Family incertae sedis	
<i>Echinerpeton intermedium</i>	

From Reisz (1972, 1986), Hook and Hotton (1991), Bennett (1996), Bailey (1997), Currie (1997), Sampson (1997), Nesbitt (2003, 2005), Kissel and Reisz (2004). Asterisks (*) denote taxa examined in this study.

individual recognition, and the most widely recognized hypothesis - thermoregulation (Romer, 1927, 1948; 1961; Romer and Price, 1940).

Most researchers agree that a thin membrane stretched between the spines to produce the sail-like morphology, supported by (1) the regular spacing of the spines observed in articulated specimens found *in situ* (Romer, 1927; Romer and Price, 1940) and (2) the existence of fractured spines

that apparently healed in place in some specimens (Enlow, 1969; Rega et al., 2002). In the instance of the type specimen of *Dimetrodon milleri* (MCZ 1365), a "floating" spine from the twenty-ninth presacral vertebra was apparently produced when it fractured and healed without reconnecting to the proximal part of the spine from which it broke off. Thus, it was presumed to have healed in place while suspended by the sail membrane (Romer and Price, 1940; Pivorunas, 1970).

When an allometric increase in sail size relative to body mass was hypothesized for a suspected phylogenetic series of *Dimetrodon*, Romer (1948, 1961) suggested that the sail may have served a thermoregulatory function because (1) increasingly massive ectotherms would have a difficult time achieving activity temperature during the mornings via an external heat source in the absence of an accessory appendage to facilitate external heat transfer (Bramwell and Fellgett, 1973; Spotila, 1980; Turner and Tracy, 1986); and (2) if the structure were indeed implicated in thermoregulation, then the two-dimensional sail surface would have had to increase disproportionately with the cube function of body mass (Pivorunas, 1970; Bramwell and Fellgett, 1973). Furthermore, the trunk vertebrae of

Dimetrodon and *Edaphosaurus* display longitudinal grooves on both the anterior and posterior faces of the neural spine, producing a figure-8 cross-sectional appearance (Figure 3C). These recesses were hypothesized to contain blood vessels that would have aided in vascularizing the sail membrane (Romer, 1927; Ricqlès, 1974a). The apparent evidence for vascularization of the dorsal sail has been implicated by many authors (Bramwell and Fellgett, 1973; Ricqlès, 1974a; Tracy et al., 1986; Bennett, 1996; Florides et al., 2001) as controlled blood flow to bodily appendages provides a more efficient means of transferring heat to and from the core of the body than simple convection (Turner and Tracy, 1986).

Statement of the Problem

Challenges to the Thermoregulatory Hypothesis

For genera exhibiting the most extreme cases of neural spine elongation (e.g., *Edaphosaurus* and *Dimetrodon*) at least two major problems complicate the thermoregulatory hypothesis. Firstly, whereas the possibility existed that controlled blood flow through the sail might have helped sail-backed synapsids maintain a more stable internal

temperature, even with the sail it would have taken up to four hours for a large ectothermic *Dimetrodon* (~250 kg) to achieve optimum activity temperature during the morning (Haack, 1986). Theoretical models have demonstrated a lack of *Dimetrodon*'s effectiveness in controlling internal temperature, exposed the dorsal sail's inability to efficiently dump excess body heat (but see Bennett, 1996), and have raised other concerns, especially the trade-offs in regards to the metabolic costs of producing a dorsal sail (Bramwell and Fellgett, 1973; Haack, 1986; Florides et al., 2001).

Secondly, despite the wide popularity and recognition of the dorsal sail, almost nothing was known about its ontogenetic development and intrinsic properties until recently (Rega et al., 2005; Sumida et al., 2005). Preliminary histological sectioning of neural spines of the genus *Dimetrodon* has revealed important clues about biomechanics and development, bringing into question some of the popular views discussed above (see Background). Sumida et al. (2005) demonstrated that the figure-8 cross-sectional morphology of the spine changed through ontogeny. In addition, Rega et al. (2005) presented an alternative hypothesis to account for the presence of the anterior and

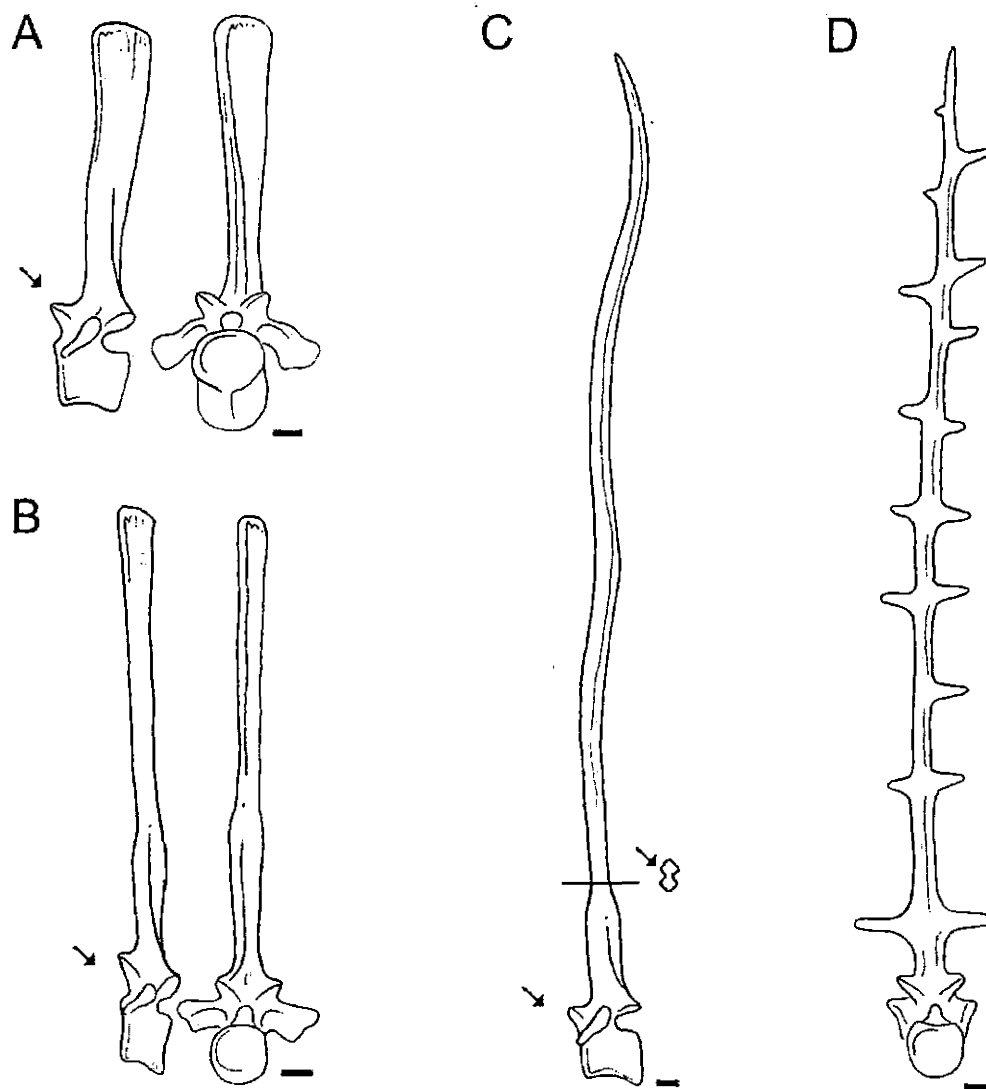


Figure 3. Morphological diversity of hyperelongate neural spines. A), left lateral and anterior views of dorsal vertebra of *Sphenacodon ferox* (Case et al., 1913); B), left lateral and posterior views of dorsal vertebra of *Ctenospondylus casei* (Romer and Price, 1940); C), left lateral view of dorsal vertebra of *Dimetrodon giganhomogenes* (modified from Bailey, 1997), transverse section demonstrates the figure-8 cross-sectional morphology; D), posterior view of dorsal vertebra of *Edaphosaurus cruciger* (modified from Bailey, 1997). Arrows denote anterior. Scale bars ~ 1 cm.

posterior grooves along the neural spines. The authors offered a biomechanical explanation for the figure-8 cross-sectional shape (Figure 3C), arguing that a double-cylinder morphology reinforced the strength of these membrane-tending struts. This conclusion is consistent with the morphology of dorsal fin spines in billfish, which also show the figure-8 morphology in cross-section with longitudinal anterior and posterior grooves. In fact, grooves in elongate biological structures occur frequently in nature (e.g., leaf petioles and feathers) and help to reduce bending (and thus breakage) imposed by tensile forces while still allowing some torsional flexibility (Etnier, 2001; Vogel, 1988, 2003). These suggestions, along with the observation that the cortex in the area of the groove is nearly avascular and lacks any radiating canals (or Volkmann's canals), diminish the likelihood that the anterior and posterior grooves found in hyperelongate neural spines served the purpose of housing large blood vessels. Clearly, a poorly vascularized dorsal sail would drastically reduce its effectiveness as a thermoregulatory device (Haack, 1986).

Obscure Origins of the Dorsal Sail

As much of the research has focused on adaptive hypotheses applied to the dorsal sails of *Dimetrodon* (e.g., Bramwell and Fellgett, 1973; Haack, 1986) and *Edaphosaurus* (e.g., Bennett, 1996), further problems persist with regards to the identification of the dorsal sail itself; specifically whether or not it existed in certain taxa whose ambiguously intermediate spine-heights render the assignment of this condition equivocal (e.g., *Sphenacodon*; Figure 3A). Not surprisingly, moderately elongate neural spines are known to have evolved before the immense dorsal sails of *Edaphosaurus* and *Dimetrodon* could have adopted any of the secondary adaptations discussed above. This invokes several questions that previous studies have not been able to address. What function, if any, was served by intermediate elongation of the neural spines in basal edaphosaurids and sphenacodontids? What circumstances facilitated the dramatic elaboration of this condition in derived forms (i.e., *Edaphosaurus* and *Dimetrodon*)? When in the evolutionary history of edaphosaurids and sphenacodontids did the elongate spines extend beyond the dorsal limits of the epaxial musculature to produce the dorsal sail? The first question is difficult to address |

because the earliest known members of the Edaphosauridae already display the hyperelongate, cylindrical struts for neural spines, although they fall within the relative height ranges for presumed hump-backed dinosaurs and artiodactyl mammals (Figure 4). On the other hand, the neural spines of basal sphenacodontids present a graded series of intermediate spine heights and thus a greater level of structural ambiguity. This problem requires more attention and is discussed in detail below.

Figure 3 illustrates the broad diversity of vertebral morphologies in synapsids with hyperelongate neural spines. In terms of gross vertebral morphology, edaphosaurids are generally distinguished from sphenacodontids by the presence of laterally directed tubercles or crossbars along the neural spines (Figures 2D,3D), although they are lacking in a possible aberrant edaphosaurid, *Lupeosaurus* (Sumida, 1989). The earliest known edaphosaurids in the fossil record (e.g., *Ianthasaurus*) possessed exaggerated neural spines with a subcircular cross-section and display the tubercles mentioned above only on the anterior neural spines with fewer tubercles located caudally (Reisz and Berman, 1986; Modesto and Reisz, 1990). In a proposed phylogenetic series of *Edaphosaurus* (i.e., *E. boanerges* -

E. cruciger - *E. pogonias*) the tubercles become increasingly concentrated and develop into transverse crossbars (Romer and Price, 1940). All edaphosaurids in which neural spines are known exhibit hyperelongation, having average neural spine heights that are at least 10 times as high as the vertebral centrum (Figure 4).

In contrast, basal sphenacodontids displayed relatively lower neural spines (exemplified by *Sphenacodon* and the apparently conservative but incompletely known *Ctenorhachis*; Hook and Hotton, 1991), but show a gradual phylogenetic trend toward increasing spine-height. The neural spines in *Sphenacodon* and *Ctenospondylus* (Figure 3A,B) show a progressively greater degree of elongation beyond the primitive form (greater than four times the height of the centrum) and are laterally compressed, with a blade-like morphology superficially resembling the anterior thoracic vertebrae of some modern artiodactyls (personal observation). Still, the dorsal neural spines of *Ctenospondylus* differ from *Sphenacodon* by the presence of an expanded base bearing a "shoulder-like constriction" at the region believed to designate the dorsal extent of the epaxial muscles, a condition referred to as "dimetrodont" (Romer, 1927; Romer and Price, 1940; Reisz et al., 1992).

In this feature, *Ctenospondylus* spines bear a closer resemblance to *Edaphosaurus* and *Dimetrodon*. This interpretation is equivocal, however, as this condition sometimes exhibits regional variation within a single vertebral column and some spines have been described as "weakly dimetrodont" (Romer and Price, 1940). Thus, some level of uncertainty exists as to whether forms like *Sphenacodon* and *Ctenospondylus* displayed a muscular hump or a short, dorsal crest or "sail."

Bailey (1997) attempted to provide a simple means of delineating sail-backed and "hump-backed" fossil vertebrates utilizing the neural spine-to-centrum height ratio (Figure 4). His analysis showed a marked difference in spine-height between sail-backed synapsids (represented by *Edaphosaurus* and *Dimetrodon*) and certain dinosaurs which he believed to bear humps resembling those of modern artiodactyls. However, Bailey's taxon sampling was limited and he did not include any synapsids with intermediate spine-heights (e.g., *Ctenorhachis*, *Sphenacodon*, and *Ctenospondylus*). When these taxa (along with a broader sampling of spines) are added to Bailey's original dataset, the complexity of the issue becomes clear (Figure 4).

**Elongation of neural spines relative to centrum height
in long-spined tetrapods**

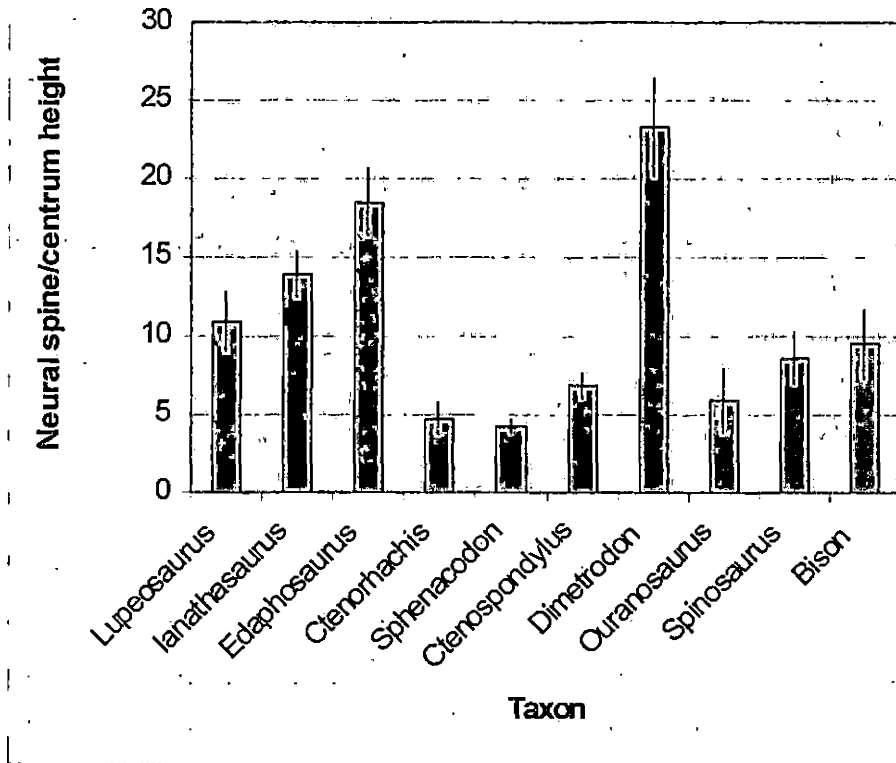


Figure 4. Preliminary reanalysis of the data presented by Bailey (1997), incorporating additional taxa. Basal synapsid taxa include *Lupeosaurus*, *Ianthasaurus*, *Edaphosaurus*, *Ctenorhachis*, *Sphenacodon*, *Ctenospondylus*, and *Dimetrodon*. "Humped" dinosaurian taxa include *Spinosaurus* and *Ouranosaurus* for comparison. The extant artiodactyl *Bison* was also included. Error bars represent 1 standard deviation.

The basal synapsids show a more or less continuous distribution of spine-heights, some of which overlap with the distributions of *Bison* and some dinosaurs. Even the

exaggerated spines of *Lupeosaurus* and *Ianthasaurus* fall close to the range of *Bison* and alleged hump-backed dinosaurs in their neural spine-to-centrum height ratios, but differ in their overall shape.

Whereas Bailey (1997) was probably correct in suggesting that the exaggeration of spine-height in certain fossil taxa is not enough to qualify the existence of an elaborate sail (based on his comparisons with *Bison* and other hump-backed mammals), he does not provide a conclusive means of separating sail-backed and hump-backed forms, neglecting potential overlap in height distributions between and even within genera. Bailey also suggested that the thermoregulatory hypothesis for large reptiles was suspect and concluded that moderately elongated blade-like neural spines in some dinosaurs instead indicated the presence of a hump, possibly associated with fat storage. More recently, such spines have been shown to exhibit biomechanical advantages in dinosaurs, artiodactyls, and other terrestrial vertebrates, helping to stabilize the trunk region or to redistribute inertial forces on the limbs effectively throughout the body during cursorial locomotion (Ebel et al., 1998; Vogel, 1988, 2003). This idea has been extended to Middle Triassic ctenosauriscid

archosaurs (Ebel et al., 1998; Ebel, 2000) and may well apply to basal sphenacodontids.

Goals and Application of Histological Techniques

The problems posed above serve to emphasize the elusive nature of understanding dorsal sail evolution and the lack of a unified set of criteria for diagnosing sail structure and function. Above all, the virtually continuous distribution of spine-heights across taxa and structural ambiguities, including the questionable significance of the dimetrodont differentiation, obscure this transition, calling for new methods to describe and distinguish between sail-backed and sailless forms and to elucidate the subtleties of sail structure and function.

A few recent studies integrating large-scale functional processes with the histological organization of bone tissue have proven to be somewhat successful (Currey, 1984, 1987, 2002; de Margerie, 2002; Margerie et al., 2004; Lee, 2004; Plochocki et al., 2007). Among amniotes, Currey (1987, 2002) has demonstrated that the integrity of modern reptile bone is not structurally inferior to that of modern mammals and birds, but in many extinct amniotes the

cortical bone tends to be highly porous and presumably more compliant. Germain and Laurin (2005) also examined this phenomenon and suggested that this condition indicated an amphibious lifestyle or a lesser degree of terrestriality for some early amniotes. Unfortunately, the statistical approaches used in the latter study mix methodologies intended for continuous and meristic data, making their exclusively "continuously based" conclusions erroneous. On the other hand, experimental studies on the limb bones of birds have exposed correlations between growth, mechanics, and histological organization, demonstrating a high occurrence of laminar bone tissue with circumferential primary osteons in skeletal regions that are subjected to high torsional loads during flight (Margerie, 2002). The circumferential arrangement of the woven bone scaffolding is interpreted as an adaptation to maintain the bone's integrity when faced with torsional loading.

Other factors, such as growth dynamics, can further influence the structural architecture of tetrapod bone, and this can be observed clearly in the histological organization (Enlow, 1963; Currey, 1984, 2002; Margerie et al., 2004; Lee, 2004). Useful reviews of the histological properties of recent and fossil tetrapod bone have been

provided by Enlow (1963, 1969; Enlow and Brown, 1956, 1957, 1958), Ricqlès (1968, 1969, 1974a,b; Ricqlès et al., 1991), and Francillon-Vieillot (1990).

Despite broad acceptance of the utility of examining osteohistology in basal tetrapods, no systematic application of these methods of architectural and developmental analysis in pelycosaurian-grade synapsids has been attempted. Rega et al. (2002, 2005) and Sumida et al. (2005) initiated a case study with the single genus *Dimetrodon* (discussed above). In the present study, neural spine osteohistology is further examined across a broad range of basal synapsid genera with hyperelongate neural spines. The main questions addressed include: Are there family and genus-level distinctions in the histological structure of the specimens to be examined? Can the histological organization of neural spines indicate the presence or absence of a dorsal sail in certain genera? Is there a relationship between the histological structure and function of the neural spines? If so, what mechanical or other functional properties are manifested at the histologic level? Finally, what structural or functional trends become apparent in light of basal synapsid phylogeny?

I presented preliminary results of comparative microstructural analyses of two sphenacodontid taxa, *Sphenacodon* and *Dimetrodon*, at the CSUSB Winter-2006 poster session and subsequent professional symposia (Huttenlocker et al., 2006, 2007), highlighting differences in neural spine histology between these two closely related taxa. For instance, the neural spines of *Sphenacodon* display extensive Sharpey's fibers throughout the cortex (Figure 5B), extrinsic fibers which penetrate the bone tissue and indicate broad attachment sites for the epaxial musculature throughout ontogeny in that genus. The presence of a dorsal crest or sail might be precluded if this histological profile were to be found along the entire length of the spine. Such extensive fibers are largely absent in the strut-like spines of *Dimetrodon* (Figure 5A) and, thus, the histological profile may be a good indicator of sail-backed (*Dimetrodon*?) versus sailless (*Sphenacodon*?) genera. However, serial sections from strategic locations along the length of the spine are necessary for improved resolution and to examine any histovariability within the spines.

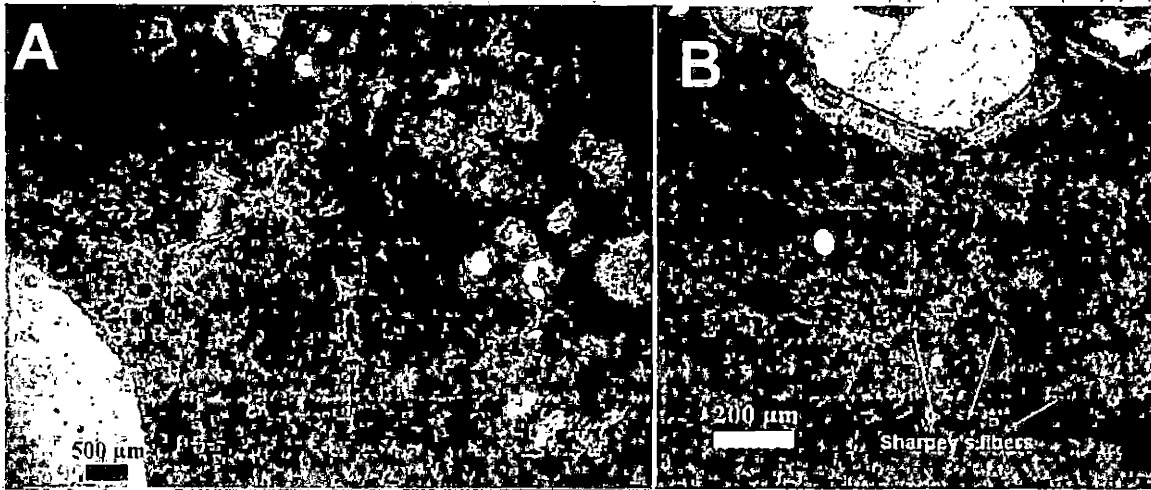


Figure 5. Transverse sections through neural spines of selected synapsids. A), transverse section through the distal portion of an anterior dorsal neural spine in *Dimetrodon* cf. *D. giganhomogenes*. Note the avascular lamellar bone in the region of the groove (left portion of the photograph). B), transverse section through the distal portion of a neural spine in *Sphenacodon ferox* (viewed with cross nicols). Note the thin cortex with large resorption cavities and extensive Sharpey's fibers, indicating high stresses and broad attachment of the epaxial musculature.

Moreover, the arrangement of the primary canals and trabecular architecture might indicate differential stresses and growth dynamics of these elements between the two closely related genera. The cortex displayed in *Dimetrodon* (Figure 5A) is thick and dense trabeculae constitute the medullary region, reinforcing the strength of the membrane-tending strut. From a microanatomical and functional perspective, the neural spines of *Dimetrodon* and

Sphenacodon seem to demonstrate little support for the hypothesis of thermoregulation, but conversely exhibit apparent biomechanical adaptations. It is important to note, however, that the data described above are tentative because histovariability along the length of the neural spine has not been taken into account in Figure 5. Thus, careful histological examinations from the base of the spine to the tip are provided in the following chapters to fully represent aspects of the neural spine's growth, mechanics and evidence of soft-tissue interaction with the bone.

Materials and Methods

The initial investigation presented in this study is largely qualitative and descriptive (Chapters Two and Three), as the microanatomical features of the spines in many of these taxa have never been formally described. In Chapter Four, quantitative analysis of histomorphometric data is performed to assess statistical correlations between histologic structure, phylogeny, and other phylogenetically-independent variables. Thin-sectioning was performed in the sectioning facilities at Western University of Health Sciences, Pomona (supervision of Dr.

Elizabeth Rega) and Denver Museum of Nature and Science (supervision of Dr. Kenneth Carpenter and Bryan Small) following the protocol outlined by Chinsamy and Raath (1992) and Wilson (1994) for fossil bone (detailed below).

Due to the limited availability of specimens and the comparative approach required for destructive analysis, the present study is divided into two major comparative investigations: analysis of hyperelongate neural spines in (1) Sphenacodontidae and (2) Edaphosauridae. This division is appropriate and Sphenacodontidae is the obvious first choice for study because fossil material is readily available, more is known about the histology of sphenacodontids (based on recent interest in *Dimetrodon* and my preliminary analyses of *Sphenacodon*), and there appears to be a more complete record of basal or conservative forms, providing useful information about the primitive structure of the spines. This initial survey (Chapter Two) then establishes a strong foundation for subsequent investigation of the family Edaphosauridae (Chapter Three). References are made below to the known histological structure of neural spines in the sauropsid *Captorhinus* for outgroup comparison (Sumida, 1990). The third phase of the project (Chapter Four) utilizes cladistic methodology and

involves the mapping of newly revealed histological characters onto both existing and newly generated cladistic frameworks (discussed in more detail below). This final phase is crucial because it has the potential to reveal relevant phylogenetic trends in neural spine form and function and may reveal whether certain features are correlated with phylogeny or phylogenetically-independent variables.

Fossilized specimens that have been thin-sectioned include representatives of the basal synapsid families Edaphosauridae and Sphenacodontidae. Within the Sphenacodontidae, spine material has been studied in the following taxa: *Sphenacodon*, *Ctenospondylus* (not sectioned), and various species of *Dimetrodon*. Edaphosaurid taxa examined here include: *Lupeosaurus*, *Ianthasaurus*, and *Edaphosaurus* (see Table 1). In addition to specimens in the vertebrate paleontology collection at California State University, San Bernardino (formerly UCLA-VP), material has been borrowed from the following institutions: Carnegie Museum of Natural History, Pittsburgh (CM); Denver Museum of Nature and Science, Denver (DMNH); and Sam Noble Oklahoma Museum of Natural History, Norman (OMNH). Due to the destructive nature of

the sectioning techniques and the rarity of complete specimens much of the material available for sectioning consisted of fragmentary or partial neural spines from multiple individuals, but neural spines from complete vertebrae were sectioned whenever possible (Appendix B).

Thin-sectioning equipment and other supplies included: cold mounting medium for embedding specimens; Ward petrographic slides; quick-setting epoxy resin for mounting specimens; low-speed Isomet precision saw with circular diamond blade; Buehler grinder/polisher with waterproof grinding paper (400, 600, and 800 grit); Nikon petrographic microscope with digital image capture device; Adobe PhotoShop, and National Institutes of Health's ImageJ image-analysis software for description of the specimens, measurements and calculation of quantitative microanatomical data.

The methods adopted here for histological sectioning follow closely to those of Chinsamy and Raath (1992) and Wilson (1994). The procedure encompasses five major steps (modified from Chinsamy and Raath, 1992): (1) measurements and photography of specimens; (2) embedding of specimens in epoxy; (3) sectioning embedded specimens; (4) mounting and

polishing; and (5) photographing and analyzing thin-sections.

Prior to the histological sectioning, it was necessary to record any information that might have been lost once the specimens were destroyed. This procedure ensured that gross anatomical data will be available to future researchers even after the specimens have been sectioned. Relevant data include approximate position of vertebra along the vertebral column and maximum height and width of neural spine if that information is available (summarized in Appendices B and C). Qualitative features on the external surface of the bone (e.g., muscle scars and vascular striations) are equally important, so careful photography of specimens has proven useful for post-sectioning analysis. In some instances, it was necessary to cast duplicate specimens to retain their original dimensions, especially in the case of exceptionally rare specimens. Specimens which have been cast include a pathological *Sphenacodon* spine (CM 73367) and two dorsal vertebrae from a specimen of the enigmatic edaphosaurid *Lupeosaurus* (UCLA VP 1651).

Once all appropriate data were recorded and casting and photography were completed, specimens were cut into

blocks for embedding. For this study, several points of interest have been chosen along the length of a given spine to ensure that the data obtained were not only useful, but also comparable across genera. Figure 6 illustrates the standardized sectioning that was performed for all genera, including a basal section, a midpoint section (approximated for fragmented spines), and a tip section. Additional sections were produced across the "changing point" (Pivorunas 1970; Bennett, 1996), defined here as a cross-sectional shape change from the base of the spine to the more distal portion, particularly in spines demonstrating pronounced "dimetrodont" differentiation (Romer and Price, 1940). Cutting down the specimens into blocks with a circular saw at these strategic locations (Figure 6) facilitated more efficient sectioning and helped to conserve embedding materials. Two types of embedding materials were used, depending on the size of the blocks. A cold mounting medium which required a catalyst was used for large specimens. The specimens were placed in a solution of industrial resin (200 ml) and methyl ethyl ketone, or MEK (1.5 ml), which served as the catalyst. The samples were placed in a vacuum for two minutes to evacuate

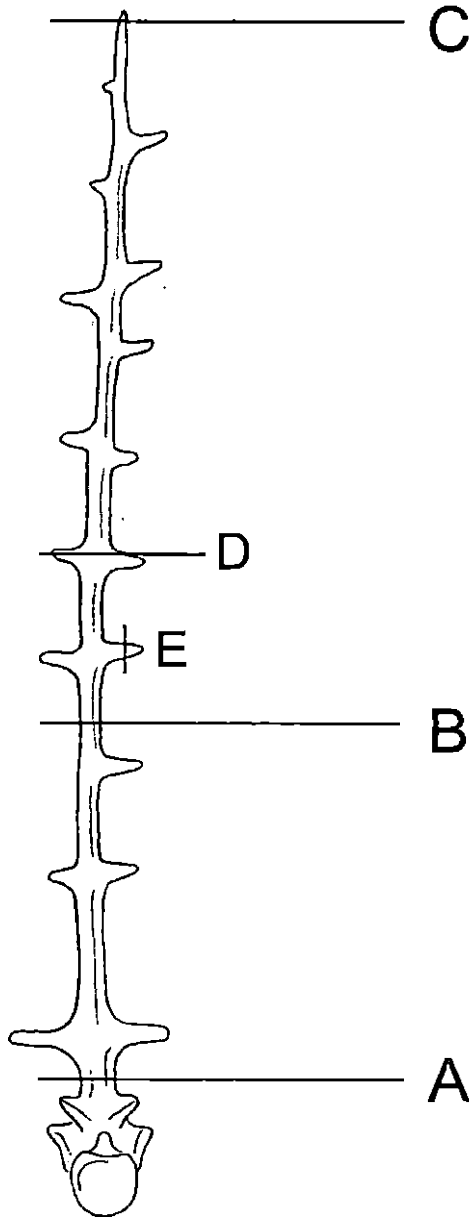


Figure 6. Illustration of a dorsal vertebra indicating the locations along the neural spine where sections were cut for histological analysis. A), basal (proximal) and "changing point" sections; B), midpoint (distal) section; C), tip section; D), section along the longitudinal axis of a lateral tubercle; E), section along the transverse axis of a lateral tubercle. Sections "D" and "E" are applicable only to edaphosaurids.

bubbles and left in open-air overnight for the sample to completely harden. Smaller specimen blocks were embedded using a quick-setting epoxy resin that was also used for mounting the specimens to the petrographic slides. Quick-setting resin is more efficient than the cold mounting medium because it is less expensive, more accessible, and sectioning can begin within minutes after embedding the specimen.

A low-speed Isomet precision saw with a 5-inch diameter circular diamond blade was used to cut the blocks once the embedding process was complete. The blocks were fitted into a chuck with the surface of interest (Figure 6A-E) exposed to the diamond blade. Very thin slices (~1-2 mm in thickness), including transverse and longitudinal slices, were cut to prepare for mounting and polishing of the thin-sections.

After the slices were produced, they were mounted onto slides with quick-setting epoxy resin by spreading a very thin layer directly onto the smooth surface of the sliced specimen and mounting it onto a petrographic slide. Once the epoxy resin hardened, it was possible to grind down the specimen mechanically using a grinder/polisher with waterproof grinding paper of varying grits (preferably 400,

600, and 800 grit). The thickness of each section was worked down with coarser grit paper (400), but finer grit (800) was necessary to polish away striations on the specimen produced during the grinding process. When the resulting sections were approximately 15-25 micrometers thick, or thin enough for light to pass through, the thin-sections were finished. All subsequent interpretations comprised a three-part analysis which is presented in Chapters Two, Three, and Four.

CHAPTER TWO
COMPARATIVE ANATOMY AND OSTEOHISTOLOGY OF
HYPERELONGATE NEURAL SPINES IN
SPHENACODONTIDAE

Introduction

A dorsal sail supported by hyperelongate neural spines of the presacral vertebrae developed in at least two lineages of Late Paleozoic synapsids, including the omnivorous and herbivorous Edaphosauridae and the carnivorous Sphenacodontidae (Figure 1). Among these forms, the sphenacodontids persisted as the dominant terrestrial predators in North America and Europe from the latest Pennsylvanian through the Early Permian Period (~300 Mya to 269 Mya) until they were ultimately replaced by their therapsid relatives during the Middle Permian (Vaughn, 1969; Reisz, 1986; Hook and Hotton, 1991; Reisz et al., 1992). The earliest known fossils that can be attributed to this family are represented by the type species *Sphenacodon ferox* (Figure 2B) from Upper Pennsylvanian and Lower Permian deposits of north-central New Mexico, USA (Romer and Price, 1940; Eberth, 1985; Reisz, 1986). The species *Sphenacodon ferocior* appears to

have succeeded *S. ferox* in the Lower Permian Cutler Group deposits of New Mexico and is distinguished by its slightly larger size (20% larger) and relatively elongate neural spines which are up to 45% longer than those of *S. ferox* (Berman, 1978), indicating positive allometry of the neural spines with respect to body size within the genus (Romer and Price, 1940; Berman, 1978), as has been recognized in the genus *Dimetrodon*.

Following this initial succession, an extensive radiation of sphenacodontids is recorded in Lower Permian deposits throughout the southwest and mid-continental regions of North America and as far east as present-day Germany (Berman et al., 2001, 2004). This record spans Asselian through Kungurian-aged (uppermost Lower Permian) deposits and includes *Ctenospondylus* and other genera in which elongation of the neural spines was taken to its extreme, such as *Secodontosaurus* and especially the speciose *Dimetrodon* (Figure 2A; Table 2). The evolutionary radiation of *Dimetrodon* species in the North American southwest and mid-continent has been characterized by temporal trends in phyletic size increase associated with a

Table 2. Taxonomy of Sphenacodontidae (modified from Reisz, 1986).

Valid taxa assignable to Sphenacodontidae Williston 1912

- *Genus *Sphenacodon* Marsh 1878
 - **S. ferox* Marsh 1878
 - = *Elcabrosaurus baldwini* Case 1907
 - **S. ferocior* Romer 1937
- *Genus *Dimetrodon* Cope 1878
 - D. limbatus* (Cope) Romer and Price 1940
 - = *Clepsydrops limbatus* Cope 1877
 - = *D. incisivus* Cope 1878
 - = *D. rectiformis* Cope 1878
 - = *D. semiradicatus* Cope 1881
 - D. natalis* (Cope) Romer 1936
 - = *Clepsydrops natalis* Cope 1878
 - D. macrospondylus* (Cope) Romer and Price 1940
 - = *Clepsydrops macrospondylus* Cope 1884
 - = *D. platycentrus* Case 1907
 - D. dollovianus* (Cope) Case 1907
 - = *Embolophorus dollovianus* Cope 1888
 - **D. giganthogenes* Case 1907
 - **D. grandis* (Case) Romer and Price 1940
 - = *Theropleura grandis* Case 1907
 - = *Bathyglyptus theodori* Case 1911
 - = *D. maximus* Romer 1936
 - D. milleri* Romer 1937
 - D. booneorum* Romer 1937
 - D. loomisi* Romer 1937
 - D. angelensis* Olson 1962
 - **D. occidentalis* Berman 1977
 - D. teutonis* Berman, Reisz, Martens and Henrici 2001
- Genus *Secodontosaurus* Romer 1936
 - S. obtusidens* (Cope) Romer 1936
 - = *Theropleura obtusidens* Cope 1880
 - = *Dimetrodon longiramus* Case 1907
- Genus *Ctenospondylus* Romer 1936
 - C. casei* Romer 1936
 - C. ninevehensis* Berman 1978
- Genus *Ctenorhachis* Hook and Hotton 1991
 - C. jacksoni* Hook and Hotton 1991

Table 2 (continued). Taxonomy of Sphenacodontidae.

Sphenacodontidae incertae sedis

Sphenacodon(?) *britannicus* (von Huene) Paton 1974 (= *Oxyodon britannicus* von Huene 1908)

Dimetrodon(?) *kempae* Romer 1937

"Haptodontine" sphenacodontians have been excluded. *Ctenorhachis* was described and assigned to Sphenacodontidae by Hook and Hotton (1991). *Dimetrodon teutonis* was described by Berman et al. (2001). Genera and species that have been examined histologically are denoted by an asterisk (*).

relative increase in the surface area of the dorsal sail, which displays positive allometry with respect to body size (Romer and Price, 1940; Tracy et al., 1986). In general, the neural spines of *Dimetrodon* are greater than 18 times the height of the vertebral centrum (and as much as 30 times in the massive *D. grandis*) and are usually subdivided into a mediolaterally compressed to subquadrate proximal region, and a distal region having a more figure-8 (or rarely subcircular) cross-sectional shape (Figure 7A,B). This disparity in cross-sectional geometry between the proximal and distal portions of the spine, which occurred to a lesser degree in the genus *Ctenospondylus*, has been termed "dimetrodont" differentiation (Romer and Price, 1940).

Bone Microstructure in the Postcrania of Sphenacodontians and Early Amniotes

Although the fossilized remains of sphenacodontians (including haptodont-grade synapsids, sphenacodontids, and therapsids; Figure 1) have largely helped to reveal the diversity, paleoecology, and biogeography of early terrestrial predators, they have also helped to demonstrate other aspects of early amniote biology through their osteohistological composition. Broad surveys of bone microstructure in extinct and extant vertebrates have briefly described the long bone histology of basal synapsids like *Ophiacodon*, *Edaphosaurus*, and the sphenacodontid *Dimetrodon*, and have even sampled the neural spines of the latter two taxa (Enlow and Brown, 1956, 1957, 1958; Enlow, 1969). These studies revealed the predominance of slow-growing lamellar-zonal bone tissue in the postcranial skeleton of these and other early tetrapods and reptilian-grade amniotes.

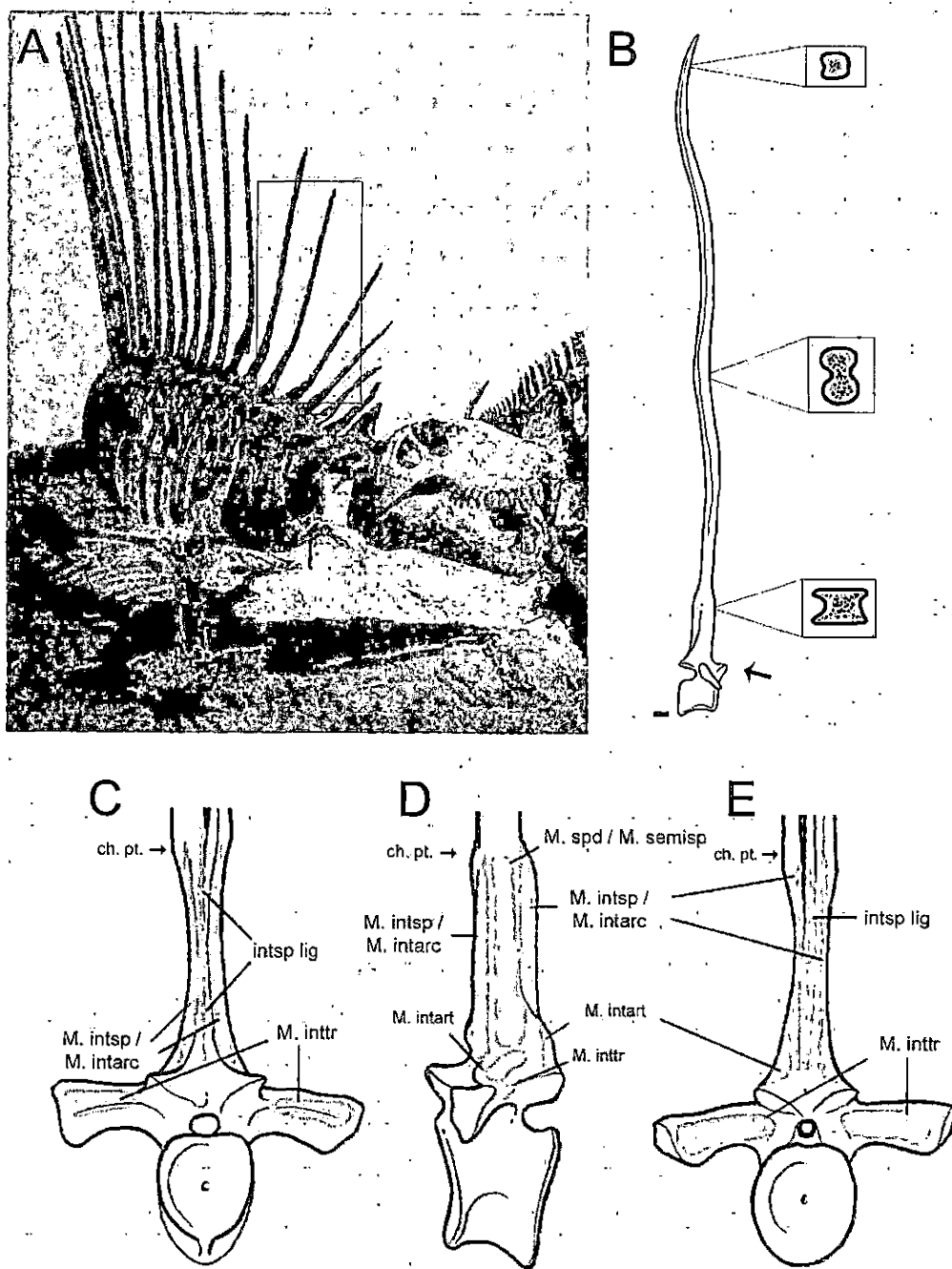


Figure 7. Gross morphology of the neural spine in the genus *Dimetrodon*. A), Articulated cast of *D. limbatus*, MCZ 1347, demonstrating the distribution of neural spine heights along cervical and dorsal regions, and their division into a laterally compressed, subquadrangular proximal region and rod-like distal region; B)

Generalized *Dimetrodon* vertebra in right lateral view (arrow denotes anterior), demonstrating changes in cross-sectional shape along the length of the neural spine (adapted from Pivorunas, 1970); C-E) Proximal region of a typical mid-dorsal vertebra in anterior ("C"), left lateral ("D"), and posterior ("E") views with muscular origins/insertions illustrated (vertebrae redrawn from Romer and Price, 1940; muscular attachments modified from Olson, 1936). Scale bar in "B" equals 10 millimeters. Abbreviations provided in Appendix A.

Subsequent surveys have suggested a dichotomy between bone deposition rates and tissue-types between pelycosaurian-grade synapsids and the more derived therapsid sphenacodontians, with evidence of slow, cyclical growth in the former group and more rapid, often sustained growth in the latter (Ricqlès, 1974a,b; Bennett and Ruben, 1986; Ray et al., 2004; Chinsamy and Hurum, 2006). In general, the long bones of *Dimetrodon* appear to have followed the former pattern, having a cortex composed largely of lamellar-zonal bone tissue but with interbedded regions of fibrolamellar bone (Enlow and Brown, 1957; Enlow, 1969; Ricqlès, 1974a). In contrast, the hyperelongate neural spines of *Dimetrodon* display densely vascularized fibrolamellar bone in the lateral margins of the cortex, likely reflecting their rapid distal outgrowth relative to the other skeletal elements (Enlow, 1969;

Ricqlès, 1974a; Bennett and Ruben, 1986). Less is known about the osteohistological properties of other sphenacodontids, but a preliminary report by Huttenlocker et al. (2006) demonstrated highly vascularized fibrolamellar bone dominating the cortex in the long bones of the sphenacodontid *Sphenacodon ferocior*. They argued that the overall growth strategy of *S. ferocior* was unlike that of *Dimetrodon* or other pelycosaurian-grade synapsids for which the histology is known, but rather was more similar to that of some nonmammalian therapsids (Ricqlès, 1974a,b; Ray et al., 2004), thus emphasizing parallel evolution in basal synapsids and a diversity of bone deposition and growth strategies among sphenacodontians. No previous histologic work has focused on the axial skeleton of *Sphenacodon*, preventing comparisons of growth and mechanics in the neural spines between *Sphenacodon* and *Dimetrodon* until now.

Neural Spine Growth and Mechanics as Revealed by Osteohistology

Sumida (1990) first examined the muscular attachments and mechanics in the vertebrae of a basal sauropsid amniote, *Captorhinus aguti*, based on the osteohistological

organization of the neural spines. He noted that low-type neural spines rarely exhibited trabeculae and lacked Sharpey's fibers, whereas tall-type spines exhibited trabecular architecture within the medulla and Sharpey's fibers in the cortex, indicative of the stresses and muscular attachments imposed by the *Mm. interspinalis*, *spinalis dorsi*, and *semispinalis dorsi*.

The role of specialized, hyperelongate neural spines in the axial skeleton of sphenacodontid synapsids has been the subject of great speculation, and a purported role in the thermal ecology and behavior of derived sphenacodontids such as *Dimetrodon* has been suggested by numerous authors (Romer, 1948, 1961; Pivorunas, 1970; Bramwell and Fellgett, 1973; Ricqlès, 1974a; Tracy et al., 1986; Florides et al., 2001). Much less is known, however, about the mechanical adaptations of the neural spines, their potential role in the structural integration of the axial skeleton, or whether or not a dorsal crest or sail existed in early members of the Sphenacodontidae (e.g., *Sphenacodon*).

In his ambitious monograph on the mammalian vertebral column, Slijper (1946:120) noted that, in terrestrial vertebrates, the "neural spines must be considered as levers, transmitting the muscular force to the vertebral

bodies" and throughout the vertebral column. Slijper also noted with reference to Wolff's Law that, because the shape of vertebrate bone models in response to the stresses it experiences, the "shape of the neural spines may be perfectly adapted to the attachment of the muscles and ligaments, especially to those muscles and ligaments attached directly to the bone" (1946:89). Olson (1936) reconstructed the muscular insertions of the epaxial muscles of *Dimetrodon* (Figure 7C-E), as well as several other early tetrapods, based on the distinct dimetrodont differentiation, the presence of muscle scars on the vertebrae and proximal neural spine, and comparisons with the extant green iguana (*Iguana iguana*). Nevertheless, muscular reconstructions of fossil vertebrates are often not feasible at the gross anatomical level, because muscular or tendinous entheses do not always attach directly to the bone, but are sometimes periosteally mediated (Slijper, 1946; Benjamin et al., 2002; Heironymus, 2006), and superficial muscle scars have been suggested only to be interpretable in half of the tendinous muscle attachments in extant vertebrates (Hieronymus, 2006). Thus, to have a better understanding of their mechanical features and soft-tissue interactions, one must investigate

various aspects of shape, pathology, and histological properties of neural spines (Slijper, 1946; Sumida, 1990; Benjamin et al., 2002; Hieronymus, 2006).

Recent reports of a series of dorsal neural spines attributable to *Dimetrodon giganhomogenes* (examined in the present study) have emphasized their histomorphometric and structural adaptations, and also pathological responses, which may in turn imply fundamental mechanical properties of the spine (Rega et al., 2005; Sumida et al., 2005). The present study serves to supplement these reports by describing fully the histological properties of the spines, and comparing their findings with additional specimens attributable to the genus *Dimetrodon* and, for the first time, the basal sphenacodontid *Sphenacodon*. The osteohistological composition of dorsal neural spines attributed to different species of *Dimetrodon* is first described and histovariability is examined along the length of the spine, as well as evidence of muscular attachments, potential ontogenetic changes in microstructural properties, and other aspects of neural spine microanatomy which may contribute to subgeneric variation within the genus *Dimetrodon*. These features are then compared to the genus *Sphenacodon*, which has also been analyzed for

histovariability and muscular insertions to assess the extent of the epaxial musculature along the length of the neural spine and the presence or absence of a dorsal crest in this taxon. Such a comparative method within the family Sphenacodontidae will provide an evolutionary context for the biology of the dorsal sail and will shed light on its evolutionary origins and possibly functions among early sphenacodontians.

Materials and Methods

Selection of Taxa

A list of all currently recognized taxa comprising the family Sphenacodontidae is presented in Table 2. Among these, the genera *Sphenacodon* and *Dimetrodon* were sampled for histological sectioning due to the availability of specimens representing these taxa. Specimens of *Ctenorhachis* and *Ctenospondylus* were not available for destructive analysis during the timeframe of this study due to their rarity, nor was *Secodontosaurus* which lacks complete neural spine material (although an associated vertebra preserves the changing point with a strut-like distal spine, subcircular in cross-section as in *Lupeosaurus* and the small sphenacodontid *Dimetrodon*

milleri; Romer and Price, 1940). The genera *Sphenacodon* and *Dimetrodon* provide the best preserved and greatest abundance of neural spine material, so several specimens representing these taxa were available for destructive analysis and comparative examination (Appendix B).

A series of neural spines showing consecutive healed fractures (Rega et al., 2005; Sumida et al., 2005) and an associated tibia, all attributed to a single adult specimen of *Dimetrodon giganhomogenes*, have been examined and sectioned for histological analysis (Figures 8-9). The specimen, FMNH UC 1134, is from the Kungurian-aged (Lower Permian) Clear Fork Group of north-central Texas (Arroyo Formation of Romer and Price, 1940). Two partial skeletons referable to *Dimetrodon* cf. *D. grandis* (DMNH 16131) and *Dimetrodon* cf. *D. giganhomogenes* (DMNH 30597) from the Lower Permian Clear Fork Group of Haskell County, Texas (Vale Formation of Romer and Price, 1940) were also sampled and distal portions of mid-dorsal neural spines were sectioned (Figure 10). In addition to these three partial skeletons, two more specimens were examined for gross anatomical comparisons. Among these is a disarticulated postcranial skeleton which records a developmental pathology in the formation of the distal portions of the

posterior dorsal neural spines. The specimen is from the Hennessey Group of Cleveland County, Oklahoma, and is attributed here to *Dimetrodon* sp. (OMNH 1727). The species *Dimetrodon loomisi* has been reported from time-correlative deposits southwest of Grandfield, Tillman County, Oklahoma (Daly, 1969, 1973), but the comparative material at hand is not complete enough to attribute to *D. loomisi* with confidence. The second comparative specimen is a fully articulated cast (Figure 7A) of a presumed adult female *Dimetrodon limbatus* (MCZ 1347) from the Admiral Formation at the Godwin Creek locality (Romer and Price, 1940), eastern Baylor County, Texas.

Three representatives of the genus *Sphenacodon* were sampled for histologic sectioning. These included the following: (1) a thin-sectioned neural spine fragment (UCMP 68436), housed in the historical histological collections of UCMP, and referable to *Sphenacodon* cf. *S. ferox* from the Camp Quarry, Lower Permian Cutler Formation (Asselian stage) of north-central New Mexico (Figures 5B, 11C,B); (2) an isolated dorsal neural spine (UCLA VP uncatalogued; field no. C-61-29) referable to *Sphenacodon ferox* from the Miller Bonebed, Lower Permian Cutler Formation (Asselian stage) of Rio Arriba County, New Mexico (Figures 11A,B,

12); and (3) an isolated dorsal neural spine preserved with a healed fracture callus (CM 73367) referable to *Sphenacodon* cf. *S. ferocior* from the Permo-Carboniferous (latest Ghzelian?) Red Tanks Member of the Bursum Formation, Valencia County, New Mexico (Figures 13B, 14). Partial skeletons of *Sphenacodon ferox* (UCMP 34226) and *Sphenacodon ferocior* (UCMP 34218; Figure 13A) were examined for gross anatomical comparisons. A complete list of histologically examined specimens and comparative material, including provenance data, is presented in Appendix B.

Histological Methods

Thin-sectioning equipment and other supplies included: cold mounting medium for embedding specimens; Ward petrographic slides; quick-setting epoxy resin for mounting specimens; low-speed Isomet precision saw with circular diamond blade; Buehler grinder/polisher with waterproof grinding paper (400, 600, and 800 grit); Nikon petrographic microscope with digital camera; Adobe PhotoShop, and NIH ImageJ image-analysis software for description of the specimens and for measurements of microanatomical structures.

The histological procedure employed here closely follows the protocols outlined by Chinsamy and Raath (1992) and Wilson (1994). It encompasses five major steps (modified from Chinsamy and Raath, 1992): (1) measurements and photography of specimens; (2) embedding of specimens; (3) sectioning embedded specimens; (4) mounting and polishing; and (5) photographing and analyzing thin-sections. Data such as approximate position of vertebra along the vertebral column and maximum height and width of neural spine were recorded when available and qualitative features on the external surface of the bone (e.g., muscle scars and vascular striations) were photographed prior to sectioning. In some instances, it was necessary to cast specimens to retain their original dimensions, especially in the case of exceptionally rare specimens. Resin casts were made to preserve the gross anatomical features of the pathological *Sphenacodon* cf. *S. ferocior* neural spine (CM 73367). Subsequently, the specimens were cut into small blocks for embedding. Several points of interest (Figure 6) were selected along the length of a given spine to ensure that the data obtained were not only useful, but also comparable across genera. These included a basal (proximal) section and a midpoint (distal) section.

Additional sections were produced across the "changing point" (Pivorunas, 1970; Bennett, 1996), defined here as a change in histological organization and/or cross-sectional shape from the base of the spine to the more distal portion, particularly in spines demonstrating pronounced dimetrodont differentiation (Romer and Price, 1940). This was performed across the healing callus at the level of the changing point in the pathological *Sphenacodon* spine, CM 73367.

Completed sections were examined using a Nikon Eclipse LV100 POL petrographic microscope with an integrated digital image capture system. Histomorphometric data were quantified using the image analysis software NIH ImageJ, published and distributed by the National Institutes of Health. Relevant calculations included: bone density, which is defined here as the proportion of mineralized bone matrix area (excluding vascular and medullary spaces) relative to the total cross-sectional area of the bone; cortical porosity, which is the ratio of vascular canal area within the cortex to the mineralized cortical bone area and is expressed as a percentage; relative bone wall thickness (or RBT), which is the ratio of the average cortical thickness to the average cross-sectional diameter

and is also expressed as a percentage (Chinsamy, 1993); total cross-sectional area in mm^2 ; minimum second moment of area (I_{\min}) measured in mm^4 ; maximum second moment of area (I_{\max}) measured in mm^4 ; relative maximum to minimum bending rigidity (I_{\max}/I_{\min}); and torsional rigidity (J) which is the sum of I_{\min} and I_{\max} (Plochocki et al., 2007). RBT (Chinsamy, 1993) is a variation of R/t (cross-sectional radius to cortical thickness) and K (internal diameter to external diameter), each of which have been previously applied to assess whether a bone has been selected for varying measures of strength (e.g., ultimate or impact strength) or for stiffness (Currey and Alexander, 1985). Values of I_{\max} and I_{\min} describe relative resistance to bending stresses, whereas J describes resistance to torsional stresses. A complete list of histomorphometric data is presented in Appendix D.

Results

Dimetrodon -

General Description. Although the dorsal neural spines exhibit some variation in the morphology of both proximal and distal regions across the various species of *Dimetrodon*, all of the specimens examined are similar in

that they exhibit some amount of dimetrodont differentiation. For example, the base of the spine of *Dimetrodon limbatus* is somewhat compressed mediolaterally and is subquadrangular in cross-section, with diminutive paired ridges running vertically along the anterior and posterior margins of the spine. By contrast, the larger *D. giganhomogenes* exhibits a much more robust base and the paired ridges are developed into exaggerated horns separated by a deep V-shaped notch (Figure 8A). In both species, however, these ridges disappear distally and are replaced by a more figure-8 cross-sectional shape (Figures 7B, 9A) as is typical of most members of the genus (Appendix C). The V-shaped notch in *D. giganhomogenes* continues dorsally into the fore and aft median grooves of the distal spine where it was purported by some authors to have housed an efferent blood vessel (Romer, 1927; Ricqlès, 1974a). In *D. giganhomogenes* and other large-bodied specimens the proximal-distal changing point is approximately 55-60 mm from the base of the spine, as in mature specimens of *Ctenospondylus* (personal observations) and reportedly in *Ctenorhachis* (Hook and Hotton, 1991). The maximum vertical extent of the dorsal neural spines in the genus ranges from 18 times the height of the vertebral

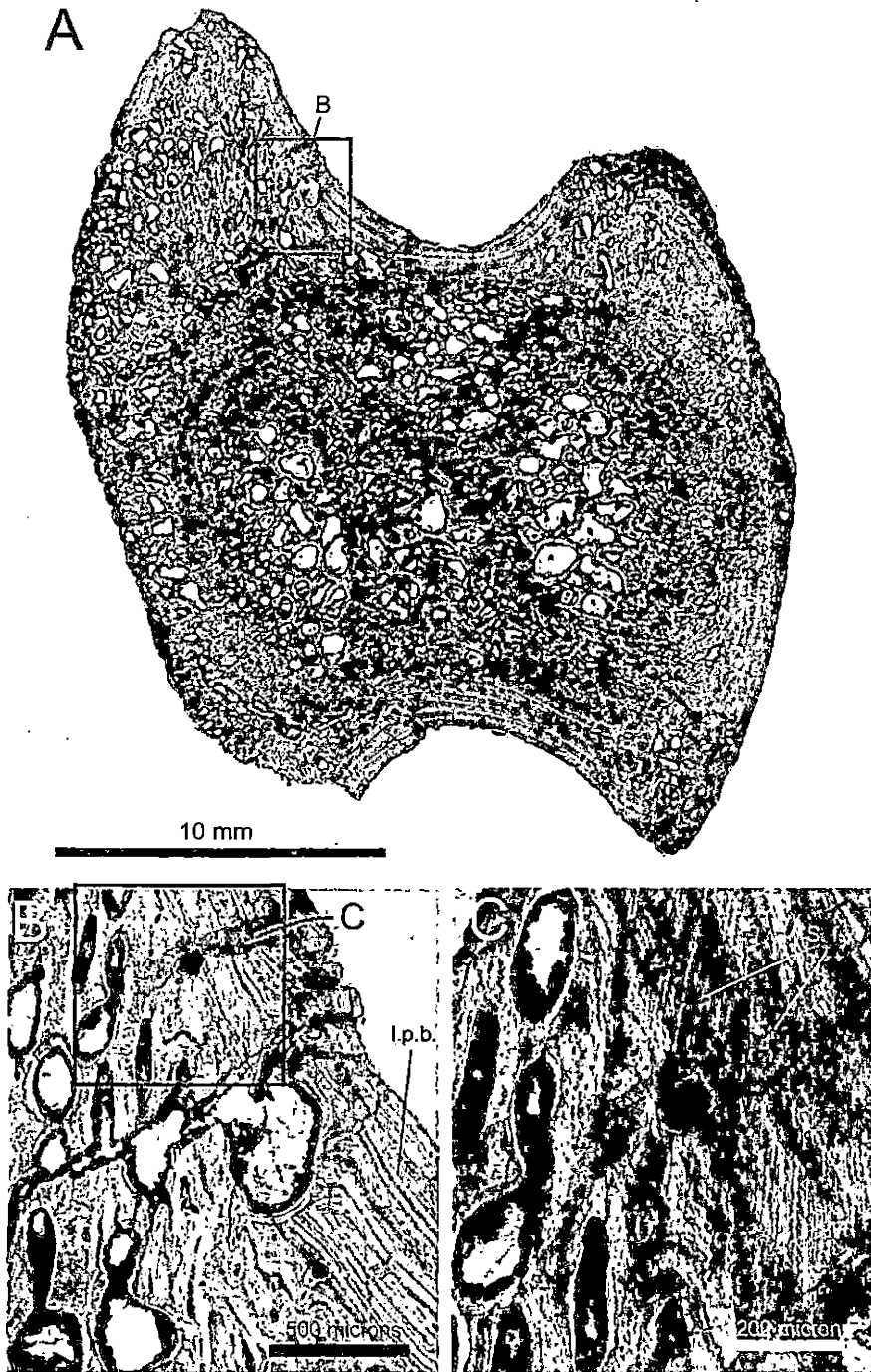


Figure 8. Proximal region of dorsal neural spine of *Dimetrodon giganhomogenes* (FMNH UC 1134). A), Transverse section of proximal region at low magnification, preserving details of the anterior and posterior grooves, densely vascularized lateral

cortex, woven bone in the horns (upper left), and a cancellous medullary region which preserves highly reconstructed cortical bone with a figure-8 cross-section in younger layers (photomicrograph courtesy S. Sumida and E. Rega); B), Transverse section at increased magnification viewed with polarized light, showing fibrolamellar bone and large, elongate resorption cavities within the horn and lamellar primary bone in the medial wall of the cortex bordering the groove; C), Area in "B" at high magnification viewed with polarized light, revealing deeply penetrating Sharpey's fibers within the cortex in the region of the horns and surrounding the resorption cavities. Abbreviations provided in Appendix A.

centrum in the diminutive *D. teutonis* and *D. occidentalis*, to as much as 32 times the height of the centrum in the massive *D. grandis* (Romer and Price, 1940; Berman et al., 2001).

FMNH UC 1134 displays a series of healed fractures as reported by Rega et al. (2005), located at the level of the proximal-distal changing point. However, aside from localized responses to injury, the histological profile of the specimen (Figures 8-9) corroborates previous descriptions of the microstructure of *Dimetrodon* spines (Enlow and Brown, 1957; Enlow, 1969; Ricqlès, 1974a). In particular, the lateral cortex is composed of extremely well-vascularized fibrolamellar bone tissue (discussed in

detail below). In addition to confirming these earlier surveys, the newly sectioned material also provides previously unknown information regarding fine details of the microstructure and ontogenetic transformations (e.g., cross-sectional shape changes, enthesal migration, and cancellous bone conversion). These new findings are reported below and serve to supplement the observations of Enlow and Brown (1957), Enlow (1969), and Ricqlès (1974a).

Proximal Region. Like the distal struts of the spine, the base exhibits variation across different species of *Dimetrodon* in terms of its cross-sectional shape which may be correlated with body size, or more explicitly with the relative degree of development of the associated epaxial musculature. Based on patterns of proximal muscle scars, Olson (1936) restored the epaxial muscles of *Dimetrodon* (Figure 7C-E). Following Slijper (1946), it is suggested here that the mechanical stresses experienced in the spine's base, associated with the development of the epaxial musculature, played a large role in shaping the spine proximally during ontogeny. For example, the base of the spine of the robust, large-bodied *D. giganhomogenes* displays a quadrangular cross-sectional shape with enlarged, paired horns anteriorly and posteriorly (Figure

8A). The inner cortex (Figure 8A) reveals, however, that the horns had not developed until later in ontogeny, at least in this level of the spine (if present, horns or small ridges may have been situated even lower in the spine earlier in ontogeny). This region bears well-vascularized, fibrolamellar cortical bone undergoing cancellous conversion, but preserving a figure-8 cross-sectional morphology typical of the distal region. This phenomenon was recently reported by Sumida et al. (2005), who suggested that cross-sectional shape of the spine may not be taxonomically informative unless ontogenetic trajectory is considered.

The formation of the proximal horns has not been considered in detail, but it is often disputed whether such remodeling and reorganization of the cortex is primarily governed by either developmental or mechanical constraints (Currey, 2002; Margerie, 2002; Margerie et al., 2004; Lee, 2004). Histological investigation reveals that the cortex in the proximity of the horns experienced marked secondary resorption and remodeling, with woven bone, elongate resorption cavities (Figure 8B) and dense, intermingling Sharpey's fibers often oriented at oblique angles (Figure 8C). These characteristics are consistent with cortical

remodeling near regions of muscular or tendinous entheses (Slijper, 1946; Benjamin et al., 2002; Heironymus, 2006) and have been identified even in other much smaller species of *Dimetrodon*, in particular a specimen tentatively attributed to *D. occidentalis* by Madalena et al. (2007). The authors suggested that the marked remodeling of the horns indicated rapid growth and possibly a growth spurt. However, the remodeling in this region may alternatively be explained by enthesal migration of the epaxial musculature distally along the spine during normal growth as evidenced by the deep, obliquely-oriented Sharpey's fibers in this region.

Distal Region. The distal spines in *Dimetrodon* range from subcircular in cross-section in small-bodied species such as *D. milleri* to figure-8 in larger species, but a quadrangular shape is purportedly maintained throughout the entire length of the neural spine in the largest species, *D. grandis* (Appendix C). The present examination confirms that the cortical bone is dominated by well-vascularized fibrolamellar tissue, but additionally reveals marked avascularity in the region of the anterior and posterior grooves which consist of lamellar bone (Figures 9A, 10A). The medullary region reveals much greater cross-sectional

bone mass than the tall-type spines of *Captorhinus* (Sumida, 1990) or *Edaphosaurus* (Ricqlès, 1974a), and is dominated by dense fine-cancellous bone which formed via the conversion of compact cortical bone. Thus, great histovariability exists in the cross-sectional profile of the distal spine. In general, the bone exhibits high cortical porosity in this region (13.5%), a thick bone wall (~15%), and great resistance to torsion and lateral bending, due to the laterally expanded, double-cylinder morphology of the distal spine (Appendix D).

The high cortical porosity is owed to an abundance of longitudinally-oriented primary osteons in the lateral cortex (Figures 9B, 10B). In fact, Enlow and Brown (1957:204) noted the pronounced vascularity of the cortex, stating that "in no skeletal element yet examined ... do the vascular canals number as many as they do in the spine of *Dimetrodon*." Possible avascularity of the anterior and posterior grooves (Rega et al., 2005) indicates that a well-vascularized lateral periosteum would make a better candidate for the source of controlled blood-flow to the sail during thermoregulation. However, from a developmental perspective, extensive vascularization would

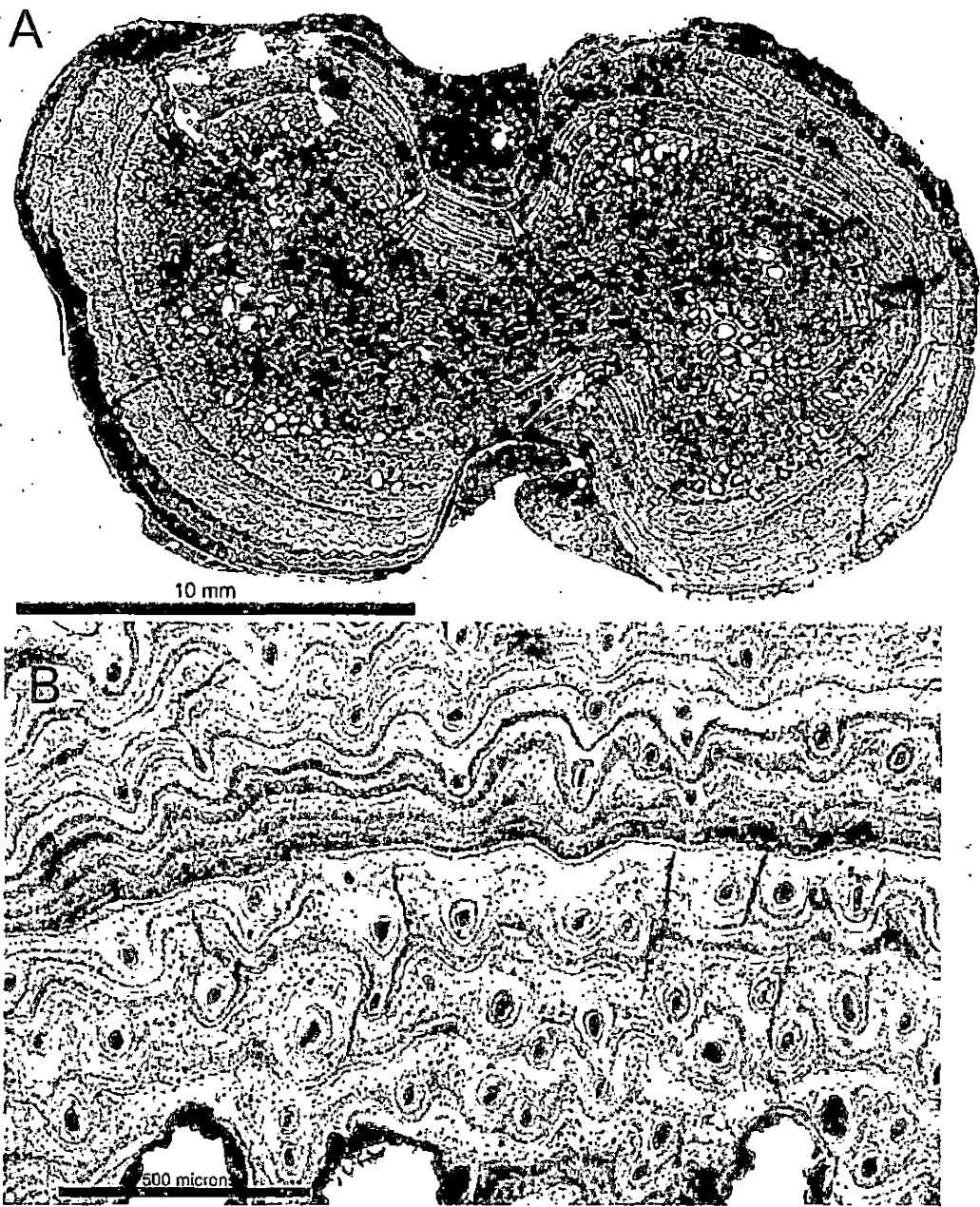


Figure 9. Distal region of dorsal neural spine of *Dimetrodon giganhomogenes* (FMNH UC 1134). A), Transverse section of distal region at low magnification, showing the typical figure-8 cross-sectional shape, lamellar bone in the anterior and posterior grooves, a highly vascularized lateral cortex composed predominantly of fibrolamellar bone, and a dense or fine-cancellous medullary region; B),

Transverse section through the cortex at high magnification viewed with non-polarized light, showing primary osteons within a fibrolamellar bone matrix preserving distinct growth zones separated by lines of arrested growth (LAGs) and annuli. Note the abundance of longitudinal primary osteons, which were organized randomly in the inner cortex, but became arranged in more regular, radiating rows as bone deposition slowed (indicated by thinner growth zones in the outer cortex). Photomicrographs courtesy S. Sumida and E. Rega.

have just as likely served to meet the needs of the rapidly growing bone tissue, as fast-growing fibrolamellar bone is often well-vascularized, particularly in juveniles (Currey, 2002). In FMNH UC 1134, the primary osteons appear to have become arranged more regularly as growth slowed and were distributed radially in the outer cortex (Figure 9B). This pattern is consistent in other species of *Dimetrodon*, including a large individual tentatively attributed to *D. grandis* (Figure 10B).

At high levels of magnification, short bundles of Sharpey's fibers were also found within the lateral cortex of the distal spine under polarized light in FMNH UC 1134. The bundles differed from those found in the proximal region of the spine in their size and

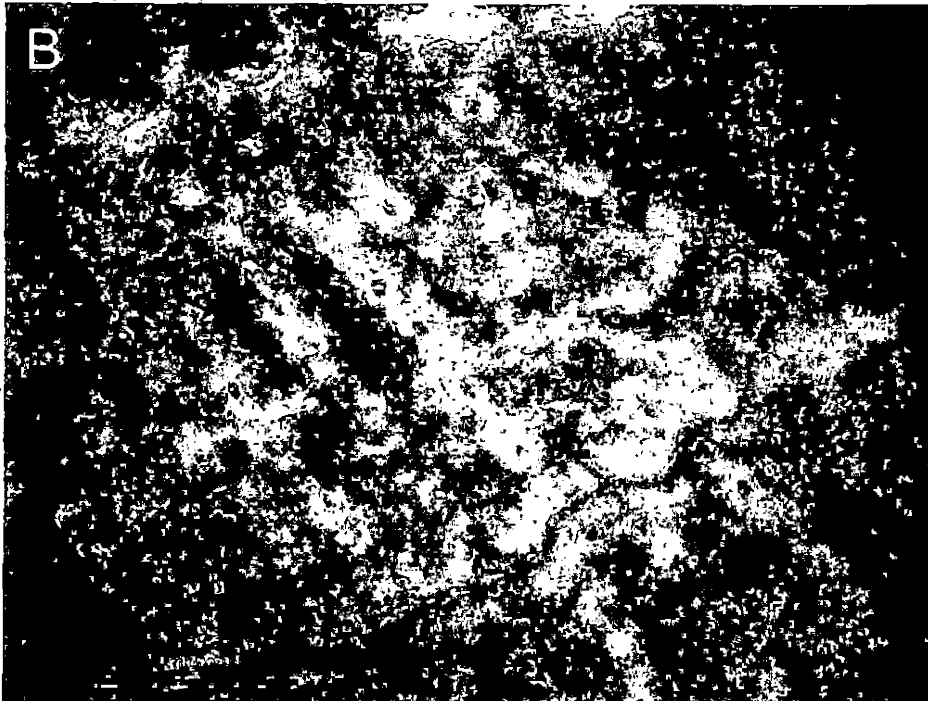
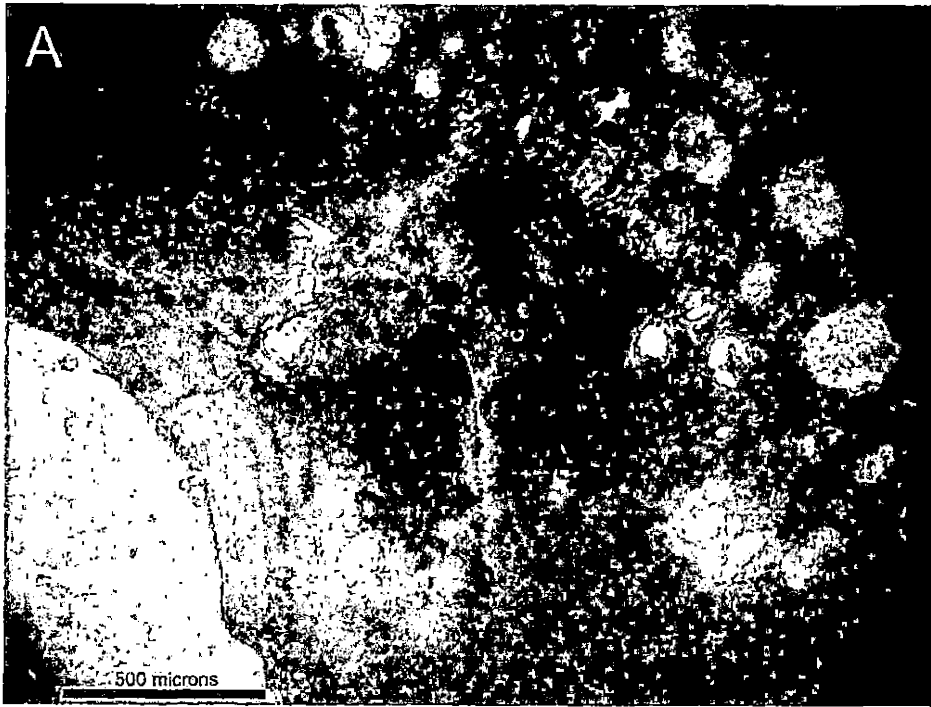


Figure 10. Distal region of mid-dorsal neural spines of *Dimetrodon* cf. *D. giganhomogenes* (DMNH 30597) and cf. *D. grandis* (DMNH 16131) viewed with non-polarized light. A), Transverse section of DMNH 30597 in the

region of the groove. Note the thick cortex composed of thin, densely packed lamellae and marked avascularity of the groove. B), Transverse section of *Dimetrodon* cf. *D. grandis*, DMNH 16131, showing the well-vascularized lateral cortex. Over-preservation obscures details of growth zones and restlines, but note the extreme size of the specimen and regular, radiating spacing of longitudinal primary osteons suggest maturity and slowed growth, reminiscent of mature *D. giganhomogenes* specimens.

distribution, often localized within individual lamellae and varying in orientation. The bundles resemble those figured in the spines of *Edaphosaurus* (Enlow, 1969; Ricqlès, 1974a), although they are not as prominent, and may indicate the migration of the periosteum or that of an associated collagenous sail membrane.

Sphenacodon -

General Description. The dorsal neural spines of *Sphenacodon* are often described as "blade-like" as they are mediolaterally compressed throughout, narrowly oval in cross-section, and widen anteroposteriorly toward the distal tip. External details reveal distinct patterns of surface texture between proximal and distal portions of the spine (the significance of which is discussed below), with a transition from roughened periosteal bone indicative of

muscle scars proximally to vertical striations distally. In mature specimens attributed to *Sphenacodon ferocior*, such a transitional zone exists between 55-60 millimeters above the zygopophyses. This point in *Sphenacodon* is approximately the height of the changing point in mature specimens of *Dimetrodon* and *Ctenospondylus* (see above).

In histological profile, the neural spines of *Sphenacodon* are typified by fibrolamellar and parallel-fibered bone tissue (as in the long bones; Huttenlocker et al., 2006), indicating both rapid and intermediate rates of deposition. Pronounced vascularization (cortical porosity approximately 6.0 to 7.5%) also corroborates fast bone-growth. However, unlike the predominantly radial orientation of osteons in the long bones, the primary osteons of the neural spines are longitudinally oriented as in *Dimetrodon*. The microstructure of the neural spines further resembles *Dimetrodon* in the presence of dense fine-cancellous bone in the medullary region produced by cancellous conversion of compact cortical bone, generally moderate to high vascularity, and apparent adaptations for resistance to torsion and bending (although resistance to bending is predominantly in the anteroposterior direction; Appendix D).

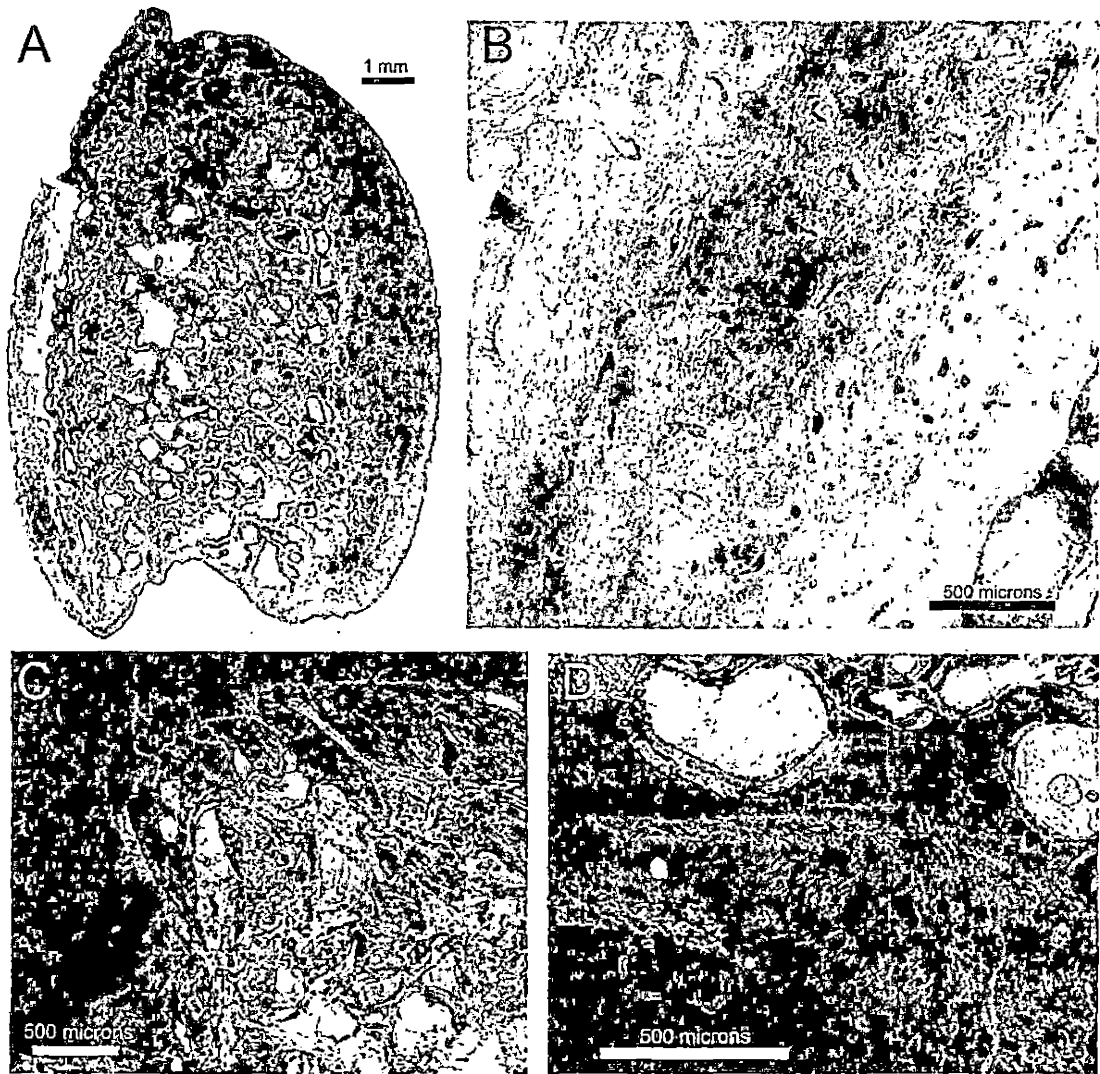


Figure 11. Transverse sections through proximal region of dorsal neural spines of *Sphenacodon ferox*. A), Proximal region of UCLA VP uncatalogued specimen (field no. C-61-29) shown at low magnification; B), Cortex of "A" shown at high magnification viewed with polarized light, revealing numerous reticular primary osteons in a fibrolamellar bone matrix; C), Posterior ridges of UCMP 68436 viewed with cross nicols, showing elongate resorption cavities in the cortex and numerous Sharpey's fibers, resembling the condition in the proximal horns of *Dimetrodon*; D), Lateral cortex of UCMP 68436 viewed with cross nicols, showing numerous resorption cavities with extensive remodeling along the medullary margin and

Sharpey's fibers deeply penetrating the cortex at an oblique angle (indicating attachments of epaxial muscles).

Proximal Region. The base of the neural spine is oval to subtriangular in cross-section due to the presence of paired ridges along the posterior margin of the spine (Figure 11A). There is an abrupt transition between the cancellous medullary region and the compact cortex, which is composed of fibrolamellar bone containing randomly-oriented, globular osteocyte lacunae and numerous reticular and longitudinal primary osteons (Figure 11B). Marked remodeling appears to have occurred within the cortex in the region of the posterior ridges, just as in the proximal horns of *Dimetrodon*. Likewise, this region displays woven bone, large elongated resorption cavities, and deeply-penetrating Sharpey's fibers (Figure 11C), likely indicating attachments of the paired *M. interspinalis*. Extensive Sharpey's fibers also continue onto the lateral margins of the proximal spine (Figure 11D), preserving evidence of the attachments of the *Mm. spinalis dorsi* and *semispinalis* (Figure 15) as in tall-type spines of *Captorhinus* (Sumida, 1990).

Distal Region. The cortex is unusually thin distally (RBT 4.8%) and the boundary with the cancellous medullary region is markedly abrupt, more so than in the proximal region of the spine. These features, coupled with the dense trabecular network of the medullary region, indicate rapid reclamation of primary cortical bone by the cancellous medulla. The dense trabecular architecture of the medullary region may be a characteristic feature of sphenacodontids, as a similar condition is found in the spines of *Dimetrodon*. In *Sphenacodon*, the distal region of the neural spine is herein distinguished from the proximal region by a transition from superficial muscle scars into vertical striations on the lateral periosteal surface. These external features are also associated with changes in the histological profile of the spine. Figure 12 demonstrates the relationships between the vertical striations localized in the distal region of the spine and the abundant, longitudinally-oriented primary osteons within the cortex. Although cortical porosity is slightly lower distally (Appendix D) abundant primary

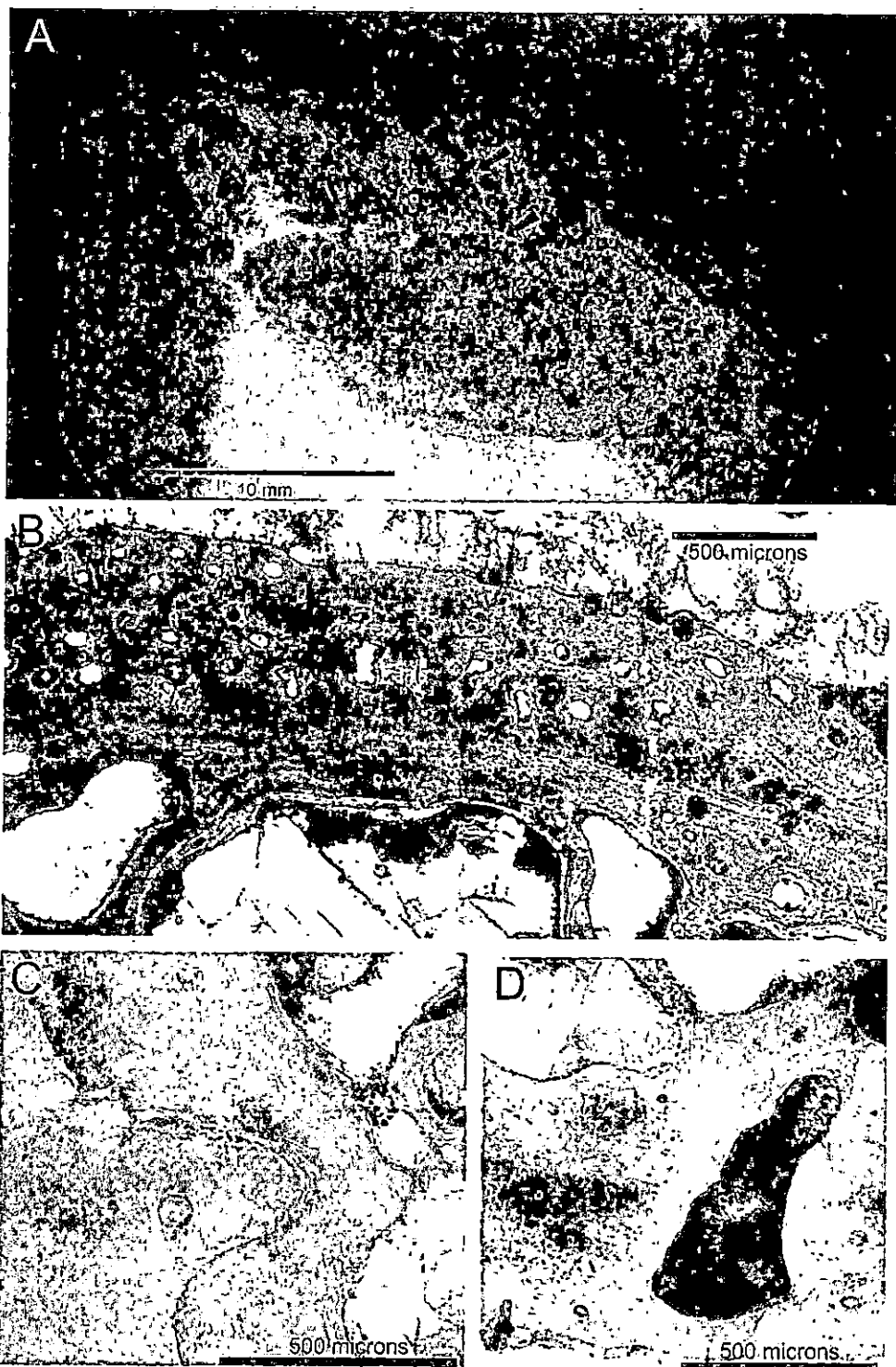


Figure 12. Distal region of dorsal neural spine of *Sphenacodon ferox* (UCLA VP uncatalogued). A), Distal fragment of spine viewed posteriorly and laterally at

an oblique angle, showing a large striation on the external surface penetrating the cortex and forming a large primary osteon (arrows), demonstrating that the superficial striations represent periosteal or subperiosteal vascular channels; B), Lateral cortex viewed with non-polarized light, composed of alternating sheets of parallel-fibered and fibrolamellar bone and densely vascularized with large primary osteons (absorbed subperiosteally); C-D), Lateral cortex at high magnification viewed with polarized light, showing large subperiosteal vascular channels in the process of becoming incorporated within the cortex.

osteons exist in the lateral margins of the spine, some of which are greater in diameter than those found in the proximal region (Figure 12C,D) and there is greater variation in the size of the primary osteons. In cross section, one specimen (uncatalogued UCLA VP specimen) records a large external striation penetrating the cortex where it is preserved as a primary osteon internally (Figure 12A). Thus, it is likely that the abundance of vascular canals in the lateral cortex of both *Sphenacodon* and *Dimetrodon* is correlated with the mode of deposition. The abundant primary osteons of the cortex existed within a fibrolamellar and parallel-fibered bone matrix (Figure 12B) which likely incorporated periosteal blood vessels within the rapidly growing subperiosteal osteoid before it

mineralized. This relationship suggests that the vertical striations on the surface of the spine are vascular in origin. Other instances of the incorporation of blood vessels into the cortex are recorded within the figured specimen (Figure 12C-D). Similar striations have been reported in the sphenacodontid *Ctenorhachis jacksoni* (Hook and Hotton, 1991) and are visible on the neural spines of *Ctenospondylus* (personal observation).

Pathological observations. Pathologies, such as healed fracture calluses, are often found in the neural spines of sail-bearing tetrapods, such as the ctenosauriscid archosaur *Arizonasaurus* (Nesbitt, 2005) and most notably in the sphenacodontid *Dimetrodon* (Romer and Price, 1940; Enlow, 1969; Rega et al., 2002, 2005). Pathology in the neural spines of *Dimetrodon* has not been described here, as the first detailed account of these pathologies is in preparation elsewhere (Rega et al., 2002, 2005). However, a recently discovered pathology in a dorsal neural spine of *Sphenacodon* cf. *S. ferocior* (CM 73367) is briefly described here due to its implications for spine mechanics and soft-tissue restorations of the dorsum.

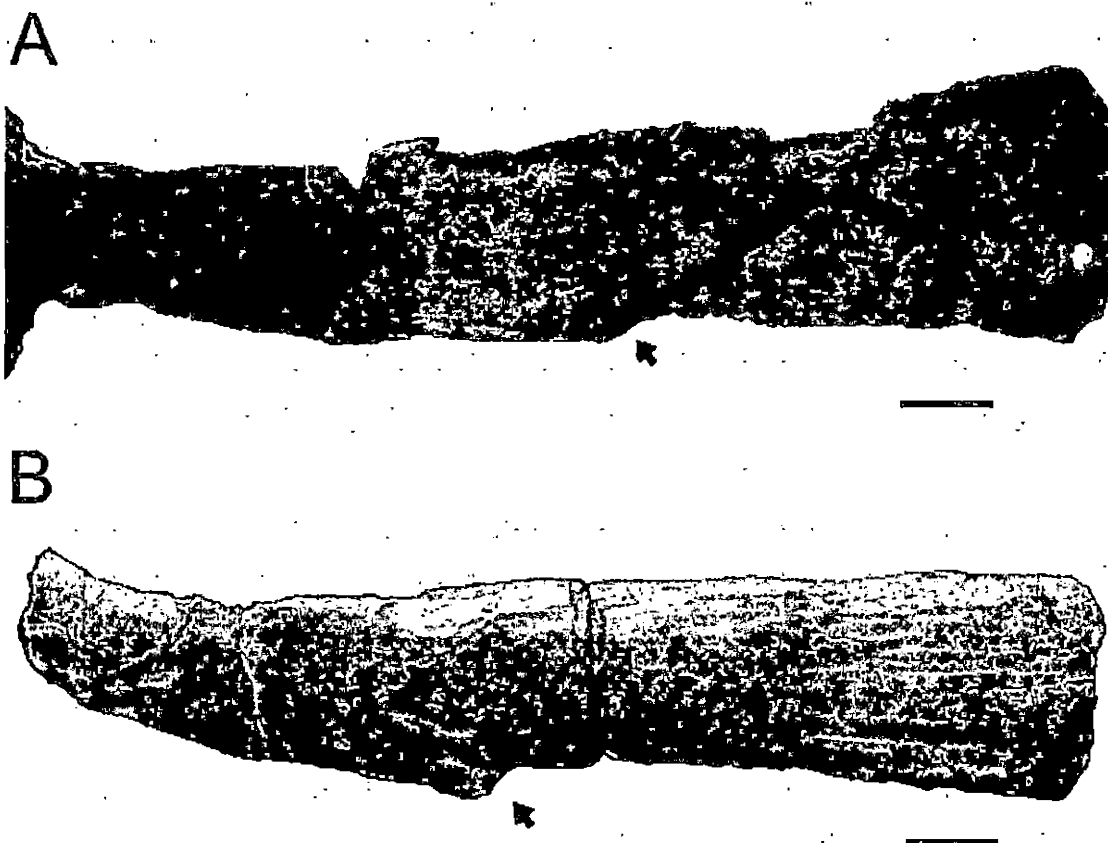


Figure 13. Healing calluses in dorsal neural spines of *Sphenacodon*. A), *Sphenacodon ferocior* (UCMP 34218); B), *Sphenacodon* cf. *S. ferocior* (CM 73367). Note that the fractures (arrows) exist within a transitional location between the proximal epaxial-embedded (denoted by faint muscle scars) and distally protruding (denoted by vertical vascular striations) regions of the spine.

A cursory survey of pathological *Sphenacodon* specimens has revealed rare but multiple occurrences of healed spine fractures in the genus (personal observations), with specimens tending to display woven-textured bone at the

transition between the proximal (epaxial-embedded) and distal portions of the neural spine (Figure 13). The healing callus in CM 73367 is restricted to the posterior portion of the spine, located just distal to the paired posterior ridges (Figures 13B, 14A). Extensive deposition of unorganized, woven fibrolamellar and cancellous bone tissue is recorded in cross-section (Figure 14A) and apparently resulted in a cross-sectional shape change from oval to subtriangular. The lateral cortex apparently became thickened with the deposition of well-vascularized, fast-growing fibrolamellar bone with large resorption cavities (Figure 14B). The inner cortex, formerly oval in cross-section, shows evidence of rapid resorption and cancellous conversion, and the compact cortical bone has been remodeled into a fine-cancellous scaffolding on the left side of the spine (Figure 14C). This scaffolding resembles the callus bridges of *Dimetrodon* (Enlow, 1969) and emphasizes variable, localized responses to injury as noted in healing calluses of *Dimetrodon* (Rega et al., 2005).

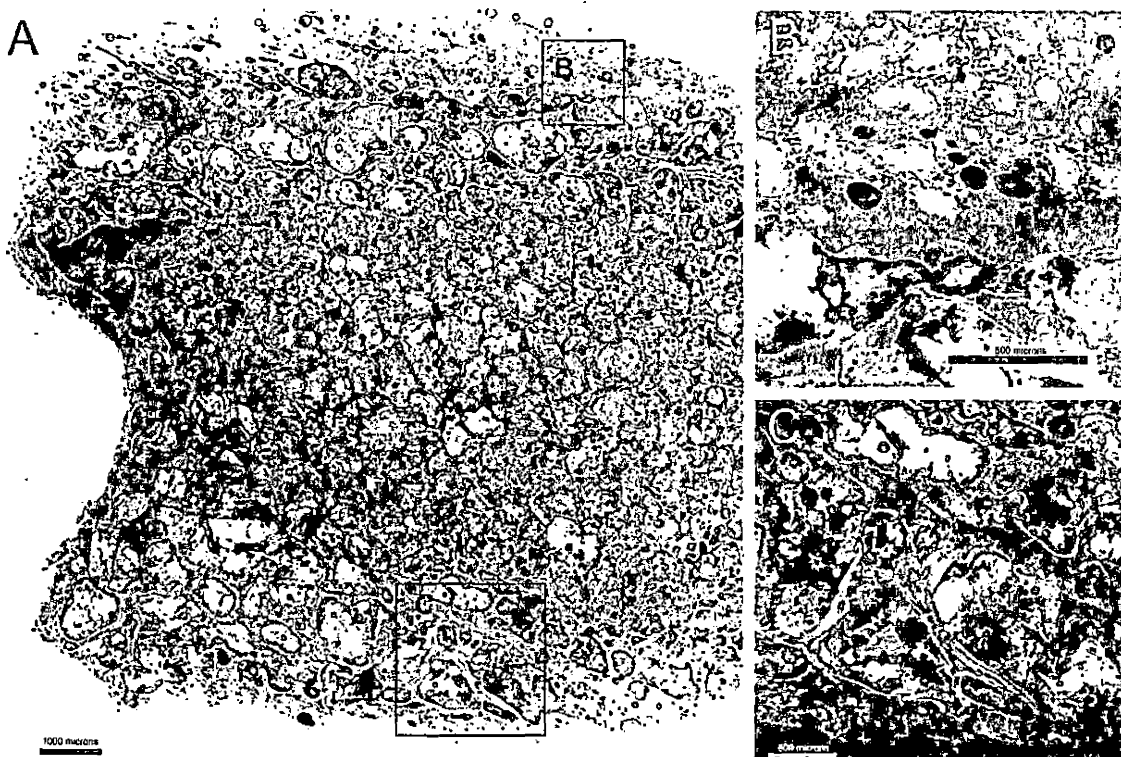


Figure 14. Transverse section through healing callus of *Sphenacodon* cf. *S. ferocior* (CM 73367) viewed with polarized light. A), Section through spine viewed at low magnification, showing extensive deposition of unorganized, woven fibrolamellar and cancellous bone tissue, localized in the posterior region of the spine, and resulting in a change in cross-sectional shape; B), Densely vascularized cortex composed of a woven fibrolamellar bone matrix; C), Extensive remodeling of cortical bone into a fine-cancellous scaffolding, resembling callus bridges in pathological specimens of *Dimetrodon*.

Discussion

Histovariability and the "Changing Point" of Sphenacodontid Neural Spines

The discovery of histological variation along the length of the neural spine necessitates a discussion of its implications for the distribution of muscular attachments in other sphenacodontids of varying spine lengths. Although not all sphenacodontids demonstrate unambiguous dimetrodont differentiation of the spines, the new interpretations of external surface markings and internal histological features along varying regions of the spine allows an alternative means of inferring the presence or absence of a dorsal crest in sphenacodontids.

For example, a changing point demarcating the proximal and distal regions of the spine has been observed in a cast of an adult specimen of *Ctenospondylus* cf. *C. casei* (uncatalogued CSUSB specimen, formerly UCLA VP) and is associated with changes in surface texture indicative of the soft-tissue correlates (e.g., muscle scars, vertical vascular striations, etc.). This transition occurs between 55-65 mm above the level of the zygopophyses, comparable to that of adult specimens of *Sphenacodon ferocior* from the Early Permian Anderson Quarry in New Mexico (personal

observation, 2007) and to the specimens of *Sphenacodon* and *Dimetrodon* described above. Across these genera, the height of the transition zone does not appear to correlate with spine height, at least in adults; that is, the transition zone remains at a roughly fixed height in adults, regardless of the continued lengthening of the distal most portion of the spine which shows much greater variation (up to 30% longer in *Ctenospondylus* than in *Sphenacodon*). Although the microanatomical transition of muscle scars and striations across this changing point can be observed on the surface of the bone in a pattern similar to that of *Sphenacodon*, there is additionally an anteroposterior "shoulder-like constriction" (Reisz, Berman, and Scott, 1992) in *Ctenospondylus* that is apparent at the gross anatomical level, reminiscent of the condition in *Dimetrodon* (Romer and Price, 1940). This shape change is taken to an extreme in many species of *Dimetrodon* that show a marked difference in cross-sectional shape from proximal to distal regions of the spine (discussed above).

As shown in *Sphenacodon*, however, changes in histology are not always associated with marked changes in cross-sectional shape at the gross anatomical level. In the blade-like neural spines of the genus *Ctenorhachis*, a

Sphenacodon-like transition zone was unwittingly described by Hook and Hotton (1991:41) in their discussion of a slight constriction of the spines with the emergence of "longitudinal striations that range from faint to prominent" at that level, approximately 50-60 millimeters above the zygopophyses. The striations were likely homologous to the vertical vascular striations described above in *Sphenacodon*. Hook and Hotton suggested that the spines of *Sphenacodon* were primitive for sphenacodontids because they were not known to be divided into proximal and distal portions, and inferred that *Ctenorhachis* displayed a sail, the shortest of any known sphenacodontid. However, the new data suggest that the soft-tissue correlates of *Sphenacodon*, in which the neural spines are equivalent in height to those of *Ctenorhachis* but resemble those of *Ctenospondylus* in their overall shape, were likely identical to those of *Ctenorhachis*. Therefore, a dorsal crest may have been a primitive characteristic of the family as microanatomical data support its apparent ubiquity among known representatives of Sphenacodontidae, even in the absence of a distinct changing point.

Pathological Evidences of a Dorsal Crest in Basal Sphenacodontids

The presence of a dorsal crest in sphenacodontids of relatively low to moderate spine heights, such as *Sphenacodon* and *Ctenorhachis*, is further supported by circumstances of their preservation and pathological features. A comprehensive examination of pathological responses in sphenacodontid bone is beyond the scope of this study and is in preparation elsewhere (Rega et al., 2002, 2005). However, pathological conditions are briefly considered here due to their implications for spine mechanics and restorations of the dorsal crest.

If the microstructural organization of proximal muscle scars and Sharpey's fibers indicate the location of muscular and tendinous attachments, then 50% of the neural spine or less was "anchored" by the epaxial muscles (Figure 15), whereas the remaining distal portion was "free" (although may have been embedded in a thin collagenous webbing as in other crested vertebrates, e.g., the chamaeleonid genus *Trioceros*; Case, 1909). Given the variable lengthening of the distal portion of the spine, it is important to note that this region would have been vulnerable to large bending moments and, thus, greater

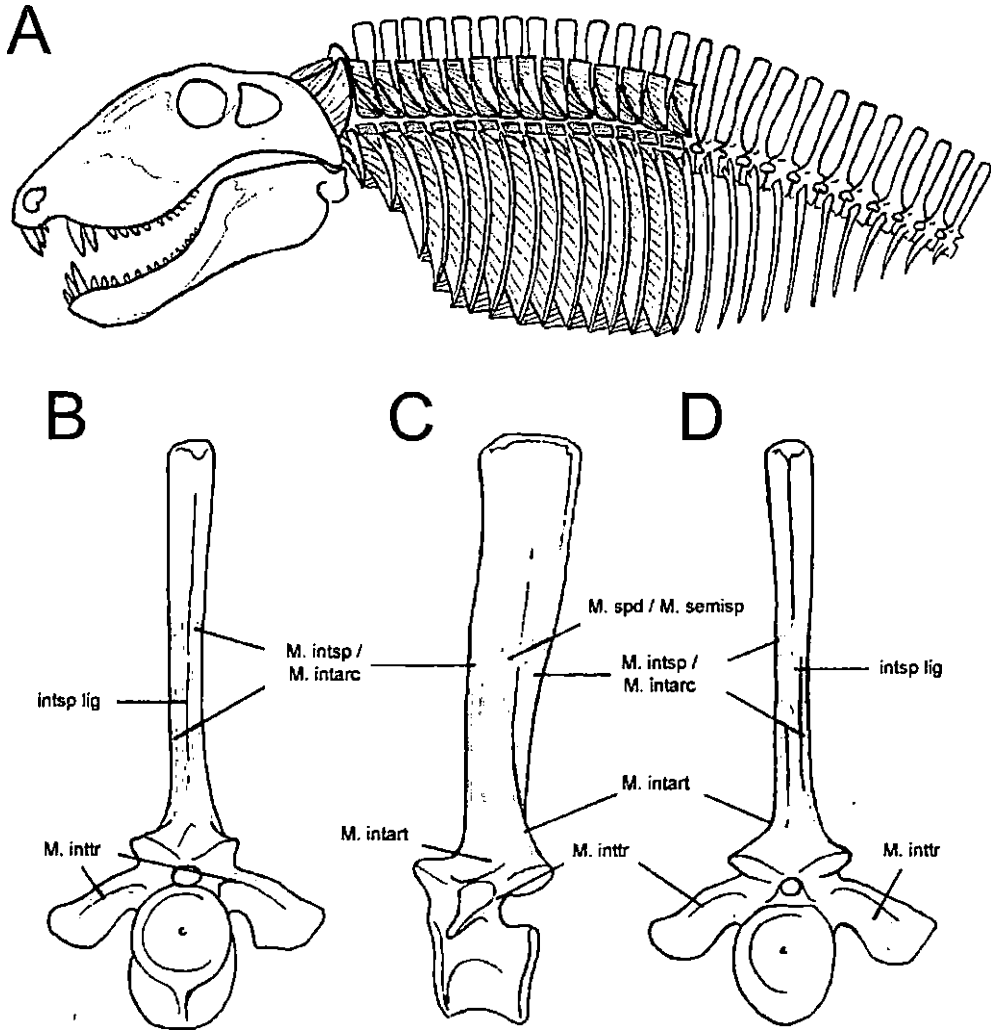


Figure 15. Restoration of short segmental epaxial musculature (sensu Olson, 1936) in the genus *Sphenacodon*. A), Anterior axial skeleton of *Sphenacodon* (modified from Romer and Price, 1940) with short segmental muscles superimposed onto the cervical and dorsal regions; B-D), Proximal region of a mid-dorsal vertebra in anterior ("B"), left lateral ("C"), and posterior ("D") views with muscular origins/insertions illustrated (vertebrae redrawn from Case et al., 1913; muscular attachments based on personal observations and restorations of *Dimetrodon* from Olson, 1936).

probability of failure at the fixed point. It is also important to note that the histomorphometric data suggest that the spines of *Sphenacodon* were well adapted for resisting fore and aft bending, but were not selected as strongly to resist lateral bending (Appendix D). Given these requisites, it is not surprising to find occasional fractures in the spines of *Sphenacodon*, all of which appear to be located within the "anchored" transitional zone of the spine as predicted. It is also at this location in the spine (i.e., the changing point) that fractures are commonly found in *Dimetrodon*.

In addition to the occurrence of healed fractures, many sail-backed synapsids have been discovered in which the vertebral column is dorsally hyper-extended (opisthotonic posture). Such posture has been described in articulated dinosaur skeletons and attributed to "death throes" and postmortem contraction of interspinal ligaments among other explanations (see Faux and Padian, 2007 for a review), but is unique in sphenacodontids in that the distal portions of the spines overlap significantly. These incidences were noted by Hook and Hotton (1991) who identified a similar postmortem posture in the type and referred specimens of *Ctenorhachis jacksoni*. The distal

ends of the spines were likely protruding to some extent, as the distal overlap of the spines upon contraction of the interspinal ligaments would not be possible if the neural spines were entirely restricted by the epaxial musculature. Thus, multiple pathological evidences apparently support the existence of a short, dorsal crest even in conservative sphenacodontids like *Ctenorhachis* and *Sphenacodon*.

Conclusions

Histovariability along the length of the neural spine in *Dimetrodon* records the transition from the proximal (epaxial-embedded) to the distally protruding portion of the neural spine. Microstructural similarities between the genera *Dimetrodon* and *Sphenacodon* offer unambiguous evidence of the presence of a short, dorsal crest in the latter genus, even in the absence of gross morphological changes. These findings emphasize that gross morphology does not always reveal changes in soft-tissue correlates (Hieronimus, 2006), and histological features may demonstrate great variability along the length of a single bone, even in the absence of obvious gross morphological markers.

Healed fracture calluses in neural spines attributed to the genus *Sphenacodon* are similar to those reported in supposed sail-backed tetrapods (e.g., *Dimetrodon* and *Arizonasaurus*), and are remarkably similar to *Dimetrodon* in healing response and location of the injury. Other pathological incidences, such as the overlap of the distal portions of spines upon death in an articulated vertebral column of *Ctenorhachis* would not have been possible if the spines were restricted by extensive epaxial musculature in these sphenacodontids.

Combined evidence including normal histology and pathology support the hypothesis that conservative sphenacodontids of relatively low to moderate spine heights had already developed a dorsal crest during the course of their evolutionary history. This confounds earlier hypotheses that the dorsal sail evolved as a thermoregulatory organ, as it was not derived in "advanced" sphenacodontids, nor was it a neomorph in *Dimetrodon* (contra Pivorunas, 1970), but rather developed from the rudimentary crest exhibited in earlier sphenacodontids. A more thorough understanding of the order of character evolution in the dorsal crest, its functions, and its elaboration into the immense sail of *Dimetrodon* will be

better facilitated by an investigation of sphenacodontid temporal and phylogenetic relationships at the genus and species level. Such temporal and phylogenetic trends in the structural and functional evolution of the dorsal sail will be examined subsequently in Chapter Four.

CHAPTER THREE

COMPARATIVE OSTEOHISTOLOGY OF HYPERELONGATE

NEURAL SPINES IN EDAPHOSAURIDAE

Introduction

The North American and European family Edaphosauridae represents one of the earliest known tetrapod families to have acquired a dorsal sail (with the possible exception of a Middle Pennsylvanian taxon, *Echinerpeton*, having unknown affinities; Reisz, 1972). Early members of this family are represented by an isolated neural spine that was assigned to Edaphosauridae incertae sedis and isolated skeletal material referred to *Ianthasaurus* sp. from the Upper Pennsylvanian Sangre de Cristo Formation of central Colorado (Sumida and Berman, 1990). The more complete type material of *Ianthasaurus hardestiorum* was recovered from Upper Pennsylvanian deposits of the Stanton Formation in eastern Kansas (Reisz and Berman, 1986). Another taxon of possible edaphosaurid affinities, *Xyrospondylus ecordi*, was recovered from the same deposits in Kansas, but its validity has been called into question (Reisz, 1986). These populations are preserved in Pennsylvanian-aged

deposits that predate the first known sail-bearing sphenacodontids by at least five million years.

To date, the family has been diagnosed by greatly elongated presacral neural spines (Figure 16) that are subcircular in cross-section (except for a short, laterally compressed proximal region); neural spines which lean or curve anteriorly in the cervical region and posteriorly in the posterior dorsal or "lumbar" region (Modesto and Reisz, 1990); and laterally projecting tubercles on the presacral neural spines (except in *Lupeosaurus*), which are typically paired toward the base of the spine (Reisz, 1986; Modesto and Reisz, 1990).

Previous Analyses of Sail Structure and Function

The functions of the edaphosaurid dorsal sail and its laterally projecting tubercles have been the subject of much debate in the literature (Romer and Price, 1940; Pivorunas, 1970; de Ricqlès, 1974a; Reisz and Berman, 1986; Modesto and Reisz, 1990; Bennett, 1996). Numerous authors have advocated a thermoregulatory function for the sail of the sphenacodontid *Dimetrodon*, largely due to the fact that the sail demonstrates positive allometric

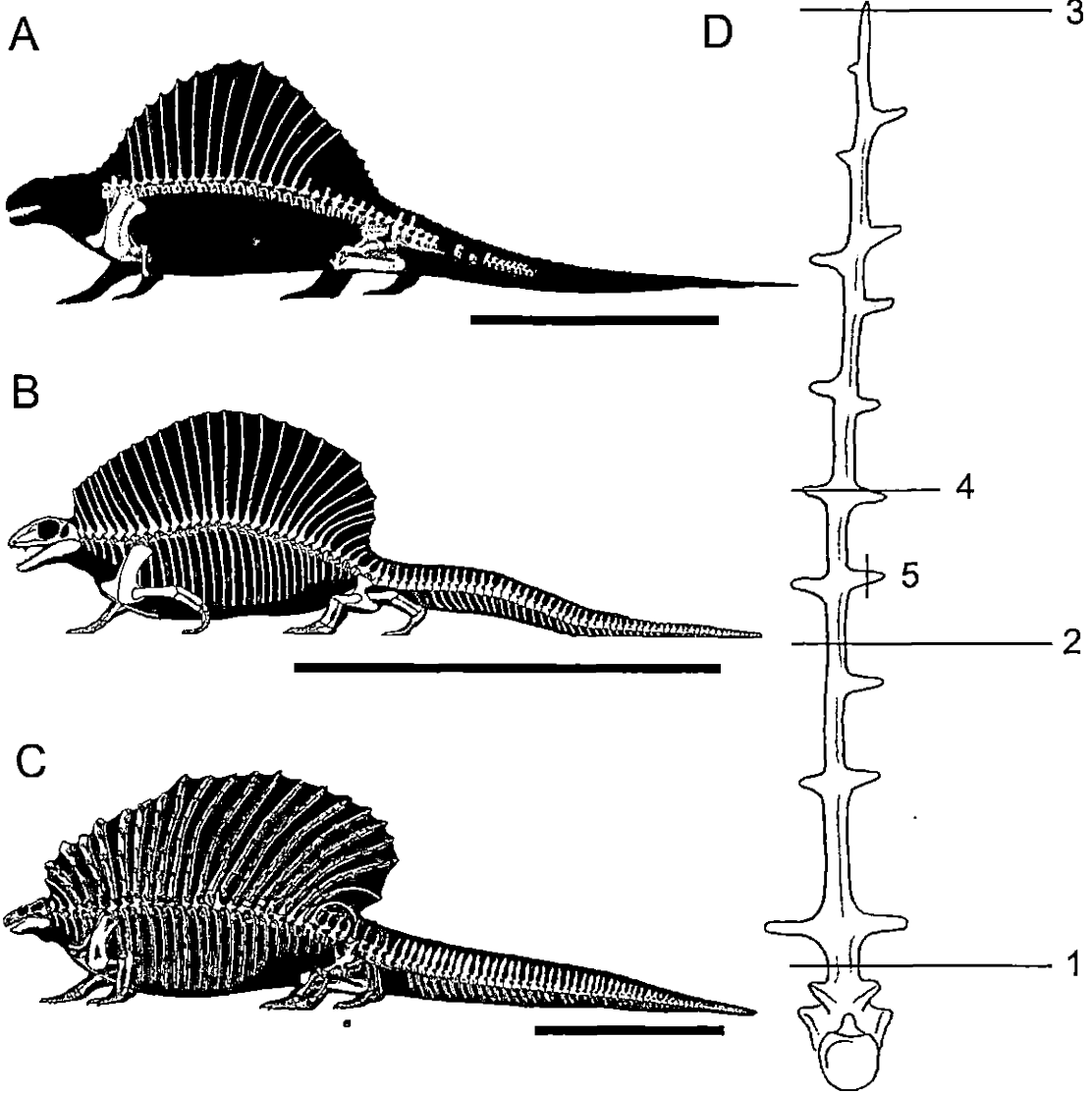


Figure 16. Edaphosauridae postcranial reconstructions and neural spine anatomy. A), *Lufesaurus kayi* (modified from Romer and Price, 1940); B), *Ianthasaurus hardestiorum* (modified from Modesto and Reisz, 1990); C) *Edaphosaurus pogonias* (modified from Romer and Price, 1940); D) Illustration of a dorsal vertebra in anterior/cranial view (modified from Reisz, 1986), indicating the locations along the neural spine where sections were cut for histological analysis. 1), basal (proximal) and changing point sections; 2), midpoint (distal) section; 3), tip section; 4), section along the longitudinal axis of a lateral tubercle; 5), section

along the transverse axis of a lateral tubercle. Sections "4" and "5" are applicable only to *Ianthasaurus* and *Edaphosaurus*. Scale bars with skeletal reconstructions ~ 0.5 meters.

growth with respect to body size (Romer, 1948, 1961; Pivorunas, 1970; Bramwell and Fellgett, 1973; Ricqlès, 1974a; Tracy et al., 1986). The presence of longitudinal grooves along the anterior and posterior surfaces of the neural spines, purported to accommodate blood vessels, also suggested to some authors that the sail was well vascularized (Romer, 1927; Romer and Price, 1940; Ricqlès, 1974a), thus facilitating its supposed thermoregulatory function. Ricqlès (1974a) was the first to attempt a reconstruction of the vascular system supplying the sail of *Dimetrodon* and *Edaphosaurus* based on a rudimentary histological survey of basal synapsid bone. He argued that the well vascularized cortical bone of *Dimetrodon* neural spines would have facilitated heat exchange more efficiently than it did for *Edaphosaurus*. He pointed out that if *Edaphosaurus* were to have had a membrane involved in thermoregulation, then peripheral vessels and tubercles were necessary to increase the efficiency of heat exchange, as the outer cortices of the spines were not as well

vascularized as in *Dimetrodon*. Thus, he hypothesized that, in *Edaphosaurus*, the tubercles provided a necessary connection between an internal artery represented by a central cavity within the spine (termed central "canal" or "channel" of Ricqlès, 1974a) and the external surface of the sail for convective heat flow to occur and be transferred to and from the viscera. A more recent study by Bennett (1996) hypothesized that the lateral tubercles of *Edaphosaurus* could have served a thermoregulatory function by increasing turbulent airflow across the sail membrane and thus facilitating more rapid cooling of the body.

Unlike *Dimetrodon*, the sail of *Edaphosaurus* does not appear to have exhibited positive allometric growth, with larger species displaying proportionately shorter neural spines (Romer and Price, 1940; Modesto and Reisz, 1990). This phenomenon and the presence of lateral tubercles suggested to some authors that the spines and tubercles of edaphosaurids were embedded within a thick membrane which may have served as a fat storage structure rather than a thermoregulatory organ (Romer and Price, 1940; Pivorunas, 1970). According to this hypothesis, the tubercles served as support structures embedded in a thick, connective

tissue sheath. Other hypotheses have been proposed regarding the function of the sail, including individual recognition (due to variations observed in the distribution of the lateral tubercles of *Ianthasaurus*) and defense (Modesto and Reisz, 1990).

Taxonomic and Histologic Perspectives

The Edaphosauridae represents a diverse family of nonmammalian synsids, with as few as eight but possibly as many as 11 omnivorous and herbivorous species spanning approximately 30 million years from the Late Pennsylvanian to the late Early Permian of North America and Europe (Table 3). Among these forms, great diversity exists in the sail's size and ornamentation (Figure 16). Although the internal structure and microanatomical properties of the neural spines of *Edaphosaurus* have been examined (Enlow and Brown, 1957; Enlow, 1969; Ricqlès, 1974a), they were not studied systematically and other edaphosaurid genera have not been examined at all, complicating interpretations of the sail's functional and structural evolution and leading to the lack of a comparative framework. For example, Ricqlès (1974a) and Bennett (1996) agreed that the communication between the central cavity and lateral

Table 3. Taxonomy of Edaphosauridae (based in part on Reisz, 1986).

Valid taxa assignable to Edaphosauridae

- *Genus *Edaphosaurus* Cope 1882
 - E. cruciger* Cope 1882
 - = *Dimetrodon cruciger* Cope 1878
 - = *Edaphosaurus microdus* Cope 1884
 - E. pogonias* Cope 1882
 - = *Naosaurus claviger* Cope 1886
 - = *Brachycnemius dolichomerus* Williston 1911
 - E. novomexicanus* Williston and Case 1913
 - E. boanerges* Romer and Price 1940
 - E. colohistion* Berman 1979
- Genus *Glaucosaurus* Williston 1915
 - G. megalops* Williston 1915
- *Genus *Lupeosaurus* Romer 1937
 - L. kayi* Romer 1937
- *Genus *Ianthasaurus* Reisz and Berman 1986
 - I. hardestiorum* Reisz and Berman 1986

Edaphosauridae incertae sedis

- Edaphosaurus*(?) *raymondi* Romer and Price 1940 (= *Naosaurus raymondi* Case 1908; *Ianthasaurus*?)
- Edaphosaurus*(?) *credneri* Romer and Price 1940 (= *Naosaurus credneri* Jaekel 1910)
- Xyrospondylus ecordi* (Peabody) Reisz, Heaton, and Pynn 1982 (= *Edaphosaurus ecordi* Peabody 1957)

Lupeosaurus has been tentatively assigned to Edaphosauridae by Sumida (1989) and Modesto and Reisz (1990).

Genera examined histologically in the present study are denoted by an asterisk (*).

tubercles of *Edaphosaurus* played a crucial role in the thermoregulatory abilities of that genus. However, if other edaphosaurid genera display a similar histological profile (i.e., avascular outer cortex of the spines) yet lack tubercles (e.g., *Lupeosaurus*) or display poorly

vascularized tubercles, then it is unlikely, or at least equivocal, that thermoregulation played a critical factor in the functional evolution of the edaphosaurid sail.

Here, structural and developmental aspects of the dorsal sail in three genera of Edaphosauridae (i.e., *Lupeosaurus*, *Ianthasaurus*, and *Edaphosaurus*) are described and summarized, and an attempt is made to identify genus-level distinctions in the sail's mechanics and development as revealed by the histology of the hyperelongate neural spines. The results of this study will allow structural and functional interpretations of the dorsal sail to be made within a phylogenetic context.

Materials and Methods

Selection of Taxa

A list of all currently recognized edaphosaurid taxa is provided in Table 3. Due to the availability of postcranial material, three genera were selected for thin-sectioning, including *Lupeosaurus*, *Ianthasaurus*, and *Edaphosaurus*. The Lower Permian genus *Glaucosaurus* was not sampled because it is only known from a single specimen represented by an incomplete skull and lower jaw (Modesto, 1994). Two vertebrae (a mid-dorsal and a posterior dorsal)

from a partial skeleton referred to *Lupeosaurus* cf. *L. kayi* (UCLA VP 1651; Figure 17) were sampled for histological sectioning. The specimen is from the Lower Permian (probably Artinskian-aged) Admiral Formation (Petrolia Formation of Hentz, 1988) near Lake Kickapoo, Archer County, Texas. Its external, gross morphology was described in detail by Sumida (1989). Sumida (1989) and Modesto and Reisz (1990) tentatively referred *Lupeosaurus* to the family Edaphosauridae.

Two uncatalogued vertebrae, including a mid-dorsal (Figure 18 A, B) and a posterior dorsal (Figure 18 C), referred to an adult specimen of *Ianthasaurus hardestiorum* (Mazierski and Reisz, 2006) were donated for sectioning by the vertebrate paleontology lab of Robert Reisz at University of Toronto. These specimens were collected from the type locality of *Ianthasaurus* (Reisz and Berman, 1986) in the Upper Pennsylvanian (Kasimovian-aged) Rock Lake Shale Member of the Stanton Formation, Anderson County, Kansas. This material is among the stratigraphically-oldest that can be confidently referred to the family Edaphosauridae.

Numerous specimens herein referred to *Edaphosaurus* spp. have been examined histologically for the present

study. *Edaphosaurus* fossils are abundant in the Lower Permian rocks of the southwestern United States and the genus was the most common Lower Permian edaphosaurid of the Texas-Oklahoma region (Romer and Price, 1940; Reisz, 1986), making specimens readily available for destructive analysis. An isolated neural arch (OMNH 73800; Figure 19B) with the proximal region of the neural spine from the Lower Permian (Kungurian-aged) Upper Garber Formation of Comanche County, Oklahoma was examined. In addition, a number of specimens from the Lower Permian (Artinskian or Kungurian-aged) Wellington Formation of Jefferson County, Oklahoma were sampled. These include the distal tips of two isolated neural spines (OMNH 73804 and OMNH 73809; Figure 21 A-C), a distal neural spine fragment with a lateral tubercle and the central cavity exposed (OMNH 73802; Figure 22), and a lateral tubercle (OMNH 73806). Additional specimens, including material referable to *E. boanerges* from the Geraldine Bonebed of Archer County, Texas (OMNH 1674), OMNH 73805 (Fig. 20A), and UCM 72431 were examined in order to observe superficial changes in muscle scar patterns from the proximal to distal portions of the spine in the genus. A complete list of the materials examined in

this study (including provenance data) is presented in Appendix B.

Histological Methods

Thin-sectioning equipment and other supplies included: cold mounting medium for embedding specimens; Ward petrographic slides; quick-setting epoxy resin for mounting specimens; low-speed Isomet precision saw with circular diamond blade; Buehler grinder/polisher with waterproof grinding paper (400, 600, and 800 grit); Nikon petrographic microscope with digital camera; Adobe PhotoShop, and NIH ImageJ image-analysis software for description of the specimens and for measurements of microanatomical structures.

The histological procedure employed here closely follows the protocols outlined by Chinsamy and Raath (1992) and Wilson (1994). It encompasses five major steps (modified from Chinsamy and Raath, 1992): (1) measurements and photography of specimens; (2) embedding of specimens; (3) sectioning embedded specimens; (4) mounting and polishing; and (5) photographing and analyzing thin-sections. Data such as approximate position of vertebra along the vertebral column and maximum height and width of

neural spine were recorded when available and qualitative features on the external surface of the bone (e.g., muscle scars and vascular striations) were photographed prior to sectioning. In some instances, it was necessary to cast specimens to retain their original dimensions, especially in the case of exceptionally rare specimens. Thus, resin casts were made for two dorsal vertebrae from a specimen of the enigmatic edaphosaurid *Lupeosaurus* (UCLA VP 1651). Subsequently, the specimens were cut into small blocks for embedding. For this study, several points of interest were chosen along the length of a given spine to ensure that the data obtained were not only useful, but also comparable across genera. Figure 16D illustrates the standardized sectioning that was performed, including a basal (proximal) section, a midpoint (distal) section (approximated for fragmented spines), and a tip section whenever tips were available. Additional thin-sections were produced across the changing point (Pivorunas, 1970; Bennett, 1996), defined here as a change in histological organization and/or cross-sectional shape from the base (epaxial-embedded) to the more distal (sail membrane-bearing) region of the spine, particularly in spines demonstrating pronounced "dimetrodont" differentiation (Romer and Price,

1940). Although edaphosaurids do not unequivocally demonstrate dimetrodont differentiation at the gross anatomical level (discussed in further detail below), the purported changing point has been identified at the level of the first tubercle pair in *Edaphosaurus* (Pivorunas, 1970). Sections were also cut through the lateral tubercles in the genera *Ianthasaurus* and *Edaphosaurus*.

Completed sections were examined using a Nikon Eclipse LV100 POL petrographic microscope with an integrated digital image capture system. Histomorphometric data were quantified using the image analysis software NIH ImageJ, published and distributed by the National Institutes of Health. Relevant calculations included: bone density, which is defined here as the proportion of mineralized bone matrix area (excluding vascular and medullary spaces) relative to the total cross-sectional area of the bone; cortical porosity, which is the ratio of vascular canal area within the cortex to the mineralized cortical bone area and is expressed as a percentage; relative bone wall thickness (or RBT), which is the ratio of the average cortical thickness to the average cross-sectional diameter and is also expressed as a percentage (Chinsamy, 1993); total cross-sectional area; minimum second moment of area

(I_{\min}) measured in mm^4 ; maximum second moment of area (I_{\max}) measured in mm^4 ; relative maximum to minimum bending rigidity (I_{\max}/I_{\min}); and torsional rigidity (J) which is the sum of I_{\min} and I_{\max} (Plochocki et al., 2007). A complete list of histomorphometric data is presented in Appendix D.

Results

Lupeosaurus -

General Description. The neural spines of *Lupeosaurus* are generally subcircular in cross-section with shallow anterior and posterior grooves running longitudinally along the length of the spine, which is approximately 10-12 times the height of the centrum in mid-dorsal vertebrae. Lateral tubercles are absent from the neural spines of this genus. The spine bears a gradual antero-posterior constriction 45-55 millimeters above the anterior zygapophyses where the spine's cross-sectional shape transitions from slightly compressed or subquadrangular to subcircular distally. Although a true "changing point" as defined for sphenacodontids is not always obvious at the gross anatomical level in edaphosaurids, microanatomical changes in the patterns of muscle scars and Sharpey's fibers mark the transition between the proximal and distal portions of

the spine. The height of this transition appears to have been consistent across the entire dorsal series, even in posterior dorsal vertebrae having much shorter neural spines. A slightly bulbous expansion midway up one of the neural spines sectioned here has been interpreted as a healing callus (Sumida, 1989) and is described only briefly below. Healed fractures in hyperelongate neural spines are often interpreted as evidence for the presence of a sail membrane (Romer, 1927; Romer and Price, 1940; Enlow, 1969; Rega et al., 2002).

Proximal Region. The base of the neural spine is subtriangular just above the zygapophyses, but becomes somewhat quadrangular just distal to this region and proximal to the changing point. The anterior and posterior margins of the proximal spine bear paired ridges as in the neural spines of the sphenacodontid *Dimetrodon* (and described below in *Edaphosaurus*), likely representing the attachment sites of the interspinal musculature (Olson, 1936). Transverse sections reveal abundant cancellous bone within the "medullary" region and a relatively thin cortex composed of a lamellar bone matrix with clear growth zones and annuli and dense Sharpey's fibers, particularly in the vicinity of the anterior and posterior ridges. Laterally,

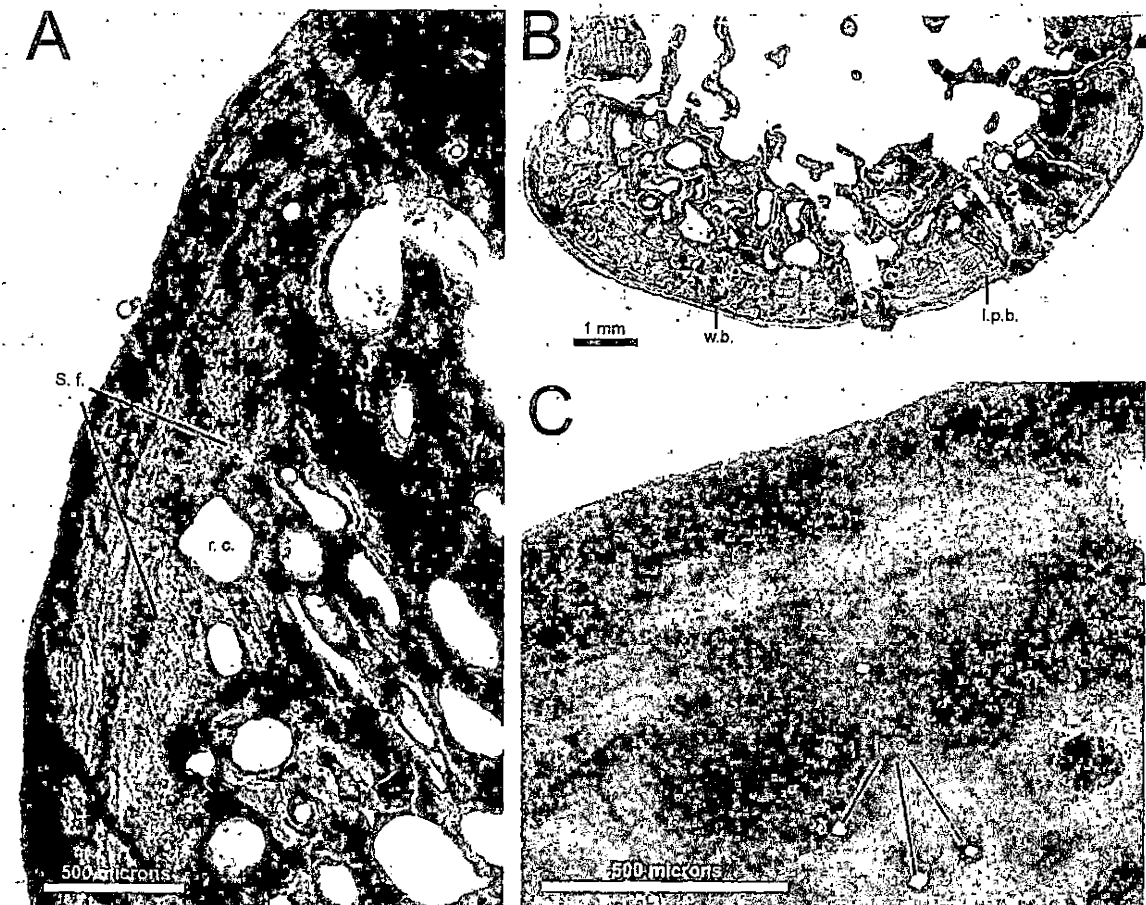


Figure 17. Transverse sections through mid-dorsal neural spine of *Lupeosaurus* cf. *L. kayi* (UCLA VP 1651) viewed with polarized light. A), Proximal section showing lamellar cortical bone, low vascularization of outer cortex and oblique orientation of Sharpey's fibers and resorption cavities (indicating the direction of the muscular insertion of the interspinalis and interarcuate muscles); B), Distal section showing thin bone wall with some secondary bone deposition and sparse trabecular structures within the cavernous medullary region (arrow denotes anterior); C), Distal section showing relatively dense cortex with a few primary osteons (p.o.), lamellar primary bone, and radially oriented Sharpey's fibers faintly present in the outer cortex.

the obliquely oriented Sharpey's fibers and enlarged resorption cavities (demonstrating secondary reconstruction of primary osteons) preserve the direction of the attachment of the interspinal and interarcuate muscles (Figure 17A).

Distal Region. Several fragmentary distal neural spines (subcircular in-cross section) were associated with the pectoral girdle of UCLA VP 1651 (Sumida, 1989), and revealed the possible presence of a central cavity in cross-section (Huttenlocker et al., 2007). Further sectioning showed that the medullary region of the distal neural spine is relatively cavernous (Figure 17B) compared to the dense proximal region, which was largely occupied by cancellous bone. In transverse section, the distal bone density is 0.52 versus 0.69 proximally (Appendix D).

The cortex is still relatively thin (10.7% RBT), but not as thin as that of the proximal region (6.8% RBT). It is composed largely of a lamellar bone matrix with faint Sharpey's fibers along the periphery and distinct lamellae forming growth zones and annuli (Figure 17B, C). The annuli are numerous and very closely spaced in the outer cortex, which is relatively avascular (Figure 17C), indicating that this was most likely a mature animal at

death. Earlier growth zones were better vascularized with numerous primary osteons, some of which have undergone secondary reconstruction, particularly near the endosteal margin. In general, the cortex is better vascularized than other edaphosaurids, having a cortical porosity of 5.0%. Endosteally, the primary bone of the cortex was reconstructed into an elaborate trabecular network, gradually transitioning into the cavernous medullary region which forms an incipient "central cavity" (discussed below). A section just below the healing callus in the mid-dorsal vertebra of UCLA VP 1651 preserves the deposition of secondary bone posterolaterally throughout the cortex (Figure 17B). This region is highly vascularized, forming a reticular vascular network, and was produced by rapidly deposited woven bone. Three or four more growth zones and annuli were deposited beyond this region, composing the outermost layers of the cortex and indicating that the individual lived for at least three more seasons post-injury. Similar healed fractures have been described histologically and figured in the sphenacodontid *Dimetrodon* (Enlow and Brown, 1957; Enlow, 1969; Rega et al., 2005).

Ianthasaurus -

General Description. The neural spines of the diminutive Pennsylvanian genus *Ianthasaurus* are more similar to those of *Edaphosaurus* than to those of *Lupeosaurus* due to the presence of paired lateral tubercles (Figure 18A, B). Like *Lupeosaurus* and *Edaphosaurus* (described below), the distal region of the neural spine is subcircular in cross-section, but does not always bear shallow anterior and posterior longitudinal grooves. The neural spines of the mid-dorsal vertebrae are typically 12 to 15 times the height of the centrum. A slight anteroposterior constriction is present at the level of the changing point (approximately ten to twelve millimeters above the zygapophyses) where the cross-sectional shape transitions from ovoid (proximally) to subcircular (distally). No obvious muscle scars could be distinguished on the proximal spine prior to sectioning.

Proximal Region. The base of the neural spine in *Ianthasaurus* is slightly compressed mediolaterally, or ovoid, in cross-section for approximately 10 millimeters before transitioning into a more subcircular cross-sectional shape distally. The histologic composition is

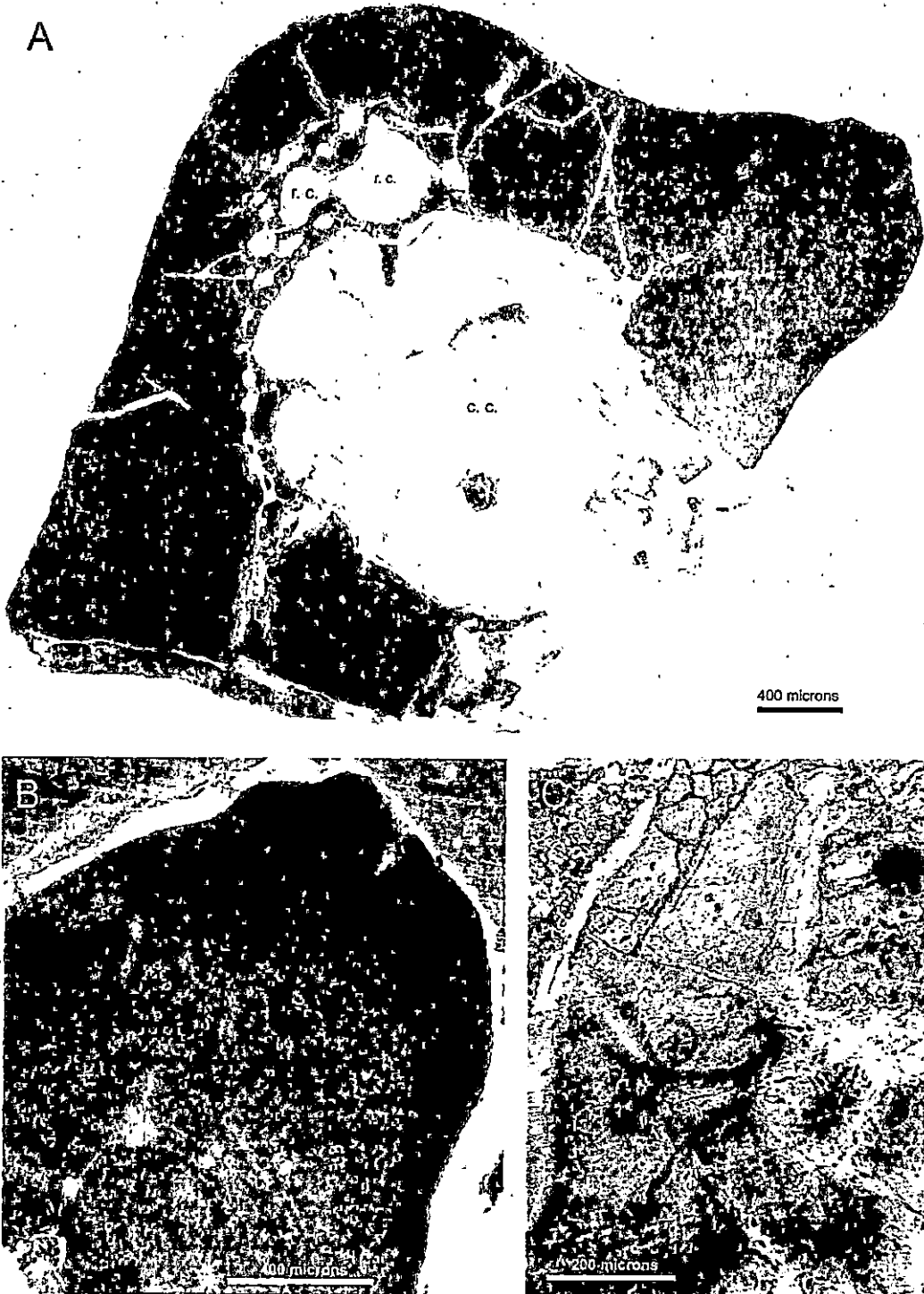


Figure 18. Sections through mid-dorsal (A, B) and posterior (C) neural spines of *Ianthasaurus hardestiorum* (University of Toronto; specimen number

to be determined) viewed with polarized light. A), Transverse distal section showing nearly avascular lamellar cortical bone, with large resorption cavities along the endosteal margin and a well-developed central cavity; B), Section through longitudinal axis of tubercle (from "A") showing low vascularization, lamellar bone, and incremental growth lines; C), Proximal section of posterior spine showing low vascularization, few distinct lamellae, and globular osteocyte lacunae near the endosteal margin.

unusual in transverse section, revealing slow-growing lamellar bone with a nearly avascular cortex (the precise cortical porosity could not be determined due to the poor state of preservation) and no distinguishable Sharpey's fibers, few distinct lamellae and no evidence of restlines (annuli or lines of arrested growth), and clusters of globular osteocyte lacunae near the endosteal margin. There is evidence of secondary reconstruction along the endosteal margin (Figure 18C) and a large central cavity is also present proximally. A well developed central cavity with a smoothly finished endosteal surface is absent from the base of the spine in *Lupeosaurus* and *Edaphosaurus*, but is present distally in the latter genus (Ricqlès, 1974a).

Distal Region. In transverse section, the distal region of a mid-dorsal neural spine (Figure 18A) displays few primary osteons in the outer cortex (cortical porosity

1.5%), is composed of lamellar bone, and, as is the case in the proximal region, shows no evidence of Sharpey's fibers. In general, the cross-sectional bone density is high (0.75) due to the thick, nearly avascular cortex. The bone wall is greatly thickened (18% RBT) relative to the neural spines of some synapsids, including *Lupeosaurus*. A thick bone wall also exists in distal spines of the sphenacodontid *Dimetrodon* (~15% RBT) and the edaphosaurid *Edaphosaurus* (~15-25%). The lamellae of the cortex are well preserved in contrast to the proximal region of the spine, particularly in the vicinity of the lateral tubercles (discussed below). Marked endosteal reconstruction occurred within the spine, producing resorption cavities within the inner cortex and a large central cavity (or "central canal" of Ricqlès, 1974a). The central cavity has been described in distal spine sections of *Edaphosaurus* (Ricqlès, 1974a), but has not been recognized in any other edaphosaurid taxon until now. The histological profile described here for *Ianthasaurus* is remarkably similar to that of *Edaphosaurus* (described below), with a thickened, nearly avascular outer cortex, endosteal reconstruction, and a well developed central cavity within the medullary region.

Lateral Tubercles. The tubercles or "cross bars" in *Ianthasaurus* are confined to the distal region of the neural spine, beginning just above the level of the antero-posterior constriction (changing point). They are always paired low in the spine, where they are most prominent, and are generally directed laterally and slightly dorsally (Reisz and Berman, 1986; Modesto and Reisz, 1990). Distally, the tubercles become more staggered in their spacing as they do in *Edaphosaurus*. There are typically no more than five pairs of tubercles arranged along the length of the spine in the known subadult specimens (Modesto and Reisz, 1990), but a recently discovered adult specimen (studied here) reveals eight pairs of tubercles along the mid-dorsal spine (Mazierski and Reisz, 2006). The most fully developed proximal tubercles often bear hyperostotic "webbing" on the ventral surface (Modesto and Reisz, 1990), a phenomenon that has not been described in the larger, geologically younger relative *Edaphosaurus*.

A transverse section through the neural spine of a mid-dorsal vertebra of the adult *Ianthasaurus* (Figure 18A) was taken at the level of the third tubercle pair, approximately 35 millimeters from the base of the spine (each tubercle pair being about 10 millimeters apart). The

section reveals very dense lamellar bone in the region of the tubercles with few primary osteons and numerous lamellae which were deposited regularly throughout the tubercles' growth (Figure 18B). The vascular composition and bone tissue-type, in conjunction with an absence of distinct growth zones or restlines, indicate that the tubercles did not grow suddenly or rapidly, but instead demonstrate a regular, incremental growth pattern over a prolonged period of time.

Edaphosaurus -

General Description. The following observations serve to supplement the published surveys of Enlow and Brown (1957), Enlow (1969), and Ricqlès (1974a) in the context of neural spine development and distal outgrowth, based on new data from systematically sectioned neural spine material.

The neural spines of the mid-dorsal vertebrae are typically 16 to 20 times the height of the centrum and bear paired, laterally projecting tubercles along the distal region of the spine. As in *Lupeosaurus* and *Ianthasaurus*, *Edaphosaurus* does not at first appear to display neural spines that are divided into clear proximal and distal portions. However, adult *Edaphosaurus* specimens examined

here demonstrate a changing point evidenced by muscle scars approximately 45 to 55 millimeters above the anterior zygapophyses (as in the similarly sized *Lupeosaurus*). Paired ridges with rough muscle scars are apparent anteriorly and posteriorly at the base of the spine (Figure 19A). These ridges continue distally across the changing point (just below the level of the most proximal tubercle pair) onto the distal region, bordering a shallow anterior and posterior groove in some large specimens, but lacking any signs of muscle scars in this region. Although shallow longitudinal grooves may be present in such specimens, the distal portions of spines in *Edaphosaurus* are largely subcircular in transverse section and do not display a double-cylinder morphology as pronounced as that which is found in most species of the sphenacodontid *Dimetrodon* (Rega et al., 2005; Sumida et al., 2005).

Proximal Region. Basal sections of *Edaphosaurus* neural spines are generally subtriangular to ovoid in cross-section, with the anterior margin of the spine generally being narrower than the posterior margin. The proximal region of the spine bears paired ridges anteriorly and posteriorly as described above in the genus *Lupeosaurus*. In addition, the base of the spine often

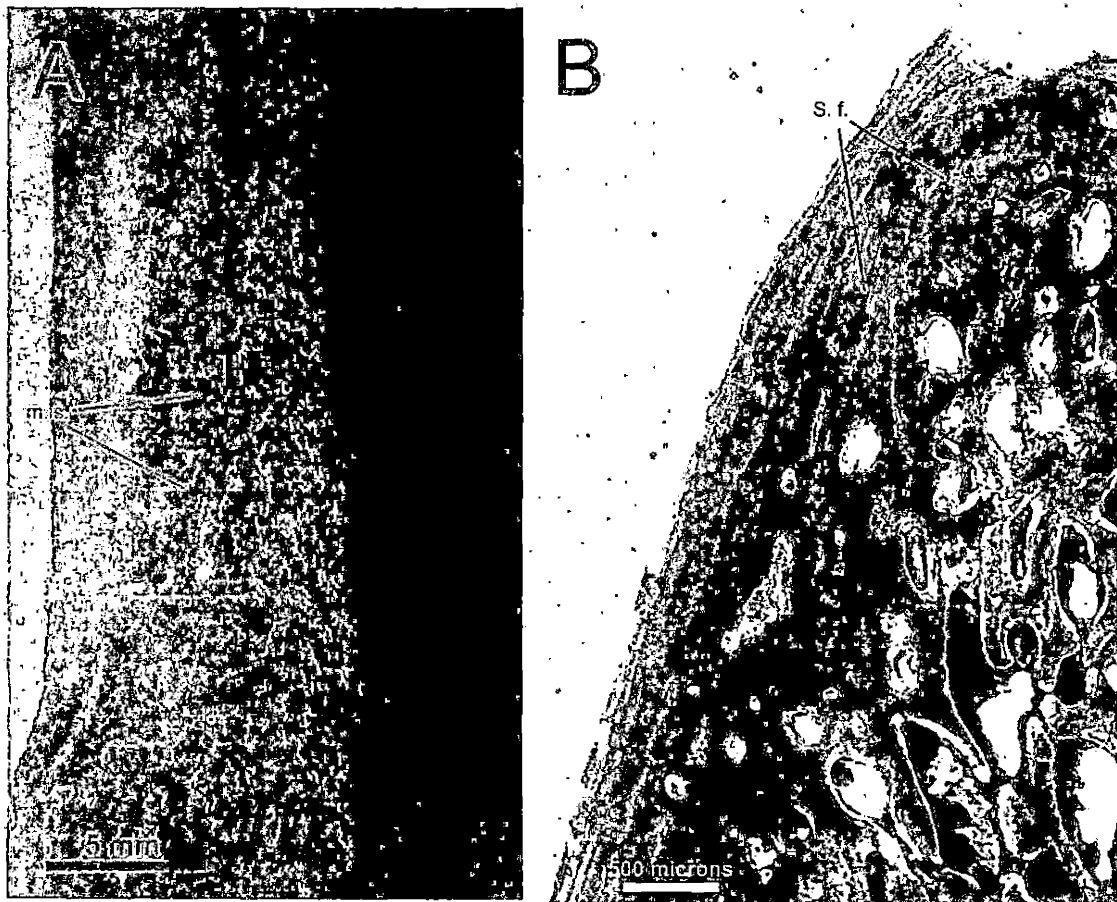


Figure 19. Proximal region of the neural spine of *Edaphosaurus* spp. A), Posterior view of the base of a mid-dorsal neural spine (OMNH 73805) showing muscle scars along the paired longitudinal ridges; B), Transverse section through the base of a mid-dorsal neural spine (OMNH 73800) - viewed with polarized light, showing lamellar cortical bone and oblique orientation of Sharpey's fibers and resorption cavities (recall the condition in *Lufesaurus*, Figure 17A).

preserves muscle scars on the anterior and posterior ridges as demonstrated by OMNH 73805 (Figure 19A) and UCM 72431. Transverse sections through the proximal region of the spine are nearly identical to those in *Lupeosaurus*, showing cancellous bone within the "medullary" region and a thin cortex, composed of lamellar bone, with abundant Sharpey's fibers (Figure 19B). The fibers and resorption cavities within the cortex and "medullary region" are arranged obliquely, thus preserving the direction of the attachment of the epaxial musculature, identical to the condition observed in *Lupeosaurus* (Figure 17A).

Distal Region. Distally, the cortical bone wall is formed by lamellar bone with visible growth zones and annuli (but no distinct lines of arrested growth), and abundant, deeply penetrating Sharpey's fibers in the outer periphery of the cortex (Figure 20A) as first documented by Enlow and Brown (1957), suggesting a close association between the periosteal bone and its surrounding soft-tissue. The medullary region is occupied by a central cavity as in *Ianthasaurus* and is encircled by a system of trabecular structures and protohaversian canals (Figure 20B, C) arranged along the endosteal margin of the cortex. The cortex is somewhat thickened as in *Ianthasaurus* and the

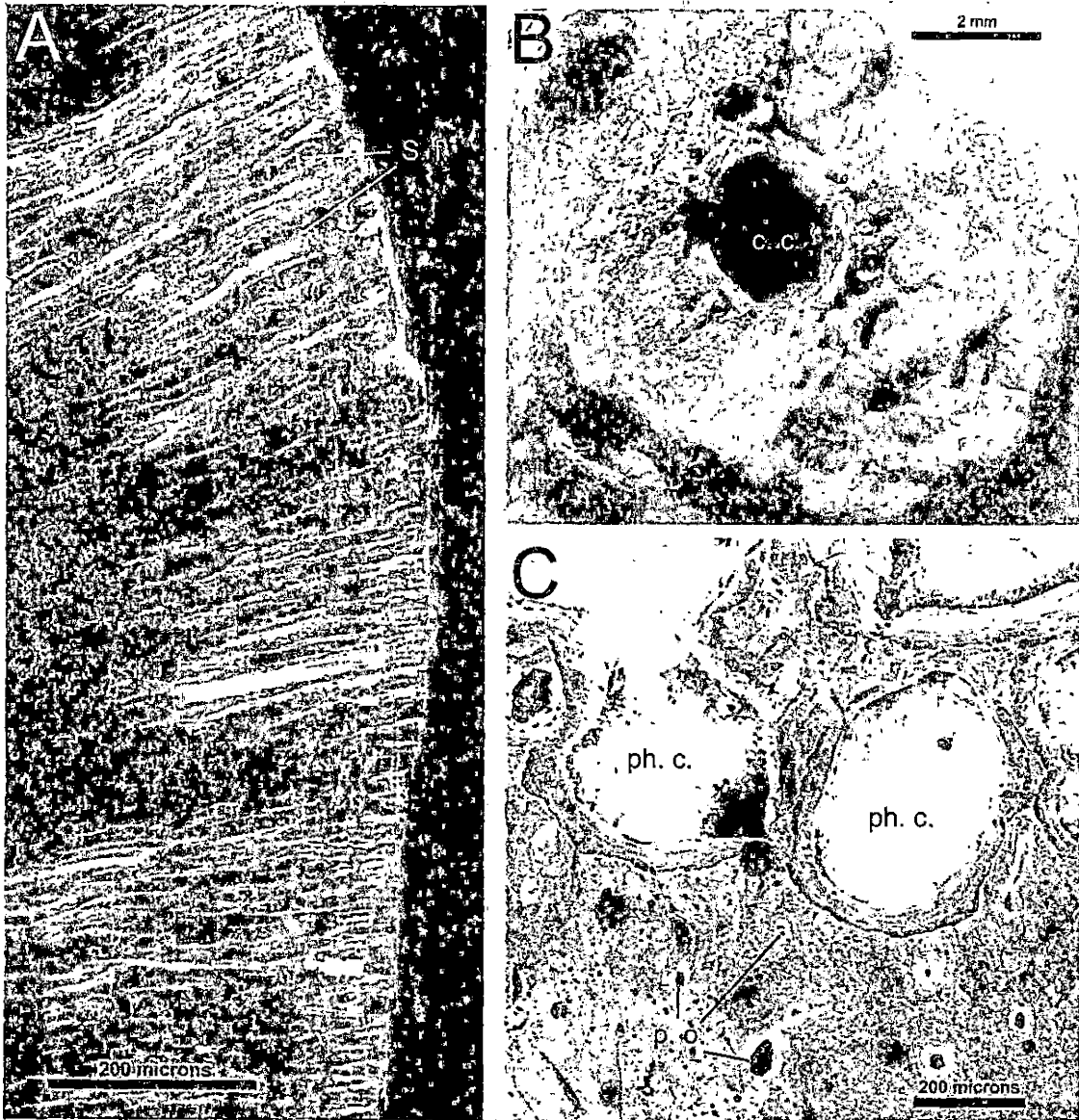


Figure 20. Distal region of the neural spine of *Edaphosaurus* spp. A), Outer cortex of the distal spine (OMNH 73809) in transverse section, viewed with polarized light, and showing abundant, deeply penetrating Sharpey's fibers (S.f.); B), Cross-section of an isolated spine fragment (OMNH 73803) showing the central cavity (c.c.); C), Transverse section through the distal spine (OMNH 73809) viewed with non-polarized light, showing large protohaversian systems (ph.c.) delineated by cement lines, forming along the endosteal margin.

sphenacodontid *Dimetrodon*. The specimens sectioned in the present study display RBTs of approximately 15%, although specimens studied previously by Ricqlès (1974a) have demonstrated RBTs as much as 25%. Overall, the cross-sectional bone density is moderately low (0.60) as in *Lupeosaurus* (0.52) due to the development of the central cavity and trabecular systems.

The central cavity and trabecular system were not fully developed in the distal most tips of the spine where appositional distal outgrowth took place. The system appears to have been produced as the resorption of old cortical bone occurred in concert with elongation of the spine, possibly as a function of minimum bone mass (MBM). This process is preserved in OMNH 73804 (Figure 21A).

The orientation of vascular canals is almost exclusively longitudinal and the peripheral margins of the cortex are largely avascular in distal sections of spines, with most of the primary osteons being located deep within the cortex and close to the endosteal margin. Ricqlès (1974a) interpreted this as evidence for decelerating growth of the neural spine during ontogeny, as vascular canals of the periosteum may become incorporated within the

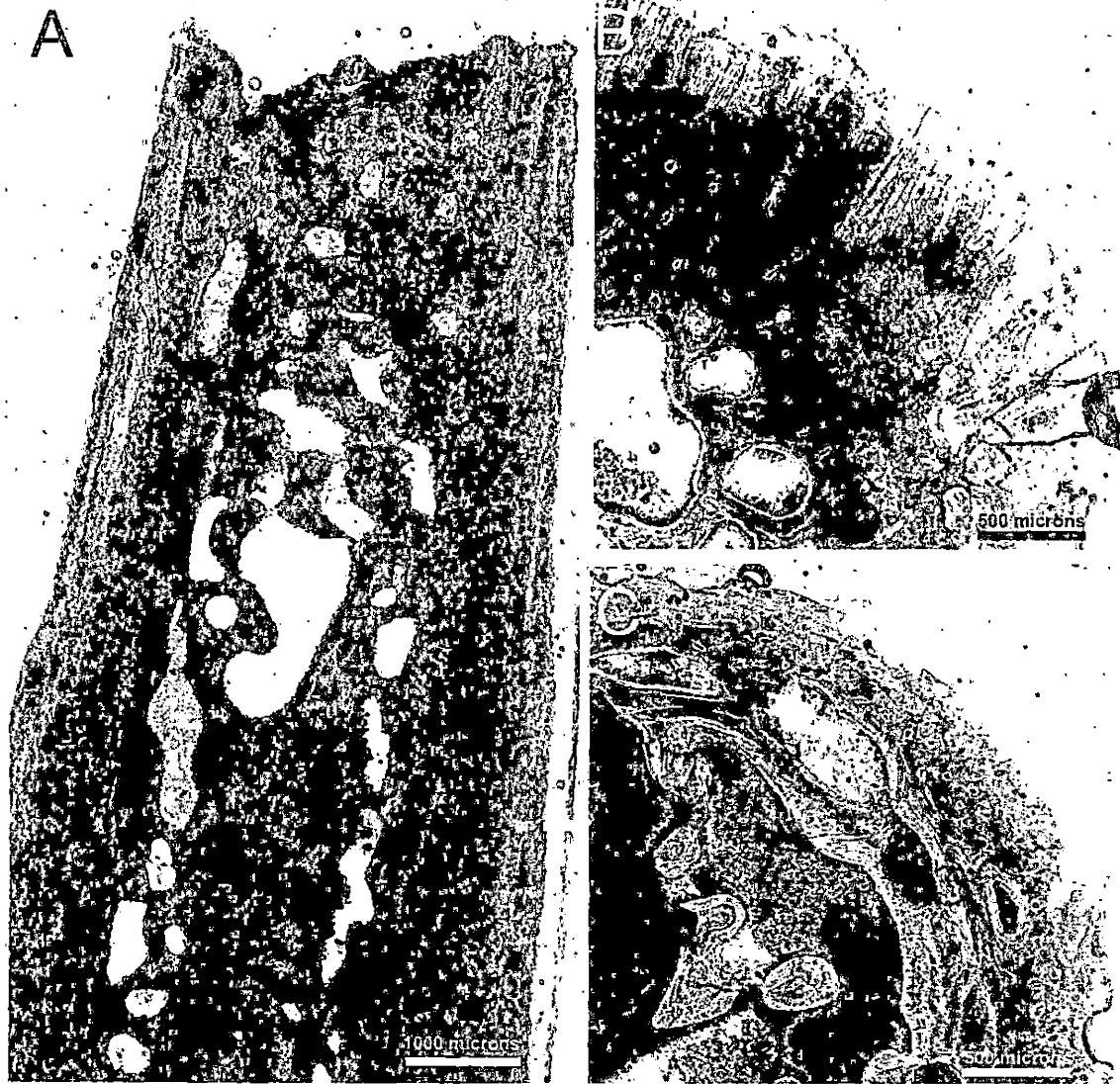


Figure 21. Tip of the neural spine of *Edaphosaurus* spp. A), Longitudinal section of spine tip (OMNH 73804) viewed in polarized light, preserving the process of the formation of the central cavity; B), Transverse section of spine tip (OMNH 73809) proximal to "C" viewed in non-polarized light, showing the typical organization of bone tissue in cross-section (i.e., dense, relatively avascular outer cortex surrounding the central cavity); C), Transverse section of spine tip (OMNH 73809) distal to "B" viewed in non-polarized light, showing a highly vascularized outer cortex with few distinct lamellae, indicating rapid distal outgrowth.

bone matrix as it is rapidly deposited early in development, but become less frequently incorporated as the rate of bone deposition decreases (Currey, 2002). A slightly different interpretation is offered here, and is supported by a series of detailed transverse sections through the spine's tip in OMNH 73809 (Figure 21B, C). The usual pattern of a dense, relatively avascular cortex with primary osteons arranged close to the endosteal margin (Figure 21B) only persists up to the spine's apex, where new periosteal bone was being rapidly deposited and incorporating the vascularization of the periosteum within the bone matrix (Figure 21C). Thus, the condition observed by Ricqlès (1974a) was not necessarily a consequence of negative allometric growth of the sail, but rather was predominantly a function of the distal elongation of the spine at its migrating apex, followed by circumferential appositional growth, increasing the diameter of the spine throughout ontogeny.

Lateral Tubercles. The lateral tubercles emanating from the neural spines of *Edaphosaurus* are generally small toward the tip of the spine, but often form large "cross-bars" closer to the base of the spine as in *Ianthasaurus* (Romer and Price, 1940; Ricqlès, 1974a; Modesto and Reisz,



Figure 22. Lateral tubercle of the neural spine of *Edaphosaurus* spp. (OMNH 73802). A), Neural spine fragment showing central cavity, trabecular bone along

the endosteal margin, and a lateral tubercle emanating from the outer cortex; B) Longitudinal section through a tubercle viewed with non-polarized light, showing a large primary osteon and several smaller canals, forming a reticular pattern of vascularization (r.b.) within a fibrolamellar bone matrix; C), Longitudinal section through a tubercle viewed with polarized light, revealing a series of growth zones over three seasons indicative of sudden and rapid growth of the tubercle.

1990). Ricqlès (1974a) suggested that transverse sections of tubercles are generally similar to those of the rest of the spine, but the central cavity is replaced by cancellous bone. However, the present analysis suggests that cancellous bone is only present in large tubercles and is not present during their early formation.

Contrary to Ricqlès (1974a), the lateral tubercles of *Edaphosaurus* did not grow similarly to the apex of the spine. This process is preserved in OMNH 73802 (Figure 22). The tubercles of OMNH 73802 are characterized by fibrolamellar bone with globular osteocyte lacunae (Figure 22B) and a reticular pattern of vascularization indicative of rapid bone deposition. Growth zones and annuli preserved in the specimen (Figure 22C) show that the tubercles may have grown at an average rate of one millimeter per year or more over two to three seasons, or greater than three

millimeters per year at their greatest period of growth. The pattern of growth zones suggests that the tubercles developed with sudden onset, where tubercles previously did not exist, followed by rapid outgrowth over few seasons. This process is in stark contrast to the incremental growth pattern of tubercles described above for *Ianthasaurus*.

Discussion

Systematic Implications and the Affinities of *Lupeosaurus*

In general, the osteohistologic composition of edaphosaurid neural spines is typified by lamellar-zonal primary bone within the cortex (although fibrolamellar bone is present in the lateral tubercles of *Edaphosaurus*), a cavernous medullary region with little cancellous bone, a distal cross-sectional bone density ranging from approximately 0.50 to 0.75, low cortical porosity ranging from 1.0% to 5.0%, and a relative bone wall thickness ranging from 10% to 25%. This characterization may prove useful in future systematic studies involving basal synapsids with hyperelongate neural spines (Huttenlocker et al., 2007).

For example, the enigmatic *Lupeosaurus kayi* was described by Romer (1937) who erected the monotypic family "Lupeosauridae" exclusively for this taxon. Nevertheless, Romer and Price (1940) suggested close affinities between *Edaphosaurus* and *Lupeosaurus*, an opinion that eventually became adopted by other authors. In an unpublished dissertation, Warren (1963) supported this view upon observing comparable ridge-like undulations of annuli on the zygapophyses of *Edaphosaurus* and *Lupeosaurus*. Reisz (1986) noted further similarities between known edaphosaurids and *Lupeosaurus*, and argued that a separate familial status for *Lupeosaurus* was not necessary. However, he declined to assign it to Edaphosauridae, relegating the genus to Pelycosauria incertae sedis. According to Reisz (1986), *Lupeosaurus* differs from other edaphosaurids in the following features: (1) lack of ectepicondylar foramen on the humerus (unique to this taxon among edaphosaurids); (2) absence of lateral tubercles on neural spines (plesiomorphic or an evolutionary reversal, as tubercles are present in *Ianthasaurus* and *Edaphosaurus*); and (3) well-developed posterior process of the iliac blade is present (plesiomorphic, but also present in the later

Table 4. New list of synapomorphies supporting a taxonomic placement of *Lupeosaurus* within Edaphosauridae.

	<u>Lupeosaurus</u>	<u>Ianthasaurus</u>	<u>Edaphosaurus</u>
1. Ventral clavicular plate expanded	Y	?	Y
2. Elongate, subcircular presacral neural spines	Y	Y	Y
3. Posterior tilt of posterior dorsal neural spines	Y	Y	Y
4. Anterior tilt of anterior cervical/dorsal neural spines	?	Y	Y
5. Moderately well-developed anterior process of the iliac blade	Y	Y	Y
6. High placement of zygopophyses and transverse processes	Y	N	Y
7. Central cavity fully developed within neural spine	P	Y	Y
8. Lateral tubercles present on neural spine	N	Y	Y

"Y" = character unambiguously present; "N" = character absent; "P" = character partially developed (i.e., central cavity); "?" = character state unknown.

described *Ianthasaurus*). *Lupeosaurus* also displays keeled cervical and anterior dorsal vertebral centra (convergent in sphenacodontids) and lacks lateral excavations in neural arches which are present in derived edaphosaurids and sphenacodontians, as well as some varanopids. Sumida (1989) tentatively referred *Lupeosaurus* to Edaphosauridae

based on the combination of (1) a greatly expanded ventral clavicular plate and (2) elongate, subcircular presacral spines. This assignment has been accepted in subsequent studies of edaphosaurid anatomy and relationships (Modesto and Reisz, 1990). Given the similarities noted by these authors and a histological profile that is distinctly consistent with edaphosaurids as described above (especially the presence of an incipient central cavity within the neural spine), the present analysis further supports a placement of *Lupeosaurus* within the Edaphosauridae. A complete list of characters supporting this hypothesis is offered in Table 4.

Growth, Mechanics, and Functional Interpretations

Thermoregulatory Requirements and the Problem of *Lupeosaurus*. As stated above, Ricqlès (1974a) argued that the better vascularized cortex of *Dimetrodon* neural spines might have facilitated heat exchange more efficiently than that in *Edaphosaurus*. Thus, he suggested that peripheral vessels (not preserved) and tubercles were necessary to maximize the efficiency of heat exchange in *Edaphosaurus*. In establishing this hypothesis, he drew upon the assumption that the tubercles provided a necessary

connection between a large artery occupying the central cavity and the external surface of the sail.

Based on higher resolution thin-sectioning in the present study, two new conclusions can be drawn regarding this hypothesized vascular configuration: (1) the central cavity originated within the distal portion of the neural spine as a result of appositional distal outgrowth and endosteal resorption and reconstruction (discussed below) and (2) the existence of transverse vascular canals connecting the central cavity to the lateral tubercles (e.g., Volkmann's canals) cannot be independently confirmed. Any vascularization within the tubercles is more likely to represent an artifact of their development. For instance, the lateral tubercles of *Ianthasaurus* appear to demonstrate relatively slow, incremental growth and are nearly avascular when viewed in cross-section (Figure 18B). By contrast, the tubercles of *Edaphosaurus* developed suddenly over few seasons, and may show a reticular pattern of vascularization indicative of their rapid growth (Figure 22B). This vascularization is most pronounced distally in the tubercle, within growth zones that developed when the tubercle experienced its most rapid period of deposition. As noted by Ricqlès, large tubercles may exhibit cancellous

bone and a large vascular canal may even be present intruding upon the trabeculae of the internal spine (Figure 22B), but, notably, these systems never communicate directly with the central cavity itself, contrary to Ricqlès' earlier suggestions.

To complicate matters even further, the thermoregulatory requirements for edaphosaurids as hypothesized by Ricqlès are not realized at all in the genus *Lupeosaurus*, which displays an incipient central cavity and a relatively avascular cortex, yet completely lacks lateral tubercles. In fact, the cortical porosity of the distal spine of *Lupeosaurus* is intermediate to other edaphosaurids and sphenacodontids, being approximately 5.0%, compared to 1.0-2.0% in *Edaphosaurus* and 13.5% in *Dimetrodon*. Some have argued that the neural spines in at least some species of *Dimetrodon* may not have been vascularized well enough to facilitate efficient heat transfer to the viscera (Rega et al., 2005). The neural spines of *Lupeosaurus* are even less vascularized, with a cortical porosity of 5.0% which falls within the average range of porosities in nonmammalian synapsid long bones (Ray et al., 2004 and unpublished data), and no transversely oriented canals have been identified

connecting the medullary region (which is also relatively cavernous, as in *Ianthasaurus* and *Edaphosaurus*) to the periosteal surface of the spine. Thus, as in other edaphosaurids, it is likely that the cavernous medullary region of the distal spine in *Lupeosaurus* is intrinsic to the very structure and development of the spine and its existence need not be explained by the presence of a single large, longitudinally oriented vascular channel.

Further Observations of the Central Cavity. The system of vascular supply and drainage as hypothesized by Ricqlès (1974a) required an internal artery supplying blood to the sail via a system of lateral tubercles and draining the sail via two veins per neural spine, each situated within the anterior and posterior groove. Thus, this system would have involved three large blood vessels per presacral vertebra with approximately 75 vertically-oriented, femoral artery-sized blood vessels vascularizing the dorsal sail. This would have made the dorsal sail particularly vulnerable to injury, remarkably expensive to produce, and would have generated enormous resistance to vascular flow.

An alternative hypothesis offered here is that the central cavity is integral to the developmental and

structural requirements of the distal neural spine, as it appears to have originated within the spine itself, with little evidence of transverse blood vessels connecting the cavity to the sail surface or exiting proximally from the neural arch. The central cavity and the trabecular systems surrounding the cavity are not fully developed in the distal tip of the spine where appositional distal outgrowth took place. Instead, one can observe the process of resorption and reconstruction of pre-existing cortical bone along the endosteal surface (Figure 21A) which appears to have occurred during distal elongation of the spine in life. The reduction of bone mass from the medullary region of the spine during elongation, coupled with a thickened cortical bone wall indicates that buckling or minimum bone mass (MBM) may have been factors governing the shape and remodeling of the spine (Currey, 2002). Thus, the shape and cross-sectional structure of the bone may provide clues to the stresses it experienced in life. For example, short spines in basal synapsids may be mediolaterally compressed because they did not experience excessive lateral bending, whereas long, cylindrical spines would have been subjected to bending forces in all directions, as in long bones. Furthermore, cross-sectional bone mass may have been

minimized in edaphosaurids relative to sphenacodontids if the spines were subjected to less extreme bending stresses during locomotion than those of sphenacodontids. Another hypothesis, although less likely, is that the central cavity provided an abundant store of marrow, as marrow is heavily concentrated in the axial skeleton of mammals, particularly in the calvariae of the skull and vertebrae (Ascenzi, 1976; Currey, 2002). The structure may represent a primitive marrow cavity, the earliest identified in the synapsid lineage.

Conclusions

Family-level distinctions are apparent in the osteohistologic structures of edaphosaurid neural spines when compared to those of sphenacodontids (see Chapter Two). Edaphosaurid neural spines are characterized by lamellar-zonal primary bone within the cortex, a cavernous medullary region with little cancellous bone, a distal cross-sectional bone density ranging from approximately 0.50 to 0.75, low cortical porosity ranging from 1.0% to 5.0%, and a relative bone wall thickness ranging from 10% to 25%. Genus-level distinctions are also evident; with *Lupeosaurus* having a slightly higher cortical porosity

compared to other edaphosaurids and sparse trabecular structures within the medullary region. *Ianthasaurus* and *Edaphosaurus* are more similar in their osteohistological profile, but the cortex of *Ianthasaurus* is nearly avascular and the lateral tubercles display evidence of slow, incremental growth (in contrast to the apparently rapid development of tubercles in *Edaphosaurus* which may display fibrolamellar and reticular bone). Species-level distinctions have yet to be explored.

Muscle scars and Sharpey's fibers associated with the paired anterior and posterior ridges at the base of the spine (likely homologous to the "horns" of *Dimetrodon*; Enlow 1969) provide evidence for the attachment of the interspinal musculature in *Lupeosaurus* and *Edaphosaurus*. It has been speculated that the space between these ridges was occupied by a large blood vessel. Although this cannot be confirmed, the observations reported here need not invoke vascular correlates to produce the anterior and posterior grooves bounded by these paired ridges. These features are interpreted as mechanical and structural in their genesis. Although a shallow groove continues dorsally without prominent ridges, it may have continued to serve a mechanical function in the distal spine as

hypothesized for the double-cylinder spines in some species of *Dimetrodon* by Rega et al. (2005) and Sumida et al. (2005). Aside from the A-P grooves, the distal spine largely retains a subcircular cross-sectional geometry, forming a hollow cylinder.

The assumptions of the thermoregulatory hypothesis as outlined by Ricqlès (1974a) are not supported by the osteohistologic profiles of any of the edaphosaurid taxa examined here. Evidence for a vascular system connecting the tubercles to an artery within the central cavity is completely absent in *Ianthasaurus* (whose tubercles are nearly avascular) and ambiguous in *Edaphosaurus*. Alternatively, the vascular organization of the tubercles is better explained by the tubercle's style of growth (i.e., slow versus rapid deposition). *Lupeosaurus* also displays an incipient cavity within the medullary region (with a few trabeculae) and modest vascularization of the outer cortex, but lacks tubercles altogether. A role in thermoregulation might have been made possible if the soft-tissue surroundings of the dorsal sail were well-vascularized, but this is speculative, cannot be tested directly, and does not explain the apparent negative allometry of the sail observed in presumed phyletic series

of *Edaphosaurus* (Romer and Price, 1940). The diverse distributions of lateral tubercles across the dorsal sail in different edaphosaurid genera and differences in the style and timing of their growth may support hypotheses of species recognition or possibly intraspecific display (Modesto and Reisz, 1990).

It is hypothesized here that the central cavity does not record the presence of a single large artery within the spine, but was produced during elongation of the spine with the likely purpose of minimizing unnecessary cross-sectional bone mass. Different bone tissue-types and vascularization imply relatively low rates of distal outgrowth in edaphosaurid spines compared to those of *Dimetrodon*. Differences in the rate of neural spine elongation, sail allometry, and cross-sectional bone density between edaphosaurids and derived sphenacodontids like *Dimetrodon* may imply different mechanical demands imposed on the sail during locomotion and related physical activities.

Due to diverse microanatomical and histomorphometric properties across genera, histological sectioning of isolated spines will facilitate more precise identifications of faunal constituents in continental

Permo-Carboniferous microvertebrate assemblages and may refine regional biostratigraphic correlations. This may be useful when only isolated neural spine material is available, which is often the case for Lower Permian microvertebrate localities across the Texas-Oklahoma region.

CHAPTER FOUR
PHYLOGENETIC SIGNAL AND PHYLOGENETICALLY-
INDEPENDENT CORRELATES: THE MECHANICAL
EVOLUTION OF HYPERELONGATE
NEURAL SPINES

Introduction

In the present study, microstructural characteristics of hyperelongate neural spines have been surveyed and described in a number of eupelycosaurian genera, expanding present knowledge of the spine's microanatomy beyond that of *Dimetrodon* and *Edaphosaurus*. The newly described material exposes both family-level similarities and subtle differences in spine architecture at both family and genus levels (Figure 23). The major observations from Chapters Two and Three are summarized in Table 5.

The data presented here allow qualitative comparisons of bone microstructure between the eupelycosaurian families Edaphosauridae and Sphenacodontidae and have helped to confirm that family and genus-level distinctions exist in the histological profiles of the neural spines. However, a truly

Table 5. Characteristics of the histological profiles of sphenacodontid and edaphosaurid neural spines.

<u>Character</u>	<u>Sphenacodontidae</u>	<u>Edaphosauridae</u>
predominant bone tissue-type	fibrolamellar (lamellar in A-P groove of <i>Dimetrodon</i>)	lamellar-zonal (fibrolamellar in tubercles of <i>Edaphosaurus</i>)
'medullary' region	occupied by dense fine-cancellous bone	cavernous with little cancellous bone or trabecular structures
bone density	~0.75	~0.50-0.75
cortical porosity	5%-15%	1%-5%
relative bone wall thickness (RBT)	5%-15% (distal) (~15% <i>Dimetrodon</i>)	10%-25% (distal) (~15-25% <i>Edaphosaurus</i>)
resistance to torsion	greatest in distal portion of neural spine	lower in distal portion of neural spine

comparative approach requires an evolutionary context to examine potential phylogenetic signal in quantitative microstructural data (Blomberg et al., 2003; Cubo et al., 2005, 2008) and to assess the order and timing of the appearances of such properties in extinct clades.

Previous studies on the comparative osteohistology of amniote bone, which have not incorporated phylogenetic data, have suggested evolutionary patterns in the distribution of bone tissue-type and growth dynamics (Amprino, 1947; Ricqlès, 1974a, b) and degree of

mineralization (Currey, 1987, 2002). Currey (1987) noted apparent functional and physiological correlates of bone histology and suggested that the properties of modern endothermic vertebrate bone (i.e., mammals and birds) arose repeated times according to (1) the size and habitat of the organism and (2) the functions of the bones within the organism (e.g., slender bones tend to be stiff and strong in bending, but not necessarily tough; see Vogel, 1988 and Currey, 2002, 2003 for discussions of stiffness versus toughness). Studies such as these have lacked a well-constrained phylogenetic framework but have exposed the highly integrated components influencing bone morphology, including historical (phylogenetic), functional (physiologic), and structural (growth and mechanical) components (Cubo et al., 2008).

A phylogenetic approach examines the distribution of organismal properties across a phylogenetic tree and assesses the extent to which the observed variation in traits (i.e., histological traits in the present study) can be explained by the phylogeny, other phylogenetically-independent correlates, or both. The tendency for closely related organisms to demonstrate

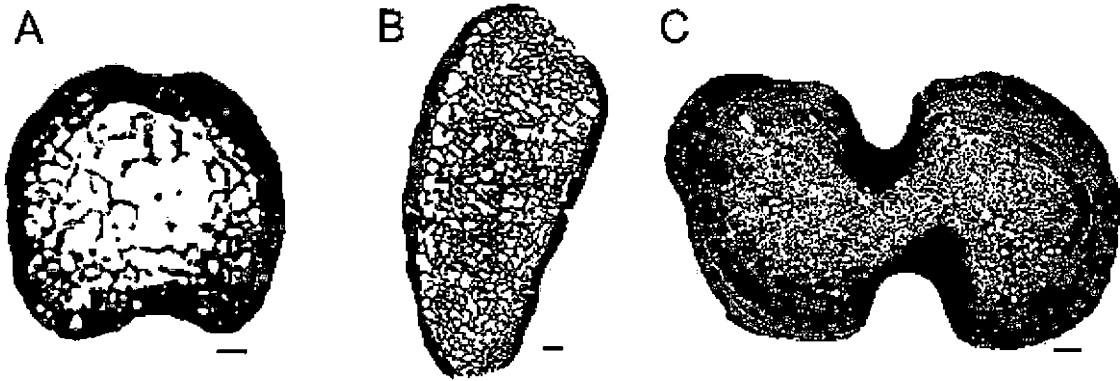


Figure 23. Comparison of cross-sectional bone mass distribution and vascularity of mid-dorsal hyperelongate neural spines in selected eupelycosaurs. A), distal spine of *Lupeosaurus kayi*; B), distal spine of *Sphenacodon ferox*; C) distal spine of *Dimetrodon giganhomogenes*. Anterior is toward top of page. Scale bars equal 1 millimeter.

quantitatively similar traits has been termed "phylogenetic signal" (Blomberg et al., 2003). The well-resolved phylogenetic relationships of pelycosaurian-grade synapsids (Reisz, 1986; Hopson, 1991; Laurin, 1993; Modesto, 1994; Laurin and Reisz, 1995) present the opportunity to study possible signal in histological properties of the neural spines, as well as other potential factors influencing the structural evolution of the dorsal sail in the eupelycosaurian families Edaphosauridae and Sphenacodontidae.

Statistical methods are employed here to assess the extent to which the histomorphometric data reported from Chapters Two and Three (Appendix D) provide reliable, predictive means for interpreting the taxonomic positions of enigmatic taxa (e.g., *Lupeosaurus*) and, thus, whether or not particular functional adaptations in the neural spines were unique to specific eupelycosaurian families. A consensus tree of eupelycosaur phylogeny is implemented and modified to accommodate previously unexamined taxa (i.e., *Lupeosaurus* and *Ctenorhachis*). The robustness of the phylogenetic hypothesis is examined, and mean pairwise dissimilarity and branch lengths (determined by Bayesian analysis of morphological data) are utilized for two separate statistical tests of phylogenetic "signal." Additionally, phylogenetically-independent contrasts are performed on the histomorphometric data to determine other possible biological correlates of bone microstructure (e.g., body mass). Therefore, an attempt is made to determine the extent to which the histological properties were influenced by historical, functional (e.g., bone mass-saving processes, MBM), and structural (e.g., modeling in response to bending stresses) constraints.

Methods

Analysis of the Reference Phylogeny

In order to study evolutionary trends in the structure of the dorsal sail, it was necessary to establish a reference phylogeny from which dissimilarity matrices could be constructed and phylogenetic signal examined (methods of phylogenetic signal discussed below), and upon which character acquisition may be mapped through time. The genera examined (listed below) and composing the clade of interest (i.e., Permo-Carboniferous pelycosaurian-grade synspsids) includes solely extinct forms. As such, sources of phylogenetically "informative" data are necessarily morphology-based. Selection of an appropriate source of phylogenetic information is potentially problematic, because published synspsid phylogenies include phylogenetically "informative" data that are not independent of the data being assessed in the present study (e.g., neural spine morphology). Thus, the robustness of the consensus tree from the literature was examined via the following methods:

First, a composite tree was constructed from several sources in the literature (Reisz, 1986; Hopson, 1991; Reisz et al., 1992; Laurin, 1993; Modesto, 1994; Laurin and

Reisz, 1995) using the tree analysis software MacClade 4 (Maddison and Maddison, 2005). The interrelationships of 16 synapsid taxa were reconstructed, including Caseasauria and Varanopidae (employed as outgroups), the eupelycosaurian taxa Ophiacodontidae, *Lupeosaurus*, *Ianthasaurus*, *Glaucosaurus*, *Edaphosaurus*, *Haptodus*, *Ctenorhachis*, *Sphenacodon ferox*, *Sphenacodon ferocior*, *Ctenospondylus*, *Dimetrodon*, *Secodontosaurus*, and the therapsids *Biarmosuchus* and *Dinocephalia*. *Biarmosuchus* and *Dinocephalia* were selected as representatives of Therapsida following Laurin (1993). Intra-relationships of Edaphosauridae were largely based on Modesto (1994) with *Lupeosaurus* placed in a basal position within the family as suggested by Sumida (1989) and Chapter Three of the present study (Table 4). Intra-relationships of sphenacodontians were based on Reisz et al. (1992) and Laurin (1993) with *Ctenorhachis* placed in a basal position within the family Sphenacodontidae according to Hook and Hotton (1991). The manually constructed tree served as the *a priori* constraint hypothesis based on the consensus of the literature (Figure 1).

Second, in addition to constructing an *a priori* tree from the literature, phylogenetic data were adopted from

the sources above and compiled in Appendices E and F. The character matrix (Appendix F) was divided between non-neural spine (characters 1-124) and neural spine (characters 125-136) characters, four of which were newly coded in the present study (characters 133-136). Character states were coded for newly added taxa (i.e., *Lupeosaurus* and *Ctenorhachis*) and the dataset transferred to a Nexus file (Appendix L) to be analyzed on the cladistics software PAUP* 4.0b (Swofford, 1999). Two analyses were performed to determine whether the resulting tree topologies accurately reflected that of the *a priori* hypothesis from the literature: (1) parsimony analysis of the complete dataset from Appendix L, and (2) parsimony analysis of the same dataset (Appendix L) excluding all neural spine characters (125-136). Performing analyses with and without the neural spine data allowed for assessment of possible conflicting phylogenetic data (i.e., homoplasy) between the axial skeleton and other regions of the skeleton. Identifying any potential homoplasy is critical before implementing a particular candidate tree for analysis of phylogenetic signal of histological traits. The output files are provided in Appendices M and N, and the resulting trees are described and compared below (see Results).

After recovering the resulting trees from the parsimony analyses with and without neural spine data, a Kishino-Hasegawa test (Kishino and Hasegawa, 1989) was performed on PAUP* 4.0b. The Kishino-Hasegawa (K-H) test is a likelihood-based analytical method designed to assess variance between the optimal tree (most parsimonious tree or MPT) and other possible reconstructions from a given dataset, thus allowing statistical comparisons of the ability of disparate phylogenetic hypotheses to explain patterns within the sampled character data. As such, the K-H test can determine whether a suboptimal hypothesis is statistically different in its ability to explain the sampled data. Accordingly, the *a priori* tree reconstructed from the literature was utilized as a constraint tree and compared against trees generated from analysis of the complete dataset as well as those generated from the analysis excluding neural spine characters.

Finally, a separate analysis of the data in Appendix L was performed on the complete dataset (including neural spine characters) using the distance criterion in PAUP* 4.0b. The resulting topology of the distance tree was similar to the *a priori* tree topology. Mean pairwise dissimilarity was derived from the resulting distance

matrix and aligned with respective ingroup pairs in Appendix G for assessment of phylogenetic correlations of histomorphometric dissimilarities (Appendices H-K).

Following the methods of Blomberg et al. (2003), raw data from Appendix D were further required to examine phylogenetic signal using the PHYSIG.M software package for MATLAB (discussed in detail below). As such, raw branch lengths were also necessary for tip data and were thus determined by subjecting the phylogenetic dataset to Bayesian analysis using the software package MrBayes (Huelsenbeck and Ronquist, 2001; Ronquist and Huelsenbeck, 2003). The dataset was trimmed to four taxa (*Lupeosaurus*, *Edaphosaurus*, *Sphenacodon*, and *Dimetrodon*) for analysis of the proximal spine data (excluding *Ianthasaurus* due to poor preservation in this region) and five taxa for analysis of the distal spine data. The M_k model, standard for morphological data (Lewis, 2001; Müller and Reisz, 2006), was employed along with the gamma distribution parameter, allowing unequal rates of character change across characters. The consensus cladistic topology (i.e., the reference phylogeny) determined above was loaded as the constraint topology, so that the Bayesian analysis would only retain trees reflecting this topology. 5,000,000 mcmc

generations were ran (two parallel analyses with four chains each) and one tree was sampled every 100 generations, resulting in the retention of 50,000 trees. Trees recovered from the first 12,500 generations were discarded for burnin. The MrBayes input file (Nexus format) is available in Appendix O. The resulting output data with raw branch lengths from the Bayesian consensus (Appendix P, four taxa; Appendix Q, five taxa) was recruited for analysis in PHYSIG (discussed below).

Quantification of Histomorphometric Characters

Quantitative microstructural data were calculated in the procedures of Chapters Two and Three, using the image analysis software NIH ImageJ, and the resulting quantities were tabulated in Appendix D. The measurements included: bone density, i.e., the proportion of mineralized bone matrix area relative to the total cross-sectional area of the bone; cortical porosity, i.e., the ratio of vascular canal area within the cortex to the mineralized cortical bone area (expressed as a percentage); relative bone wall thickness (or RBT), i.e., the ratio of the average cortical thickness to the average cross-sectional diameter (expressed as a

percentage); total cross-sectional area in mm^2 ; minimum second moment of area (I_{\min}) measured in mm^4 ; maximum second moment of area (I_{\max}) measured in mm^4 ; relative maximum to minimum bending rigidity (I_{\max}/I_{\min}); and torsional rigidity (J), i.e., the sum of I_{\min} and I_{\max} .

Relevant histomorphometric characters that were subjected to analyses of phylogenetic signal and phylogenetically-independent contrasts included: bending rigidity, bone density, cortical porosity, and RBT. However, for tests of phylogenetic correlation based on linear regressions against mean pairwise dissimilarity, it was necessary to calculate dissimilarity in the histomorphometric values for each ingroup pair. The data in Appendices H-K were determined by aligning all relevant ingroup pairs (pairs with histomorphometric data available from Appendix D) and subsequently calculating histomorphometric dissimilarity between pairs by subtracting the values available in Appendix D for each pair. Thus, the histomorphometric dissimilarity is the difference in histomorphometric values for each ingroup pair, following the methods of Cubo et al. (2005). Separate calculations were performed for proximal and distal portions of the neural spines, due to

histovariability along the length of the spine. Linear regressions were possible for all taxa in which the distal portion of the neural spine was well-preserved and adequate data available (*Lupeosaurus*, *Ianthasaurus*, *Edaphosaurus*, *Sphenacodon*, and *Dimetrodon*). *Ianthasaurus* was omitted from comparisons of the proximal region of the spine due to poor preservation in this region (Chapter Three).

Phylogenetic Signal and Phylogenetically-Independent Contrasts

Numerous methods have been developed and are available in the published literature to assess "phylogenetic signal" (Blomberg et al., 2003). Two independent methods of analysis have been implemented here, including (1) assessment of phylogenetic correlations and phylogenetically-independent contrasts via linear regressions (Cubo et al., 2005, 2008) and (2) assessment of phylogenetic signal sensu Blomberg et al. (2003) using the PHYSIG.M software package for MATLAB.

(1) Linear Regressions. In the presence of phylogenetic signal, large values of mean pairwise dissimilarity (Appendix G) for a given ingroup pair should be expected to correlate with large differences in

histomorphometric traits (Appendices H-K). Phylogenetic correlations based on the mean pairwise dissimilarity and phylogenetically-independent contrasts were each analyzed as a series of linear regressions performed on SigmaPlot 9.0 (Systat Software Inc., 2004). Mean pairwise dissimilarity of ingroup pairs was regressed against bending rigidity dissimilarity (Appendix H), bone density dissimilarity (Appendix I), cortical porosity dissimilarity (Appendix J), and RBT dissimilarity (Appendix K). Several statistical parameters were examined on SigmaPlot 9.0 in order to test for phylogenetic correlations, including the correlation coefficient (r), R-squared, and p-values to assess statistical significance of the correlation (Table 6). Additionally, raw histomorphometric properties from Appendix D were regressed against other biologically significant variables to test for phylogenetically-independent correlates of observed bone microstructural properties. Phylogenetically-independent variables adopted from Appendices C and D included: body mass, cross-sectional bone mass (sensu Cubo et al., 2005), and relative neural spine height based on the neural spine-to-centrum height ratio. The statistical results of the phylogenetic correlations and phylogenetically-independent contrasts are

provided in Tables 6 and 7. Calculated p-values below 0.05 were considered significant ($\alpha = 0.05$).

(2) PHYSIG. The statistical approaches above employed correlation in order to describe what proportion of the observed distribution of histomorphometric data is explainable by historical versus non-historical components. However, these approaches are largely parameter estimation methods and do not explore alternative hypotheses, nor do they implement randomization of data to test whether the reference phylogeny explains the observed distribution of histomorphometric data better than randomly permuted data. Recent statistical approaches developed by Blomberg et al. (2003) measure whether the observed variance of the character in question is greater than expected from a "Brownian motion" model of evolution (i.e., stochastic evolution along a hierarchical tree). The authors derived a statistic, the K-statistic, which indicates the strength of phylogenetic signal by comparing the observed variance against an analytical expectation based on tree structure (including branch lengths) and assuming Brownian motion character evolution. K values of greater than 1.0 indicate greater levels of phylogenetic signal in a trait than expected from Brownian motion character evolution. A

computer-based randomization procedure for determining K was developed by the authors, the PHYSIG.M package for MATLAB (www.biology.ucr.edu/faculty/Garland/PHYSIG.html), and is employed here.

Phylogenetic signal sensu Blomberg et al. (2003) was assessed along the reference tree with branch lengths generated in MrBayes (Huelsenbeck and Ronquist, 2001; Ronquist and Huelsenbeck, 2003) and analyzed using the PHYSIG software package. Bayesian analysis (Appendix O) was performed to retrieve branch lengths for analyses of the proximal spine data (four taxa available; Appendix P) and distal spine data (five taxa; Appendix Q). Branch lengths and raw data for bending rigidity, bone density, cortical porosity, and RBT were aligned in text files and were analyzed by PHYSIG with 10,000 random permutations of the data. The calculated K and p-values ($\alpha = 0.05$) are reported in Table 6.

Results

Phylogenetic Results and the Interrelationships of Edaphosauridae and Sphenacodontidae

Parsimony analysis of the data in Appendix L allowed comparisons of resulting tree topologies analyzed with

(Appendix M) and without (Appendix N) neural spine data. Analysis of the complete data recovered two MPTs (tree length = 209; consistency index = 0.7799; retention index = 0.8824; rescaled consistency index = 0.6882) which differed only in their reconstructions of the genus *Sphenacodon* as monophyletic versus paraphyletic. The 50% majority-rule consensus, which closely resembles the *a priori* consensus tree (but additionally suggesting the possible paraphyly of *Sphenacodon*) is depicted in Figures 24B and 25.

A separate analysis excluding neural spine data (Appendices E and F, characters 125-136) recovered five MPTs (tree length = 189; consistency index = 0.7884; retention index = 0.8883; rescaled consistency index = 0.7003) differing only in their reconstructions of the intra-relationships within Edaphosauridae (Appendix N). The higher-level relationships of eupelycosaurs reflect those of the *a priori* constraint topology from the literature, but the exclusion of neural spine data results in less resolution between MPTs within Edaphosauridae. Furthermore, the dietary specializations in the skull of the sphenacodontid *Secodontosaurus* necessitated possible reversals to the plesiomorphic eupelycosaur condition (Reisz et al., 1992; e.g., lengthening of the snout,

increased tooth count in marginal dentition). Thus, the absence of neural spine data allows *Secodontosaurus* to fall out in a relatively basal position among sphenacodontids, followed successively by *Dimetrodon* and a monophyletic clade of *Sphenacodon* plus *Ctenospondylus* (Appendix N). The enigmatic *Ctenorhachis*, which is known only from postcranial data, consistently appears as the basal-most sphenacodontid in both of the analyses, with or without neural spine data.

A K-H test was performed to assess whether the *a priori* constraint topology, manually reconstructed on MacClade 4 (Maddison and Maddison, 2005) from literature sources, described the spine and "spineless" data significantly better than the MPTs of their respective analyses. The *a priori* constraint tree was found to require only two more steps (tree length = 191) than the "spineless" topologies (tree length = 189) when compared against the spineless dataset, and a p-value of 0.1581 indicates that there is no statistical difference in the tree's ability to explain the observed data. Even greater support was found when the *a priori* constraint tree was compared with the complete dataset (Appendices L and M), as

the cladistic topologies were identical (tree length = 209; p-value = 1.0).

Furthermore, distance analysis of the complete data corroborates the *a priori* constraint topology, except for a sister taxon relationship between *Lupeosaurus* and *Glaucosaurus*, to the exclusion of *Ianthasaurus* plus *Edaphosaurus* (Figure 24A). Comparisons of the distance tree (topology plus branch lengths) and the 50% majority-rule consensus tree mapped onto a stratigraphic column suggest high levels of congruence between character-based and temporal-based branch lengths (Figure 24A, B). Congruence between temporal and character-based branch lengths may support relatively constant rates of morphological evolution in Permo-Carboniferous synapsids as suggested by Sidor and Hopson (1998).

The combined observations reported here resulted in the selection of the *a priori* tree (compiled from the literature and corroborated by the complete morphological dataset) as the preferred reference phylogeny for analysis of phylogenetic signal and phylogenetic character mapping. The topology further supports a monophyletic Edaphosauridae as the sister taxon to Sphenacodontia (the most exclusive clade including *Haptodus*, Sphenacodontidae, and Therapsida;

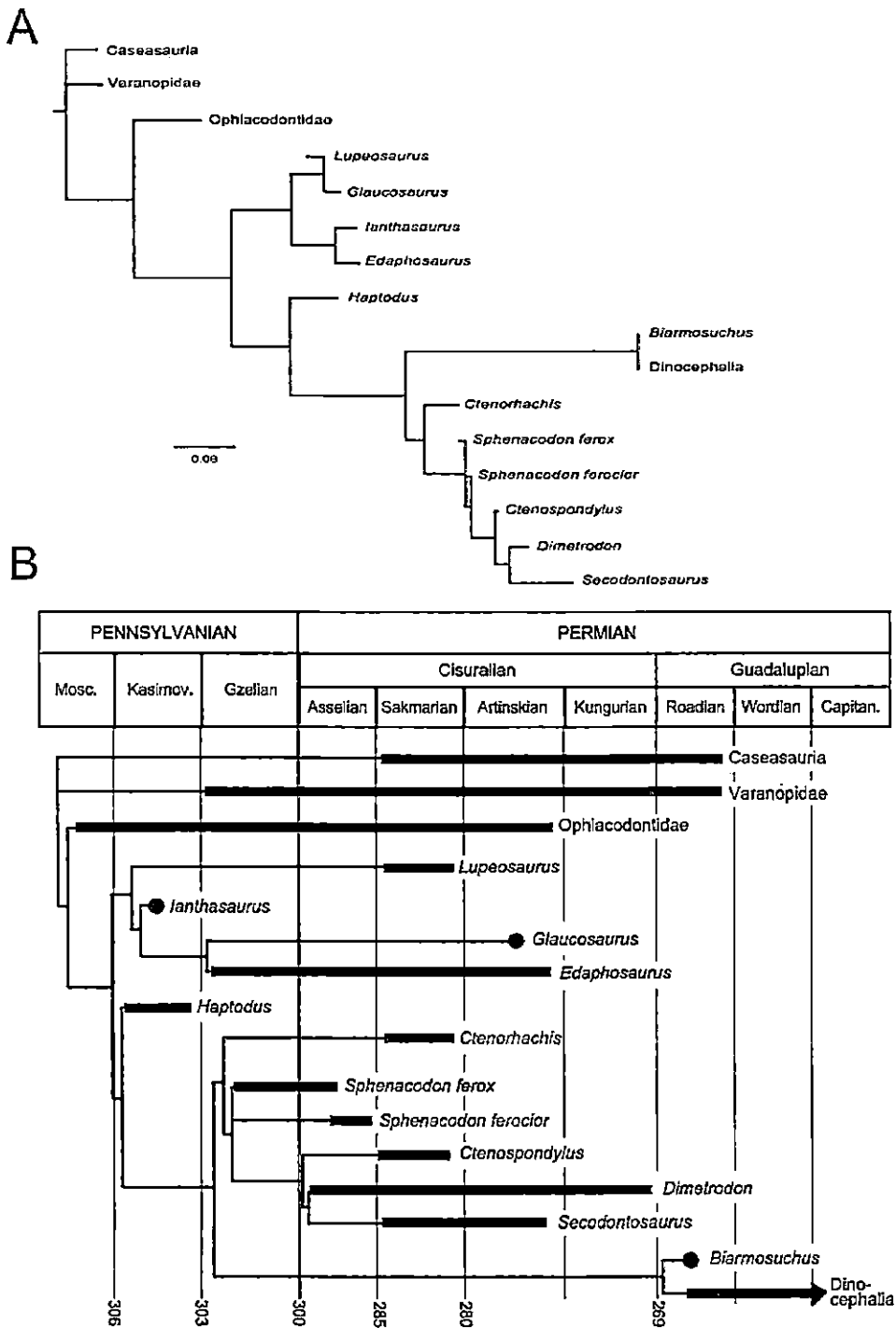


Figure 24. Comparison of (A) distance tree with branch lengths determined from character data and (B) 50% majority-rule consensus of two MPTs reconstructed against stratigraphy. Data in Appendix L was analyzed under

distance (A) and parsimony (B) criteria on PAUP* 4.0b. Note the congruence between character-based (morphological dissimilarity) and stratigraphy-based (temporal) branch lengths.

Figure 1). For the first time, *Lupeosaurus* is analytically demonstrated as the basal-most edaphosaurid, whereas *Ianthasaurus* shares a closer common ancestry with the clade uniting *Edaphosaurus* and *Glaucosaurus*. Sphenacodontidae is demonstrated to be the monophyletic sister taxon to Therapsida (Reisz, 1986; Hopson, 1991; Reisz et al., 1992). The clade of *Dimetrodon* plus *Secodontosaurus* is well-nested within Sphenacodontidae, with *Ctenospondylus* reconstructed in an intermediate position between that clade and a paraphyletic *Sphenacodon*. *Ctenorhachis* is shown to represent the basal-most sphenacodontid.

Phylogenetic Character Mapping

Subsequent to the phylogenetic analysis, it became apparent that certain characteristics of the neural spines were strongly phylogenetically-informative, whereas others demonstrated some degree of homoplasy. For example, one such trait of uncertain significance is the presence of neural spine "shoulders" (character 128) resulting in

dimetrodont differentiation in the hyperelongate neural spines of some edaphosaurids (i.e., *Edaphosaurus*) and sphenacodontids (Reisz et al., 1992). On one hand, this morphology may represent a genetically-inherited (historical) feature representing independent, phylogenetically-informative data. On the other hand, neural spine shoulders may represent a modeling response to stresses imposed on elongate spines and may thus be non-independent of the lengthening of the spines (character 126). To address this problem, the selected reference phylogeny was utilized to map and compare transformations in both discrete morphological characters and quantitative histomorphometric characters within their phylogenetic context for the first time. Neural spine characters (125-136) were mapped onto the reference phylogeny using the tree analysis software MacClade 4 (Maddison and Maddison, 2005). Examples from relative neural spine height (character 126) and neural spine shoulders producing dimetrodont differentiation (character 128) are illustrated in Figure 25. The implications for the evolution of neural spine shoulders is discussed below (see Discussion).

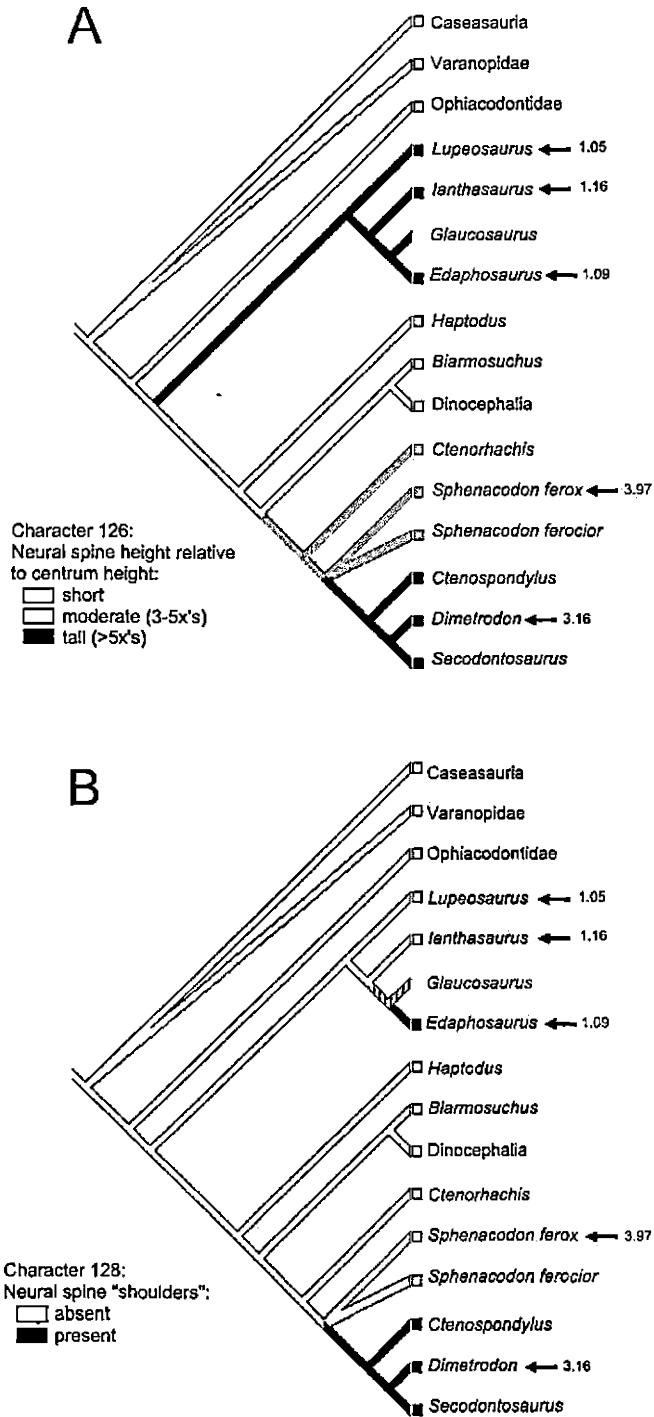


Figure 25. Phylogenetic character mapping of selected neural spine characters from Appendices E and F onto 50% majority rule consensus of two MPTs. A), Character 126,

neural spine height relative to centrum height; B) character 128, neural spine "shoulders" (denoting presence/absence of dimetrodont differentiation). Numerical values to right of tip labels denote bending rigidity of distal spine (from Appendix D).

Phylogenetic Signal and Phylogenetically-Independent Contrasts

The statistical results of the phylogenetic correlations (along with the PHYSIG analysis for phylogenetic signal) and phylogenetically-independent contrasts are provided in Tables 6 and 7. The analyses failed to recover statistically significant correlations for most variables, likely due to the small sample size available. Nonetheless, there are a few notable correlations which merit discussion below.

Approximately 79% of variation in distal bending rigidity was attributed to phylogeny, due to high maximum bending rigidity in Sphenacodontidae (Table 6). However, direction of resistance to bending was not taken into account. Bending rigidity values greater than 1.0 (Appendix D) indicate that a bone was better adapted for resistance to bending stresses in a particular direction, regardless of which direction that may be (e.g., anteroposterior versus mediolateral). Bending rigidity was

maximized in the anteroposterior direction in the spines of *Sphenacodon*, whereas bending rigidity was greatest laterally in the representative species of *Dimetrodon* quantified in the present study (i.e., *D. giganhomogenes*). Distal bending rigidity in the spines of Edaphosauridae was largely isotropic (rigidity ~1.0) due to the subcircular cross-sectional morphology across all sampled edaphosaurids. Phylogenetic signal in this character can be better evaluated with an increased sample of the cross-sectional geometry of spines in broader range of eupelycosaurs at the species level. A larger sample size of sphenacodontid spines (including several species of *Dimetrodon*) would help to further test the statistical correlations of bending rigidity, cortical porosity (discussed below), and phylogeny.

With respect to strictly historical components of spine osteohistology, no other statistically significant phylogenetic correlations in quantitative histomorphometric data were identified. A surprising result is the apparent lack of a correlation between distal cortical porosity (i.e., vascularity) and phylogeny. In Chapter Two,

Table 6. Phylogenetic correlations of histomorphometric dissimilarity on mean pairwise dissimilarity from phylogenetic data.

<u>Mean pairwise</u> <u>dissimilarity</u>	<u>character</u>	<u>PHYLOGENETIC CORRELATION (SIGMA PLOT)</u> :			<u>PHYSIG</u> :	
		<u>correlation coefficient</u>	<u>R-squared</u>	<u>p-value</u>	<u>K</u>	<u>p-value</u>
	Proximal spine					
	bending rigidity	0.446	0.199	0.196	0.205	0.502
	bone density	0.185	0.034	0.609	0.155	0.831
	cortical porosity	0.425	0.180	0.221	0.353	0.333
	RBT	0.591	0.349	0.072	0.844	0.162
	Distal spine					
	bending rigidity	0.890	0.792	<0.001	1.545	0.067
	bone density	0.134	0.018	0.633	0.243	0.286
	cortical porosity	0.322	0.103	0.242	0.250	0.048
	RBT	0.338	0.114	0.218	0.132	0.425

Table 7. Phylogenetically-independent contrasts of histomorphometric data (raw data from Appendices C and D).

<u>character</u>	<u>correlation coefficient</u>	<u>R-squared</u>	<u>p-value</u>
<u>Body mass (kg)</u>			
Proximal spine			
bending rigidity	0.202	0.041	0.744
bone density	0.309	0.096	0.613
cortical porosity	0.111	0.012	0.859
RBT	0.487	0.237	0.405
Distal spine			
bending rigidity	0.080	0.006	0.881
bone density	0.087	0.008	0.870
cortical porosity	0.376	0.142	0.462
RBT	0.064	0.004	0.904
<u>Cross-sectional bone mass (mm²)</u>			
Proximal spine			
bending rigidity	0.220	0.048	0.723
bone density	0.869	0.756	0.055
cortical porosity	0.714	0.510	0.175
RBT	0.157	0.025	0.802
Distal spine			
bending rigidity	0.631	0.399	0.179
bone density	0.282	0.079	0.589
cortical porosity	0.893	0.798	0.016
RBT	0.439	0.193	0.384

Table 7 (continued). Phylogenetically-independent contrasts of histomorphometric data (raw data from Appendices C and D).

<u>character</u>	<u>correlation coefficient</u>	<u>R-squared</u>	<u>p-value</u>
<u>Neural spine height /</u>			
<u>centrum height ratio</u>			
Proximal spine			
bending rigidity	0.621	0.386	0.264
bone density	0.740	0.548	0.153
cortical porosity	0.192	0.037	0.757
RBT	0.118	0.014	0.850
Distal spine			
bending rigidity	0.488	0.238	0.326
bone density	0.778	0.605	0.069
cortical porosity	0.214	0.046	0.684
RBT	0.790	0.625	0.531

sphenacodontids were suggested to have relatively high levels of vascularity in the lateral cortex of the distal spines. Results of the phylogenetically-independent contrasts (Table 7) suggest that cross-sectional bone mass better explains the data for cortical porosity (R-squared = 0.798; p-value = 0.016). It is likely, however, that higher cortical vascularity (and thus porosity) was related not only to greater cross-sectional bone mass, but more directly to bone deposition rates (Amprino, 1947; Ricqlès, 1974a, b). If this is true, then the observations here may corroborate the hypothesis that the vascularity observed in sphenacodontids facilitated rapid deposition of fibrolamellar and parallel-fibered bone tissue ahead of any other physiological utility.

Another notable phylogenetically-independent correlate is the weak correlation between proximal bone density and both cross-sectional bone mass (R-squared = 0.756; p-value = 0.055) and relative spine height (R-squared = 0.548; p-value = 0.152). The correlation is, however, stronger with cross-sectional bone mass. Thus, the burden of greater sail mass may have to some degree necessitated greater bone density proximally. Distal bone density also correlates

weakly with relative spine height (R-squared = 0.605; p-value = 0.069).

Discussion

Trends in Dorsal Sail Structure and Histological Organization

Comparisons of Distal Outgrowth. Bone microstructure is influenced by a number of interacting variables, including historical (phylogenetic), functional (physiologic), and structural (growth and architecture) components (Cubo et al., 2008). Amprino's rule (1947) states that bone tissue-type (e.g., fibrolamellar vs. lamellar-zonal) is directly related to the rate at which the bone was deposited. Relative size differences noted in the sails of edaphosaurids and sphenacodontids has suggested to some authors that the sail of *Dimetrodon* grew much faster than that of its predecessors as well as its edaphosaurid contemporaries (Romer and Price, 1940; Ricqlès, 1974a). This is corroborated by the histological evidence; whereas rapidly deposited fibrolamellar bone is abundant in *Dimetrodon* spines, it is largely absent in edaphosaurids (except in the rapidly growing tubercles of *Edaphosaurus*).

The relatively shorter neural spines of *Sphenacodon*, however, are characterized by pronounced vascularization in a fibrolamellar and parallel-fibered bone matrix, reflecting that of the limb bone histology (Huttenlocker et al., 2006). The implications for allometry and skeletal growth in sphenacodontids are interesting; if one assumes Amprino's rule, what it suggests is that a number of the skeletal elements in *Sphenacodon* were rapidly deposited, including the spines constituting the dorsal crest (see Chapter Two); the spines of *Edaphosaurus* may be relatively longer than those of *Sphenacodon*, but may have reached their extreme lengths not by rapid deposition over a short expanse of time, but instead gradually over a prolonged period of time, indicating that *Edaphosaurus* may have lived longer and may have grown more slowly than *Sphenacodon*, reaching its adult size later in ontogeny. This hypothesis is corroborated by previous surveys of bone histology in both groups which have suggested slow, cyclical growth in *Edaphosaurus* (Ricqlès, 1974a) and rapid growth in *Sphenacodon* juveniles with decelerating growth into maturity over a relatively short period of time (Huttenlocker et al., 2006). By contrast, the limb bone histology of *Dimetrodon* appears to reflect slow, cyclical

growth (Ricqlès, 1974a), but the dorsal neural spines record rapid, sustained growth, likely contributing to the apparent sail allometry with respect to body size in that genus (Romer and Price, 1940).

Additional implications for bone growth and vascularity have been revealed by the phylogenetically-independent contrasts performed here. The investigations in Chapter Two suggested that the distal region of the neural spines of sphenacodontids tended to be characterized by relatively high levels of porosity and thus dense vascularization. In *Sphenacodon*, large vascular striations were preserved in the process of becoming incorporated into the lateral cortex (Figure 12). Assuming Amprino's rule, the large cross-sectional bone mass was achieved through rapid deposition (as opposed to slow deposition over a prolonged period of time) and recorded by the presence of fibrolamellar and parallel-fibered bone tissue in sphenacodontids. Incidentally, the present study has revealed fast-growing fibrolamellar bone in the tubercles of *Edaphosaurus*, which demonstrate little area in cross-section, but were well-vascularized (Figure 22 B).

Functional Interpretations of Hyperelongate Neural Spines and their Mechanical Properties

Though it is difficult to ascertain the function of the dorsal sail based on microanatomy alone, osteohistological examination of the neural spines rejects the assumptions of the widely popularized thermoregulatory hypothesis, such as the significance of the A-P grooves, vascular restorations, and interspecific variation in the surface area of the dorsal crest or sail (Chapters Two and Three). Main et al. (2005) similarly rejected a thermoregulatory function for the analogous dorsal dermal plates (hypertrophied scutes) of thyreophoran dinosaurs, contrary to interpretations of earlier studies (Buffrénil et al., 1986). Based on histological evidence, they demonstrated that (1) blood was not likely to have been transported directly from within the body cavity to the outer surface of the plates; (2) earlier configurations of the external vascularization and soft-tissue of the plates was speculative or equivocal at best; and lastly (3) phylogenetic patterns revealed no general trends in scute size or shape within Stegosauria, indicating that variation in scute morphology is more likely to be a function of

species recognition rather than directional selection toward optimal thermoregulatory capabilities.

It is unlikely that the dorsal sail of eupelycosaurs was selected for thermoregulation during its early evolution. Phylogenetic trends (Figure 25A) reveal that the structure first evolved in the edaphosaurid lineage, appearing suddenly in small-bodied forms from the Kasimovian and Ghzelian (Upper Carboniferous) of North America. By contrast, the dorsal sail of sphenacodontids, the first highly-terrestrialized vertebrate predators, appeared later in the upper-most Carboniferous of North America as a short, dorsal crest, stabilized by simple laterally-compressed neural spines. Thus, the progressive lengthening of hyperelongate neural spines in the sphenacodontid lineage provides a unique opportunity to analyze how elongate biological structures adapt to changing mechanical demands over evolutionary time and may provide insights into their functional integration with the axial skeleton.

Elongate Biological Structures and the Mechanical Adaptations of the Distal Neural Spines of *Dimetrodon*.

Depending on its functional and material properties, any elongate biological structure requires a certain amount

of flexural stiffness (Etnier, 2001). Flexural stiffness restricts bending about the neutral plane, whereas torsional stiffness restricts twisting about the long-axis of the structure. The material properties and cross-sectional distribution of bone mass play a significant role in this so-called "twistiness-to-bendiness" ratio (Etnier, 2001; Vogel, 1988, 2003), in which bending resistance is maximized at the cost of torsional stiffness. Thus, as an example, high values of flexural stiffness accompanied by low values of torsional stiffness allow a structure to resist bending while still allowing twisting about the long-axis.

Since cylinders are inherently susceptible to bending stresses, many examples exist in nature in which the cross-sectional shape of an elongate structure is "modified" to accommodate the types of mechanical insult it experiences. For example, plant leaves are able to twist and cluster together to reduce drag in storms, while simultaneously retaining their cantilever function by not bending easily (Vogel, 1988, 2003). Petioles with grooves have higher twistiness-to-bendiness ratios than those without grooves, a likely adaptation to minimize structural failure. The groove also provides added

resistance to tensile forces and, in leaf petioles and bird feathers, is located on the side of the structure that is loaded in tension.

Although flexural stiffness could not be accurately quantified in the hyperelongate neural spines of eupelycosaurs examined in the present study (due to diagenesis of the material properties of fossil bone), bending rigidity and torsional stiffness were inferred based on the second moments of area and the cross-sectional distribution of bone mass (Appendix D). The distal region of the neural spine of *Dimetrodon* is exemplary of the mechanical adaptations experienced in the hyperelongate spines of derived sphenacodontids. Mid-dorsal spines of *D. giganhomogenes* and many other species are transversely expanded in cross-section, having high values of maximum bending rigidity (i.e., resistance to lateral bending). However, the distal spine deviates from the cylindrical shape observed in the neural spines of the distantly-related edaphosaurids. The transversely expanded nature of the distal spine and the presence of A-P grooves increase the twistiness-to-bendiness ratio, suggesting that slight twisting of the spines may have been possible, or even necessary, as

forces were propagated through the axial skeleton via lateral undulations of the trunk during locomotion.

Phylogenetic Distribution of Mechanical Adaptations: Cross-sectional Shape and Resistance to Lateral Bending Stresses. The phylogenetic distribution of neural spine morphologies illustrated in Figure 25 demonstrates that short, laterally-compressed spines represent the plesiomorphic condition for eupelycosaurian synapsids. The hyperelongate neural spines of edaphosaurids appeared suddenly, forming a broad dorsal sail with no known intermediate forms, and displayed a subcircular cross-sectional geometry (bending rigidity ~ 1.0). There was apparently no pronounced dimetrodont differentiation in basal forms, although derived species of *Edaphosaurus* may exhibit dimetrodont-like differentiation, delineating the proximal (epaxial-embedded) and distal portions of the spine.

There is a distinct difference in the timing of the acquisition of these characters in Edaphosauridae and Sphenacodontidae (Figure 25). By comparison, sphenacodontid gross spine morphology appears to have evolved in a stepwise fashion, initially demonstrating laterally-compressed neural spines (bending rigidity $\gg 1.0$

about the transverse plane of the trunk) and later demonstrating subcircular and laterally-expanded (figure-8) spines (bending rigidity $\gg 1.0$ about the sagittal plane) in numerous species of *Dimetrodon*. When directionality is applied to the given values for bending rigidity (Appendix D), resistance to lateral bending appears to be correlated with the relative lengthening of the neural spines (but with low statistical support). The presence of neural spine "shoulders" producing dimetrodont differentiation has been suggested here to represent either a phylogenetically-informative piece of data (see Results) or a modeling response correlated with relative spine-height. Thus, resistance to lateral bending and neural spine "shoulders" might both correlate with the relative spine-height. However, it has been suggested (Reisz et al., 1992) that, in the sphenacodontid lineage, neural spine shoulders appeared on the branch between *Sphenacodon* and *Ctenospondylus* (Figure 25B). Incidentally, the relative height of mid-dorsal neural spines of *Ctenospondylus*, which are largely blade-like and laterally-compressed, falls well below the average ranges of heights for the edaphosaurids *Lupeosaurus* and *Ianthasaurus* (Figure 4) which do not demonstrate distinct neural spine shoulders. Thus, it is

unlikely that neural spine shoulders are exclusively mechanically constrained structures (or at least that they are constrained by spine-height alone), and could therefore exhibit some degree of phylogenetic "signal" within the sphenacodontid lineage. Alternatively, the presence of neural spine shoulders may represent the existence of some unknown variable, such as increased mechanical insult from behavioral activities in post-*Sphenacodon* sphenacodontids, although this cannot be independently verified at present. Such early changes in neural spine architecture would suggest different mechanical demands on the neural spines of sphenacodontids versus edaphosaurids.

The *Sphenacodon-Ctenospondylus* condition may constitute a paraphyletic grade in the level of organization and degree of elongation of the sphenacodontid dorsal crest. Eberth (1985) suggested that *Sphenacodon* and *Ctenospondylus* may be congeneric. The results of the present analysis suggest conversely that *Sphenacodon* is paraphyletic with respect to *Ctenospondylus* and derived sphenacodontids.

Safety Factors, the Strengthening of the Vertebral Column and Terrestrial Locomotion. Currey (2002) demonstrated that in most vertebrate bones, high

probabilities of failure are coupled with high safety factors in order to deter failure or fracture. The mechanical advantage of sphenacodontid spines associated with frequent fractures in museum specimens is consonant with this principle (Chapter Two). Specifically, sphenacodontid spines were likely subjected to mechanical insult from their environment on a frequent basis, such that they adapted (*sensu* Currey, 2003) safety factors as a response to overcome such forces (e.g., bending stresses or torsion).

Interestingly, few fractured spines were observed in most examined specimens of Edaphosauridae. This does not necessarily mean that neural spines were never fractured or that the spines were mechanically superior to those of sphenacodontids, but it may suggest that their spines were less prone to insult or fatigue, having lower probabilities of failure and, thus, contributing to a lower safety factor compared to *Dimetrodon*, for example. One important exception is the pathological specimen of *Lupeosaurus* (Chapter Three). However, *Lupeosaurus* is unique among edaphosaurids in that it only developed a rudimentary central cavity, with sparse trabecular structures still present in the "medullary" region. When

taken together, minimum bone mass (MBM) and the scarcity of fractured spines in studied specimens support a low probability of failure in the spines of edaphosaurids.

Unlike *Dimetrodon*, the hyperelongate neural spines of *Edaphosaurus* do not exhibit extreme mechanical specializations and would not have been mechanically superior to those of *Dimetrodon* if subjected to similar external stresses. Moreover, edaphosaurid spines may have been selected for MBM, a phenomenon that is less evident in sphenacodontid spines which retain dense, fine-cancellous bone within the "medullary" region. The presence of a hollow, central cavity in *Edaphosaurus* suggests that the cost of producing excessive amounts of bone material outweighed the need to resist mechanical insult. Thus, it is not likely that the distal spines of *Edaphosaurus* were subjected to extreme locomotory forces nor did they play a significant role in locomotion. The sail may have been utilized as a display structure (Modesto, 1990) as analogously hypothesized for thyreophoran dinosaur plates (Main et al., 2005) and played little role in maintaining the stability of the axial skeleton.

Although edaphosaurids and sphenacodontids show subtle mechanical differences in their neural spines, the differences do not imply that MBM was not occurring at all in sphenacodontids, as it is an energy-conserving phenomenon that is observed across most vertebrate clades (Currey, 2002; Currey and Alexander, 1985). However, the mechanical demands imposed on the spines of sphenacodontids may have been such that relatively greater safety factors were in place (discussed in detail below), and hence the retention of dense, fine-cancellous bone in the "medullary" region, greater cross-sectional bone mass and, more importantly, unique distributions of cross-sectional bone mass relative to the neutral plane of the spine in derived sphenacodontids. In basal sphenacodontids like *Sphenacodon*, I_{\max} (Appendix D) of the neural spine was equal to I_y such that resistance to bending was strongest about the transverse plane of the trunk of the body. This indicates that the shapes of the neural spines of early sphenacodontids were mechanically selected to resist bending down the long axis of the vertebral column, thereby strengthening the trunk anteroposteriorly and dorsoventrally for terrestrial locomotion. Continued lengthening of the neural spines,

as exemplified in *Ctenospondylus*, has been suggested to play a role in the strengthening of the vertebral column (Romer and Price, 1940; Pivorunas, 1970; Vaughn, 1971; Ebel, 2000).

In addition to stabilizing the trunk, the extreme hyperelongate neural spines of large individuals of *Dimetrodon* (e.g., *D. giganhomogenes* and *D. grandis* which were thin-sectioned for the present study) displayed pronounced lateral expansion, producing a double-cylinder cross-sectional shape (Rega et al., 2005; Sumida et al., 2005). Although the base of the spine in *D. giganhomogenes* shows a relative distribution of second moments of area that is consistent with spines adapted to resist fore and aft (I_y) bending as in *Sphenacodon*, the distal portion of the spine demonstrates three times greater resistance to bending in the lateral direction (I_x), with an I_{\max} of 12,166 mm⁴ (Appendix D). This suggests that the greatly hyperelongated distal spines of *D. giganhomogenes*, and likely many other large *Dimetrodon* species, were mechanically selected to resist lateral bending as such stresses would have been transmitted through the spine by lateral undulations produced during terrestrial locomotion. It is hypothesized here that, in

basal sphenacodontids, a dorsal crest or sail had initially evolved as a biomechanical adaptation for trunk stability and strengthening of the vertebral column during terrestrial locomotion, but may have been co-opted in derived sphenacodontids (e.g., *Dimetrodon*) for other mechanical functions involved more directly in the locomotor capabilities of the organism. In the case of eupelycosaurs, it is possible that an elaborate dorsal sail could have been secondarily exapted in derived sphenacodontids (e.g., *Dimetrodon*) to facilitate thermoregulatory processes, but only if the soft-tissue constituents of the sail allowed for controlled heat transfer to and from the viscera.

Conclusions

Phylogenetic analysis of eupelycosaurian synapsids corroborates the current consensus of the large-scale interrelationships of eupelycosaurs. Additionally, *Lupeosaurus* and *Ctenorhachis* are recovered as basal members of Edaphosauridae and Sphenacodontidae respectively. Furthermore, the genus *Sphenacodon* is suggested to be paraphyletic. Previous investigations of sphenacodontid phylogeny have exposed little variation in

the cranial bones of *Sphenacodon*, *Ctenospondylus*, and *Dimetrodon*, other than size-correlated reductions in the dentition which occurred in parallel in all three genera (Vaughn, 1969; Berman, 1978; Eberth, 1985; Reisz, Berman, and Scott, 1992). Consequently, the major source of taxonomically-informative variation exists in the postcranial skeleton and not in the cranium. This interpretation is in opposition to the wide application of cranial characters in the phylogeny of basal synapsids. Future taxonomic assessments of sphenacodontids at the species level (e.g., the speciose *Dimetrodon*) should direct efforts toward a more thorough understanding of the nature of the variation exhibited in the axial skeleton and integrate potential sources of phylogenetic data including the proportions of the dorsal vertebral centra (Romer and Price, 1940; Rushforth and Small, 2003), ontogenetic transformations in cross-sectional geometry of the neural spines (Sumida et al., 2005), and their associated histological properties (Sumida et al., 2005; Madalena et al., 2007).

Careful investigation of previously studied and newly examined eupelycosaurian taxa has revealed familial-level distinctions in the histological

characterizations of hyperelongate neural spines.

Sphenacodontidae is characterized by abundant fibrolamellar and parallel-fibered bone tissue within the cortex, dense fine-cancellous bone in the medullary region, relatively high bone density (~ 0.75), high cortical porosity (5%-15%), and increased resistance to bending and torsional stresses in the distal portion of the spine. By contrast, Edaphosauridae is characterized by abundant lamellar-zonal bone, a cavernous "medulla" with sparse trabecular structures, moderately high bone density ($\sim 0.50-0.75$), low cortical porosity (1%-5%), and low torsional resistance in the distal portion of the spine.

Several tests of phylogenetic "signal" were performed to reveal evolutionary trends in the histological properties of the hyperelongate neural spines of edaphosaurids and sphenacodontids. Distal bending rigidity may exhibit some degree of phylogenetic signal, with edaphosaurids largely displaying isotropic rigidity and sphenacodontids displaying a wider array of bending resistance adaptations. However, increased sampling intensity is necessary to resolve the nature of this signal

in sphenacodontids. Most other variables lacked statistically significant correlations with phylogeny.

Histomorphometric data allows comparisons of distal outgrowth of the neural spines. Increased cross-sectional bone mass coupled with high rates of bone deposition is suggested to account for the increased vascularity of the lateral cortex of sphenacodontid neural spines. Comparisons between relative bone deposition rates in the spines and previously reported growth strategies inferred from long bone histology can account for size-related (ontogenetic and/or phylogenetic) allometry in the dorsal crest or sail.

Phylogenetic character mapping reveals the sudden and early appearance of an elaborate dorsal sail in edaphosaurids, in contrast to the later, gradual emergence of the "sail" in sphenacodontids (although a short dorsal crest is hypothesized to have existed in early members of the latter clade; Chapter Two). Independent acquisitions of the dimetrodont differentiation cannot be attributed to mechanical variables that were directly associated with spine-height, and may thus represent phylogenetically-informative transformations or parallel responses to some unknown mechanical variable.

Historical (phylogenetic) and functional (physiologic) explanations of bone microstructure remain contentious for the hyperelongate neural spines of eupelycosaurs. However, mechanical interpretations of bone microstructure are readily interpretable from analysis of the histomorphometric data and, thus, functional interpretations may be inferred strictly in terms of axial skeleton mechanics. The most extreme mechanical adaptations are apparent within the family Sphenacodontidae. Sphenacodontids are often portrayed as the dominant, large-bodied terrestrial vertebrate predators in their respective environments, and among the first large-bodied amniote predators in early terrestrial vertebrate communities. As such, it is not unreasonable to expect novel mechanical adaptations for trunk stability and terrestrial locomotion in the axial skeleton of these early amniote predators, as similar novel transformations occurred in parallel in the appendicular skeleton of their therapsid cousins during this geologic period (e.g., reduction of girdle elements, digit reductions, postural modifications, etc.). Nevertheless, the extent to which the spines played a role in the functional integration of the axial skeleton and their role in terrestrial locomotion

is uncertain. Moreover, the mechanical performance of the dorsal sail does not preclude its utility for other biologically significant functions. Future studies should implement computer-based biomechanical modeling (e.g., finite element analysis) and aim to design experiments capable of testing the limits of neural spine performance using multiple parameters of spine shape and material properties.

APPENDIX A
LIST OF ABBREVIATIONS

APPENDIX A. List of anatomical and institutional abbreviations used in this study.

- c.c. – central cavity
ch. pt. – changing point
CM – Carnegie Museum of Natural History, Pittsburg
CSUSB – California State University, San Bernardino
DMNH – Denver Museum of Nature and Science, Denver
FMNH UC – Field Museum of Natural History, Chicago
intsp. lig. – interspinal ligament
l.p.b. – lamellar primary bone
m.s. – muscle scars
M. intarc – interarcuate muscle
M. intart – interarticular muscle
M. intsp – interspinalis muscle
M. intr – intertransversus muscle
M. semisp – semispinalis muscle
M. spd – spinalis dorsi muscle
MCZ – Harvard Museum of Comparative Zoology, Cambridge
OMNH – Sam Noble Oklahoma Museum of Natural History, Norman
p.o. – primary osteons
ph.c. – protohaversian canal
r.b. – reticular bone
r.c. – resorption cavity
S.f. – Sharpey's fibers
UCLA VP – University of California, Los Angeles, Vertebrate Paleontology collections
UCM – University of Colorado Museum, Boulder
UCMP – University of California Museum of Paleontology, Berkeley
UT – University of Toronto, Mississauga
w.b. – woven bone

APPENDIX B
SPECIMEN/LOCALITY DATA

APPENDIX B. List of specimens examined in this study. Specimens denoted with asterisks (*) were serially sectioned and examined histologically. See Appendix A for institutional abbreviations.

Genus / species ID	Specimen number	Element(s)	Locality	Horizon
<i>Sphenacodon ferox</i>	UCMP 34226	partial skeleton	Camp Quarry, Rio Arriba Co., New Mexico	Lower Permian, Cutler Group
<i>Sphenacodon ferox</i> *	UCLA VP uncatalogued (field no. C-61-29)	isolated neural spine	Miller Bonebed, Rio Arriba Co., New Mexico	Lower Permian, Cutler Group
<i>Sphenacodon</i> cf. <i>S. ferox</i> *	UCMP 68436	isolated neural spine	Camp Quarry, Rio Arriba Co., New Mexico	Lower Permian, Cutler Group
<i>Sphenacodon ferocior</i>	UCMP 34218	partial skeleton	Anderson Quarry, Rio Arriba Co., New Mexico	Lower Permian, Cutler Group
<i>Sphenacodon</i> cf. <i>S. ferocior</i> *	CM 73367	isolated neural spine	Sierra Lucero, Major Ranch, Valencia Co., New Mexico	Upper Pennsylvanian(?), Red Tanks Member, Bursum Formation
<i>Dimetrodon limbatus</i>	MCZ 1347	articulated skeleton (DMNH cast)	Godwin Creek, Baylor Co., Texas	Lower Permian, Wichita Group
<i>Dimetrodon giganhomogenes</i> *	FMNH UC 1134	partial vertebral column and tibia	Coffee Creek, Baylor Co., Texas	Lower Permian, Arroyo Formation
<i>Dimetrodon</i> cf. <i>D. giganhomogenes</i> *	DMNH 30597	partial skeleton	Hannsz Ranch, Haskell Co., Texas	Lower Permian, Vale Formation
<i>Dimetrodon</i> cf. <i>D. grandis</i> *	DMNH 16131	partial skeleton	Hannsz Ranch, Haskell Co., Texas	Lower Permian, Vale Formation
<i>Dimetrodon</i> sp.	OMNH 1727	partial skeleton	Cleveland Co., Oklahoma	Lower Permian, Hennessey Group
<i>Ctenospondylus</i> cf. <i>C. casei</i>	UCLA VP uncatalogued	isolated neural spine (cast)	Rattlesnake Canyon, north-central Texas	Lower Permian, Admiral Formation
<i>Edaphosaurus boanerges</i>	OMNH 1674	mounted composite skeleton	Geraldine Bonebed, Archer Co., Texas	Lower Permian, Admiral Formation
<i>Edaphosaurus</i> sp.*	OMNH 73800	isolated neural arch with proximal spine	Comanche Co., Oklahoma	Lower Permian, Upper Garber Formation

<i>Edaphosaurus</i> sp.*	OMNH 73802	neural spine (distal fragment)	Jefferson Co., Oklahoma	Lower Permian, Wellington Formation
<i>Edaphosaurus</i> sp.*	OMNH 73804	neural spine (distal tip)	Jefferson Co., Oklahoma	Lower Permian, Wellington Formation
<i>Edaphosaurus</i> sp.	OMNH 73805	neural spine (proximal fragment)	Jefferson Co., Oklahoma	Lower Permian, Wellington Formation
<i>Edaphosaurus</i> sp.*	OMNH 73806	neural spine lateral tubercle	Jefferson Co., Oklahoma	Lower Permian, Wellington Formation
<i>Edaphosaurus</i> sp.*	OMNH 73809	neural spine (distal tip)	Jefferson Co., Oklahoma	Lower Permian, Wellington Formation
<i>Lupeosaurus</i> cf. <i>L. kayi</i> *	UCLA VP 1651	partial skeleton	Archer Co., Texas	Lower Permian, Admiral Formation
<i>Ianthasaurus hardestiorum</i> *	UT uncatalogued	mid-dorsal vertebra with associated vertebra	Garnett Locality, Anderson Co., Kansas	Upper Pennsylvanian, Stanton Formation (Rock Lake Shale Member)
<i>Ianthasaurus hardestiorum</i> *	UT uncatalogued	posterior dorsal vertebra with associated vertebra	Garnett Locality, Anderson Co., Kansas	Upper Pennsylvanian, Stanton Formation (Rock Lake Shale Member)

APPENDIX C
MORPHOLOGICAL COMPARISONS

APPENDIX C. Comparisons of the sail-backed synapsid taxa examined in this study. Table includes (1) global standard stage (Kasimovian through Kungurian), (2) maximum size, including estimated mass (in kilograms) and total body length (in meters) for taxa in which the information was available, (3) maximum dorsal spine height with relative neural spine-to-centrum height ratios, (4) cross-sectional shape of spine, and (5) relevant sources from the literature.

Taxon	¹ Global stage	² Max size (estimated mass / body length)	³ Max dorsal spine height (neural spine/centrum height)	⁴ Cross-sectional shape of spine	⁵ Source(s)
<i>Sphenacodon ferox</i> (Sphenacodontidae)	Ghzelian-Asselian	small/medium (52 / 1.8)	relatively low (4)	oval/laterally compressed throughout	Romer and Price 1940
<i>Sphenacodon ferocious</i> (Sphenacodontidae)	Ghzelian(?) - Asselian	medium/large (129 / 2.3)	relatively low to moderate (5-6)	oval/laterally compressed throughout	Romer and Price 1940
<i>Dimetrodon milleri</i> (Sphenacodontidae)	Sakmarian	small (47 / 1.7)	moderately high (19)	subcircular (A-P grooves absent)	Romer and Price 1940
<i>Dimetrodon occidentalis</i> (Sphenacodontidae)	Sakmarian	small (41)	moderately high (18)	predominantly figure-8	Berman 1977; Berman et al. 2001
<i>Dimetrodon teutonius</i> (Sphenacodontidae)	Artinskian	small (24)	moderately high (18)	figure-8 distally (oval/laterally compressed at base)	Berman et al. 2001, 2004
<i>Dimetrodon natalis</i> (Sphenacodontidae)	Artinskian	small (38 / 1.7)	moderately high	figure-8 distally (subquadrate base)	Romer and Price 1940; Berman et al. 2004
<i>Dimetrodon limbatus</i> (Sphenacodontidae)	Artinskian	large (140 / 2.7)	high (22)	figure-8 distally (subquadrate base)	Romer and Price 1940
<i>Dimetrodon macrospondylus</i> (Sphenacodontidae)	Artinskian	large	high?	predominantly figure-8	Romer and Price 1940
<i>Dimetrodon booneorum</i> (Sphenacodontidae)	Artinskian	small/medium (63 / 1.8)	high	predominantly figure-8	Romer and Price 1940

<i>Dimetrodon dolloviarius</i> (Sphenacodontidae)	Kungurian	large (150)	high	figure-8 distally (subquadrate base)	Romer and Price 1940
<i>Dimetrodon giganhomogenes</i> (Sphenacodontidae)	Kungurian	large (166 / 3.3)	high (24)	figure-8 distally (subquadrate base)	Romer and Price 1940
<i>Dimetrodon grandis</i> (Sphenacodontidae)	Kungurian	large (250 / 3.2)	high (32)	mostly subquadrate throughout	Romer and Price 1940
<i>Dimetrodon loomisi</i> (Sphenacodontidae)	Kungurian	medium/large (97 / 2.6)	high (22)	figure-8 distally (subquadrate base)	Romer and Price 1940
<i>Dimetrodon angeleensis</i> (Sphenacodontidae)	Kungurian	large	high	figure-8 distally	Olson, 1962
<i>Secodontosaurus obtusidens</i> (Sphenacodontidae)	Artinskian- Kungurian	medium (~72)	high	subcircular with shallow A-P grooves (oval/laterally compressed at base)	Romer and Price 1940; Reisz et al 1992
<i>Ctenospondylus casei</i> (Sphenacodontidae)	Artinskian	large (~140 / ~2.7)	moderate (7)	oval/laterally compressed throughout	Romer and Price 1940
<i>Ctenospondylus ninevehensis</i> (Sphenacodontidae)	Artinskian(?)	small/medium (~50 / ~1.8)	moderate (~6-7)	oval/laterally compressed throughout	Berman 1978
<i>Ctenorhachis jacksoni</i> (Sphenacodontidae)	Artinskian	small/medium (~60 / ~1.8)	relatively low (4)	laterally compressed	Hook and Hotton 1991
<i>Ianthasaurus hordestiorum</i> (Edaphosauridae)	Kasimovian	small (~7)	moderately high (14)	subcircular (laterally compressed proximally)	Reisz and Berman 1986; present study
<i>Edaphosaurus colohistion</i> (Edaphosauridae)	Ghzelian	medium	high	subcircular (subtriangular at very base)	Berman 1979
<i>Edaphosaurus novomexicanus</i> (Edaphosauridae)	Sakmarian	small/medium (63 / 2.4)	high	subcircular with shallow A-P grooves (subtriangular at very base)	Romer and Price 1940
<i>Edaphosaurus boanerges</i> (Edaphosauridae)	Artinskian	medium (83 / 2.6)	high (22)	subcircular with shallow A-P grooves (subtriangular at very base)	Romer and Price 1940

<i>Edaphosaurus cruciger</i> (Edaphosauridae)	Artinskian- Kungurian	large (166 / 2.9)	high (22)	subcircular with deep A-P grooves in large individuals (subtriangular at very base)	Romer and Price 1940
<i>Edaphosaurus pogonias</i> (Edaphosauridae)	Kungurian	large (186 / 3.2)	high (18)	subcircular with deep A-P grooves in large individuals (subtriangular at very base)	Romer and Price 1940
<i>Lupeosaurus kayi</i> (Edaphosauridae)	Sakmarian- Artinskian	large (166 / 3.0)	moderately high (12)	subcircular with very shallow A-P grooves (subtriangular at very base)	Romer and Price 1940; Sumida 1988

APPENDIX D
HISTOMORPHOMETRIC DATA

APPENDIX D. Histomorphometric data, including (1) bone density, (2) cortical porosity, (3) relative bone wall thickness (RBT), (4) total cross-sectional area (or “bone mass” of Cubo et al., 2005), (5) minimum second moment of area (I_{\min}), (6) maximum second moment of area (I_{\max}), (7) relative maximum to minimum bending rigidity (I_{\max}/I_{\min}), and (8) torsional rigidity (J) of dorsal neural spines for each sampled taxon. RBT calculations follow Chinsamy (1993). Calculations for “ I_{\max}/I_{\min} ” and “ J ” follow Plochocki et al. (2007). The data are based on available proximal and distal (mid-height) sections obtained from dorsal neural spines, with additional tip and tubercle data for *Edaphosaurus* (see Appendix B for complete specimen details, including provenance data).

Taxon		¹ Bone density	² Cortical porosity (%)	³ RBT (%)	⁴ Total cross-sectional area (mm ²)	⁵ I_{\min} (mm ⁴)	⁶ I_{\max} (mm ⁴)	⁷ I_{\max}/I_{\min}	⁸ J (mm ⁴)
Edaphosauridae									
<i>Lupeosaurus</i>	proximal	0.55	1.0	6.8	230	1200	1420	1.18	2620
	distal	0.52	5.0	10.7	150	1101	1155	1.05	2256
<i>Ianthasaurus</i>	distal	0.75	1.5	18.7	8.36	4.59	5.34	1.16	9.93
<i>Edaphosaurus</i>	proximal	0.65	1.0	8.0	214	1878	3761	2.00	5639
	distal (mid)	0.77	1.2	15.5	118	1010	1100	1.09	2110
	distal (tip)	0.60	2.0	14.7	36.8	102	116	1.14	218
	tubercle	0.76	2.0	--	18.7	--	--	--	--
Sphenacodontidae									
<i>Sphenacodon</i>	proximal	0.60	7.5	8.8	151	1075	1599	1.49	2674
	distal	0.56	5.9	4.8	180	812	3225	3.97	4037
<i>Dimetrodon</i>	proximal	0.77	16.0	8.8	540	5465	9244	1.69	14709
	distal	0.72	13.5	14.6	282	3854	12166	3.16	16020

APPENDIX E

LIST OF PHYLOGENETICALLY INFORMATIVE CHARACTERS

APPENDIX E. List of 136 cranial and postcranial characters used in the phylogenetic analysis. Characters 1-124 are non-neural spine characters borrowed from Reisz, Berman, and Scott (1992), Laurin (1993), Modesto (1995), and Sidor and Hopson (1998). Characters 125-136 are neural spine characters adapted from those sources and from the present study. Neural spine characters were excluded from second analysis to examine potential effects of homoplasy on the resulting tree topology (see Chapter Four, Methods).

NON-NEURAL SPINE CHARACTERS (1-124):

Characters 1-90: General synapsid and sphenacodontian characters of Reisz, Berman, and Scott (1992)

1. Skull and mandible high (0) or low and narrow (1). (RBS1992, 1)
2. Snout short (0) elongate (1). (RBS1992, 2)
3. Premaxilla ventral edge straight (0), sloping anteroventrally (1), or sloping anterodorsally (2). (RBS1992, 3)
4. Premaxilla with (0) or without (1) palatal process. (RBS1992, 4)
5. Premaxilla short (0), long and slender (1), wide (2), or robust (3). (RBS1992, 5)
6. Septomaxilla small inside naris (0) or large and superficial (1). (RBS1992, 6)
7. Nasal shorter or subequal (0) or longer (1) than frontal. (RBS1992, 7)
8. Nasal without (0) or with (1) posteroventral narial process. (RBS1992, 8)
9. Prefrontal without (0) or with (1) antorbital recess. (RBS1992, 9)
10. Nasal-maxillary suture absent (0), present but very short (1), or extensive, longer than nasal-lacrimal suture (2). (RBS1992, 10)
11. Frontal orbital lappet absent (0), present but small (1), or extends far laterally (2). (RBS1992, 11)
12. Frontal anterior and posterior process subequal in width (0) or anterior process narrower (1). (RBS1992, 12)
13. Frontal with very short (0) or long (1) anterior process. (RBS1992, 13)
14. Parietal equal to 1/4 skull roof length (0) or reduced in length (1). (RBS1992, 14)
15. Parietal narrow (0) or with broad posterolateral wing (1). (RBS1992, 15)
16. Parietal lateral edge concave or straight (0) or convex (1). (RBS1992, 16)
17. Pineal foramen 1/5 or more of parietal width (0) or less than 1/5 of parietal width (1). (RBS1992, 17)
18. Postfrontal with straight postorbital suture (0) or incised posteriorly by postorbital (1). (RBS1992, 18)
19. Pineal ridge absent (0) or present (1). (RBS1992, 19)
20. Postorbital-supratemporal contact present (0), narrowly separated (1), or wide separation (2). (RBS1992, 20)
21. Postorbital lateral surface flat (0), gently recessed (1), or strongly recessed (2). (RBS1992, 21)
22. Postorbital posterior process broad (0) or narrow (1) in dorsal view. (RBS1992, 22)
23. Postorbital region relative to preorbital length subequal (0) or preorbital longer (1). (RBS1992, 23)

24. Postparietal paired (0) or fused (1). (RBS1992, 24)
25. Maxilla ventral margin straight (0), gently convex (1), or strongly convex (2). (RBS1992, 25)
26. Posterior tip of maxilla anterior to postorbital bar (0) or beyond postorbital bar (1). (RBS1992, 26)
27. Maxilla supracanine buttress absent (0), present (1), or present with ascending process (2). (RBS1992, 27)
28. Maxilla preorbital dorsal process absent (0) or present (1). (RBS1992, 28)
29. Narial opening enlarged anteroposteriorly (0) or small (1). (RBS1992, 29; primitive/derived states reversed)
30. Lacrimal contacts (0) or excluded from (1) naris. (RBS1992, 30)
31. Jugal excluded from ventral edge of skull (0), narrow contribution to ventral edge (1), or wide contribution (2). (RBS1992, 31)
32. Jugal suborbital process narrow anteriorly (0) or expanded anterodorsally (1). (RBS1992, 32)
33. Quadratojugal anterior process long (0) or absent (1). (RBS1992, 33)
34. Squamosal excluded from (0) or contributes to (1) zygomatic arch. (RBS1992, 34)
35. Ventral margin of postorbital region straight (0) or concave (1). (RBS1992, 35)
36. Pterygoid anterior process with low (0) or high (1) dorsal flange. (RBS1992, 36)
37. Pterygoid quadrate process with (0) or without (1) medial shelf. (RBS1992, 37)
38. Pterygoid quadrate process short (0) or long (1). (RBS1992, 38)
39. Stapes dorsal process free (0), attaches to paroccipital process (1), or absent (2). (RBS1992, 39)
40. Stapes dorsal process slender (0), broad (1), or absent (2). (RBS1992, 40)
41. Stapes rod-like (0) or blade-like (1) shaft. (RBS1992, 41)
42. Basicranial articulation level with pterygoid transverse flange (0) or posterior to transverse flange (1). (RBS1992, 42)
43. Basisphenoid tubera large and laterally oriented (0), small anterolaterally (1), or small anteriorly (2). (RBS1992, 43)
44. Parasphenoid plate broad (0), narrow (1), or narrow with deep median groove (2). (RBS1992, 44)
45. Parasphenoid plate posterior accessory shelf dentigerous (0), small edentulous shelf (1), or no shelf (2). (RBS1992, 45)
46. Paroccipital process of opisthotic extends horizontally (0) or ventrolaterally (1). (RBS1992, 46)
47. Paroccipital process of opisthotic extends laterally (0) or posteriorly (1). (RBS1992, 47)
48. Paroccipital process of opisthotic broad and blade-like (0), narrow and blade-like (1), or narrow and rod-like (2). (RBS1992, 48)
49. Lateral mandibular fenestra absent (0) or present (1). (RBS1992, 49)
50. Ventral edge of angular ridged (0) or keeled (1). (RBS1992, 50)
51. Coronoid region of mandible gently convex (0) or strongly convex (1). (RBS1992, 51)
52. Prearticular nearly straight (0) or twisted posteriorly (1). (RBS1992, 52)
53. Pterygoideus process formed by articular and prearticular (0) or mainly by articular, sheathed by prearticular (1). (RBS1992, 53; Edaphosaurus modified from '0' to '1')
54. Angular reflected lamina absent (0) or present (1). (RBS1992, 54)

55. Angular ventral lamina gently convex (0) or strongly convex posteriorly (1). (RBS1992, 55)
56. Retroarticular process composite (0) or formed by articular (1). (RBS1992, 56)
57. Retroarticular process horizontal (0) or curved ventrally (1). (RBS1992, 57)
58. Marginal dentition without (0) or with (1) anterior and posterior cutting edges. (RBS1992, 58)
59. Canine length less than (0) or greater than (1) two times other maxillary teeth. (RBS1992, 59)
60. Premaxillary teeth small (0), first large (1), or all large (2). (modified from RBS1992, 60)
61. Anterior dentary teeth small (0), second large (1), or all large (2). (RBS1992, 61)
62. Precanine maxillary teeth: More than 5 (0) five or less (1), or none (2). (modified from RBS1992, 62 and SH1998, 110)
63. Premaxillary teeth five or more (0) or less than five (1). (RBS1992, 63)
64. Vomerine teeth present (0) or absent (1). (RBS1992, 64)
65. Ectopterygoid teeth present (0) or absent (1). (RBS1992, 65)
66. Pterygoid teeth arranged in three (0) or two (1) groups. (RBS1992, 66)
67. Intercentrum 1 and 2 in contact ventrally (0) or separated by atlas pleurocentrum (1). (RBS1992, 67)
68. Cervical centra ridged (0) or keeled (1) ventrally. (RBS1992, 69)
69. Cervical centra equal (0), longer (1), or shorter (2) than dorsal centra. (RBS1992, 70)
70. Dorsal centra ridged (0) or keeled (1) ventrally. (RBS1992, 71)
71. Sacral vertebrae two or less (0) or at least three (1). (RBS1992, 72)
72. Neural arches not excavated laterally (0), shallow excavation (1), or deep excavation (2). (RBS1992, 79)
73. Scapula broad (0) or narrow distally (1). (RBS1992, 80)
74. Scapula broad (0) or narrow at base (1). (RBS1992, 81)
75. Supraglenoid foramen on posterior surface (0), on lateral surface of scapula (1), or absent (2). (RBS1992, 82)
76. Posterior coracoid triceps process small (0) or enlarged (1). (RBS1992, 83)
77. Limbs short and stout (0) or long and slender (1). (RBS1992, 84)
78. Humerus deltopectoral ridge double (0) or single (1). (RBS1992, 85)
79. Ulna olecranon broad (0), narrow and elongate (1), or small (2). (RBS1992, 86)
80. Ilium dorsal groove present (0) or absent (1). (RBS1992, 87)
81. Ilium posterior process long, extending to posterior limit of ischium (0) or short (1). (RBS1992, 88)
82. Ilium anterodorsal process absent (0) or present (1). (RBS1992, 89; Edaphosaurus modified from '0' to '1')
83. Pubis lateral tubercle present (0) or absent (1). (RBS1992, 90)
84. Ischium slender distally (0) or expanded distally (1). (RBS1992, 91)
85. Femur intertrochanteric fossa prominent (0), reduced (1), or absent (2). (RBS1992, 92)
86. Femoral ventral ridge system prominent (0) or reduced (1). (RBS1992, 93)
87. Fibula distal head/shaft diameter less than 3/1 (0) or equal or greater than 3/1 (1). (RBS1992, 94)
88. Astragalus proximal neck region short (0) or long (1). (RBS1992, 95)

89. Calcaneum width and length subequal (0) or length greater than width (1). (RBS1992, 96)
90. Lateral centrale present (0) or absent (1). (RBS1992, 97)

Characters 91-96: Relevant edaphosaurid characters from Modesto (1995). Redundant characters listed above from RBS1992 have been omitted below.

91. Premaxillary dentition larger than (0) or equal to or smaller than (1) maxillary teeth in basal cross-section. (M1995, 3)
92. Caniniform region present (0) or absent (1). (M1995, 4)
93. Caniniform tooth/teeth present (0) or absent (1). (M1995, 5; primitive/derived states corrected)
94. Prefrontal ventral process tongue-like (0) or expanded medially (1). (M1995, 8)
95. Pterygoid transverse flange present (0) or absent (1). (M1995, 18)
96. Ilium anterodorsal process smaller than posterodorsal process and convex in lateral view (0) or equal to posterodorsal process size and triangular in lateral view (1). (M1995, 36)

Characters 97-124: Relevant sphenacodontian and therapsid characters adapted from Laurin (1993) and Sidor and Hopson (1998). Redundant characters listed above from RBS1992 have been omitted below.

97. Premaxilla internarial process short (0) or long (1). (L1993, 2; SH1998, 1)
98. Maxilla contact with prefrontal absent (0) or present (1). (L1993, 27; SH1998, 8)
99. Maxillary tooth row posterior extent under orbit (0) or anterior to orbit (1). (SH1998, 10)
100. Temporal fenestra muscle attachment on border of lateral fenestra absent (0) or present (1). (SH1998, 15)
101. Supratemporal bone present (0) or absent (1). (L1993, 24; SH1998, 22)
102. Vomer internarial shape slightly wide posteriorly (0) or widest near middle (1). (SH1998, 23)
103. Vomer ventral surface flat to convex (0) or bears lateral ridges with median trough (1). (SH1998, 24)
104. Bosses or ridges on palate absent (0) or present (1). (SH1998, 35)
105. Squamosal external auditory meatus absent (0) or present and shallow (1). (L1993, 37; SH1998, 52)
106. Quadrate contact primarily with paroccipital process (0) or equally with paroccipital process and squamosal (1). (SH1998, 58)
107. Basicranial joint unfused (0) or fused (1). (L1993, 39; SH1998, 68)
108. Splenial exposed medially and laterally (0) or confined medially (1). (SH1998, 90)
109. Posterior emargination of angular reflected lamina short (0) or long (1). (L1993, 56; SH1998, 96)
110. Shape of articular glenoid: longitudinal troughs (0), elongate oblique troughs (1), or screw-shaped hinge (2). (SH1998, 101)
111. Enlarged dentary tooth absent (0), present at anterior most position (1), or present in caniniform position (2). (L1993, 72; SH1998, 107)
112. Postcanines number 12 or greater (0) or fewer than 12 (1). (L1993, 73; SH1998, 112)

- 113. Vertebral type notochordal (0) or amphicoelous (1). (L1993, 85; SH1998, 123)
- 114. Glenoid elongate and screw-shaped (0) or rounded and facing posterolaterally (1). (SH1998, 131)
- 115. Humerus supinator process present (0) or absent (1). (SH1998, 142)
- 116. Humeral head broad and strap-like (0) or elongate and oval (1). (SH1998, 144)
- 117. Manual intermedium size relative to lateral centrale larger (0) or smaller (1). (SH1998, 150)
- 118. Manual digit III, second phalanx long (0) or reduced/absent (1). (SH1998, 152)
- 119. Acetabulum shape irregular oval (0) or circular (1). (L1993, 108; SH1998, 159)
- 120. Acetabulum depth shallow (0) or deep (1). (L1993, 109; SH1998, 160)
- 121. Femoral head terminal (0) or inflected medially (1). (L1993, 114; SH1998, 167)
- 122. Femoral head articular shape elongate and irregular (0) or oval (1). (SH1998, 168)
- 123. Femur posterior condyle extends more distally (0) or subequal (1) to anterior condyle. (L1993, 115; SH1998, 169)
- 124. Greater trochanter absent (0) or present (1). (SH1998, 170)

NEURAL SPINE CHARACTERS (125-136):

Neural spine characters from RBS1992 (125-130), M1995 (126, 127, 129, 131-132), and present study (133-136).

- 125. Axis neural spine expanded anteroposteriorly (0) or narrow dorsally (1). (RBS1992, 68)
- 126. Presacral neural spines short (0), elongated more than three times (1) or more than five times (2) the height of the centrum. (modified from RBS1992, 73,74; M1995, 24)
- 127. Neural spines flattened or blade-like (0) or laterally expanded (1) in cross-section. (modified from RBS1992, 75; M1995, 25)
- 128. Neural spine "shoulders" absent (0) or present (1). (RBS1992, 76)
- 129. Neural spine lateral tubercles absent (0) or present (1). (RBS1992, 77; M1995, 26)
- 130. Neural spine anterior and posterior groove absent (0), present but shallow (1), or forms a deep fissure (2). (modified from RBS1992, 78)
- 131. Anterior presacral neural spines extend dorsally (0) or curve anteriorly (1). (M1994, 27)
- 132. Posterior presacral neural spines extend dorsally (0) or curve posteriorly (1). (modified from M1994, 28)
- 133. Prominent paired "horns" bounding the median groove in proximal region of neural spine absent (0) or present (1). (New character)
- 134. Pronounced longitudinal vascular striations are absent (0) or present laterally (1) on the periosteal surface of the neural spine. (New character)
- 135. Medullary region of neural spine occupied by dense trabeculae (0) or trabeculae largely absent, instead forming a cavity (1). (New character)

136. Central cavity of neural spine with a gradual transition from the cortex (0) or distinctly separated from cortex by smooth endosteal bone. (New character; sphenacodontids are coded '?' where this character is known, as they do not possess a central cavity)

APPENDIX F
CHARACTER MATRIX

Data matrix (cont.)

	00000000011
	999999999000000000111111111122222222223333333
	1234567890123456789012345678901234567890123456
caseasauria	000??
varanopidae	00000000000000100000000000000000000000000000??
ophiacodont	00000010000000000000000000000000000000000000??
lupeosaurus	?????1??????????0???00???000000?21001?10010
ianthasaurus	?00?1?000????0???0?000010??00????021011110011
glaucosaurus	11111?0000??????00?00??????????????????????
edaphosaurus	1111110000000000000000100000000002111110011
haptodus	0000000000000000110000000000000000000000000??
biarmosuchus	00000111111111111122111111111111110000000000??
dinocephalia	00000111111111111122111111111111110000000000??
ctenorrhachis	?????00??????????????0????00?????10000001??
s_ferox	000000010000000001100000000000011000000010?
s_ferosior	000000010000000001100000000000011000000010?
ctenospondyl	00000001000000000?100000??000001201000101??
dimetrodon	00000001000000000110000000000012110201110?
secodonto	000000010000000001100000??000001211020?0???

APPENDIX G

MEAN PAIRWISE DISSIMILARITY BASED ON DISTANCE ANALYSIS OF
CHARACTER DATA

APPENDIX G. Mean pairwise dissimilarity based on distance analysis of character data (Appendix F). Pairwise distances derived from distance matrix analyzed in PAUP 4.0b.

Ingroup pairs	Mean pairwise dissimilarity
<i>Sphenacodon - Dimetrodon</i>	0.05185
<i>Sphenacodon - Lupeosaurus</i>	0.41667
<i>Sphenacodon - Ianthasaurus</i>	0.55422
<i>Sphenacodon - Edaphosaurus</i>	0.54545
<i>Dimetrodon - Lupeosaurus</i>	0.38889
<i>Dimetrodon - Ianthasaurus</i>	0.54217
<i>Dimetrodon - Edaphosaurus</i>	0.52273
<i>Lupeosaurus - Ianthasaurus</i>	0.17857
<i>Lupeosaurus - Edaphosaurus</i>	0.18919
<i>Ianthasaurus - Edaphosaurus</i>	0.06024

APPENDIX H
BENDING RIGIDITY DISSIMILARITY

APPENDIX H. Bending rigidity dissimilarity between ingroup pairs calculated from Appendix D.

Ingroup pairs	Bending rigidity dissimilarity (proximal)
<i>Sphenacodon - Dimetrodon</i>	0.20
<i>Sphenacodon - Lupeosaurus</i>	0.31
<i>Sphenacodon - Edaphosaurus</i>	0.51
<i>Dimetrodon - Lupeosaurus</i>	0.51
<i>Dimetrodon - Edaphosaurus</i>	0.31
<i>Lupeosaurus - Edaphosaurus</i>	0.82

Ingroup pairs	Bending rigidity dissimilarity (distal)
<i>Sphenacodon - Dimetrodon</i>	0.81
<i>Sphenacodon - Lupeosaurus</i>	2.92
<i>Sphenacodon - Ianthasaurus</i>	2.81
<i>Sphenacodon - Edaphosaurus</i>	2.88
<i>Dimetrodon - Lupeosaurus</i>	2.11
<i>Dimetrodon - Ianthasaurus</i>	2.00
<i>Dimetrodon - Edaphosaurus</i>	2.07
<i>Lupeosaurus - Ianthasaurus</i>	0.11
<i>Lupeosaurus - Edaphosaurus</i>	0.04
<i>Ianthasaurus - Edaphosaurus</i>	0.07

APPENDIX I
BONE DENSITY DISSIMILARITY

APPENDIX I. Bone density dissimilarity between ingroup pairs calculated from Appendix D.

Ingroup pairs	Bone density dissimilarity (proximal)
<i>Sphenacodon - Dimetrodon</i>	0.17
<i>Sphenacodon - Lupeosaurus</i>	0.05
<i>Sphenacodon - Edaphosaurus</i>	0.05
<i>Dimetrodon - Lupeosaurus</i>	0.22
<i>Dimetrodon - Edaphosaurus</i>	0.12
<i>Lupeosaurus - Edaphosaurus</i>	0.10

Ingroup pairs	Bone density dissimilarity (distal)
<i>Sphenacodon - Dimetrodon</i>	0.16
<i>Sphenacodon - Lupeosaurus</i>	0.04
<i>Sphenacodon - Ianthasaurus</i>	0.19
<i>Sphenacodon - Edaphosaurus</i>	0.21
<i>Dimetrodon - Lupeosaurus</i>	0.20
<i>Dimetrodon - Ianthasaurus</i>	0.03
<i>Dimetrodon - Edaphosaurus</i>	0.05
<i>Lupeosaurus - Ianthasaurus</i>	0.23
<i>Lupeosaurus - Edaphosaurus</i>	0.25
<i>Ianthasaurus - Edaphosaurus</i>	0.02

APPENDIX J
CORTICAL POROSITY DISSIMILARITY

APPENDIX J. Cortical porosity dissimilarity between ingroup pairs calculated from Appendix D.

Ingroup pairs	Cortical porosity dissimilarity (proximal)
<i>Sphenacodon - Dimetrodon</i>	0.085
<i>Sphenacodon - Lupeosaurus</i>	0.065
<i>Sphenacodon - Edaphosaurus</i>	0.065
<i>Dimetrodon - Lupeosaurus</i>	0.150
<i>Dimetrodon - Edaphosaurus</i>	0.150
<i>Lupeosaurus - Edaphosaurus</i>	0.000

Ingroup pairs	Cortical porosity dissimilarity (distal)
<i>Sphenacodon - Dimetrodon</i>	0.076
<i>Sphenacodon - Lupeosaurus</i>	0.009
<i>Sphenacodon - lanthasaurus</i>	0.044
<i>Sphenacodon - Edaphosaurus</i>	0.047
<i>Dimetrodon - Lupeosaurus</i>	0.085
<i>Dimetrodon - lanthasaurus</i>	0.120
<i>Dimetrodon - Edaphosaurus</i>	0.123
<i>Lupeosaurus - lanthasaurus</i>	0.035
<i>Lupeosaurus - Edaphosaurus</i>	0.038
<i>lanthasaurus - Edaphosaurus</i>	0.003

APPENDIX K

RELATIVE BONE WALL THICKNESS (RBT) DISSIMILARITY

APPENDIX K. Relative bone wall thickness (RBT) dissimilarity between ingroup pairs calculated from Appendix D.

Ingroup pairs	RBT dissimilarity (proximal)
<i>Sphenacodon - Dimetrodon</i>	0.000
<i>Sphenacodon - Lupeosaurus</i>	0.020
<i>Sphenacodon - Edaphosaurus</i>	0.008
<i>Dimetrodon - Lupeosaurus</i>	0.020
<i>Dimetrodon - Edaphosaurus</i>	0.008
<i>Lupeosaurus - Edaphosaurus</i>	0.012

Ingroup pairs	RBT dissimilarity (distal)
<i>Sphenacodon - Dimetrodon</i>	0.098
<i>Sphenacodon - Lupeosaurus</i>	0.059
<i>Sphenacodon - Ianthasaurus</i>	0.139
<i>Sphenacodon - Edaphosaurus</i>	0.107
<i>Dimetrodon - Lupeosaurus</i>	0.039
<i>Dimetrodon - Ianthasaurus</i>	0.041
<i>Dimetrodon - Edaphosaurus</i>	0.009
<i>Lupeosaurus - Ianthasaurus</i>	0.080
<i>Lupeosaurus - Edaphosaurus</i>	0.043
<i>Ianthasaurus - Edaphosaurus</i>	0.032

APPENDIX L
PARSIMONY ANALYSIS INPUT FILE

APPENDIX M

PARSIMONY ANALYSIS OUTPUT FILE (WITH SPINE DATA)

APPENDIX M. Parsimony analysis output file from cladistic analysis ran with complete dataset (characters 1-136) in PAUP 4.0b (Swofford, 1999).

P A U P *

Version 4.0b10 for Macintosh (PPC/Altivec)

Tuesday, January 22, 2008 3:04 PM

Outgroup status changed:

2 taxa transferred to outgroup

Total number of taxa now in outgroup = 2

Number of ingroup taxa = 14

Branch-and-bound search settings:

.Optimality criterion = parsimony

Character-status summary:

Of 136 total characters:

All characters are of type 'unord'

All characters have equal weight

5 characters are parsimony-uninformative

Number of parsimony-informative characters = 131

Initial upper bound: unknown (compute heuristically)

Addition sequence: furthest

Initial 'MaxTrees' setting = 100

Branches collapsed (creating polytomies) if maximum branch length is zero

'MulTrees' option in effect

Topological constraints not enforced

Trees are unrooted

Branch-and-bound search completed:

Score of best tree found = 209

Number of trees retained = 2

Time used = 0.00 sec

Tree description:

Unrooted tree(s) rooted using outgroup method

Optimality criterion = parsimony

Character-status summary:

Of 136 total characters:

All characters are of type 'unord'

All characters have equal weight

5 characters are parsimony-uninformative

Number of parsimony-informative characters = 131

Character-state optimization: Accelerated transformation (ACCTRAN)

Tree number 1 (rooted using user-specified outgroup)

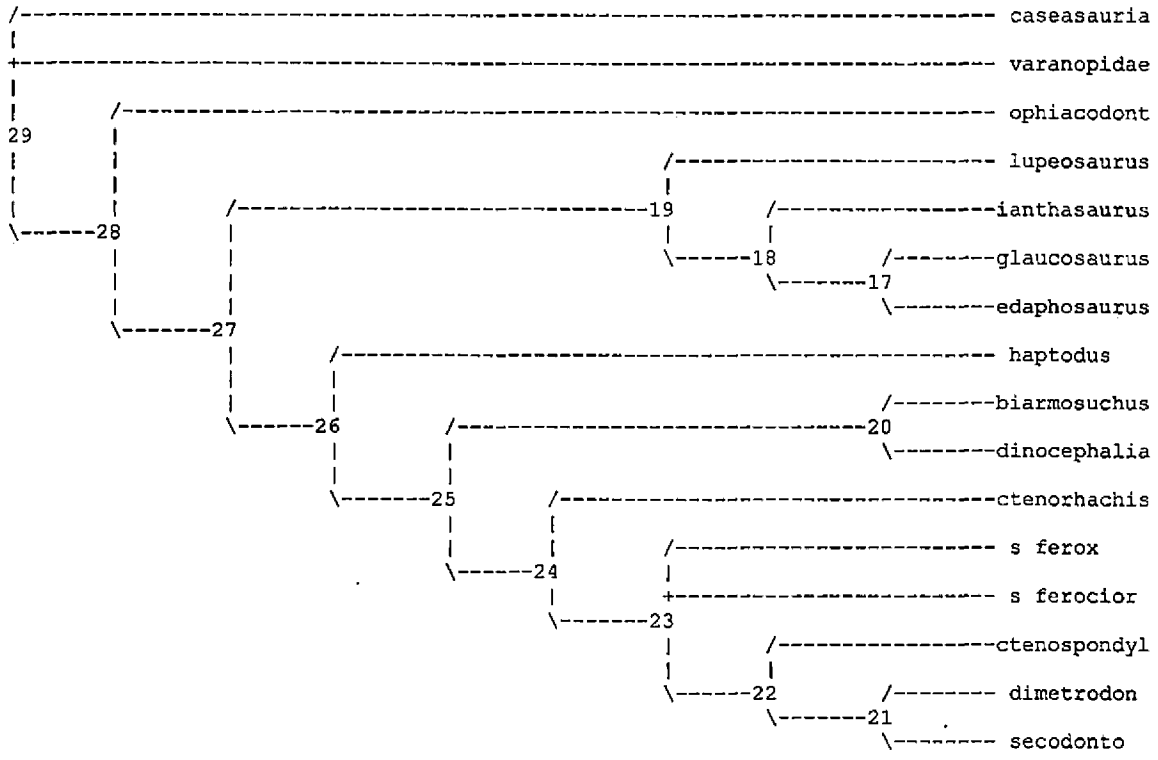
Tree length = 209

Consistency index (CI) = 0.7799

Homoplasy index (HI) = 0.2201

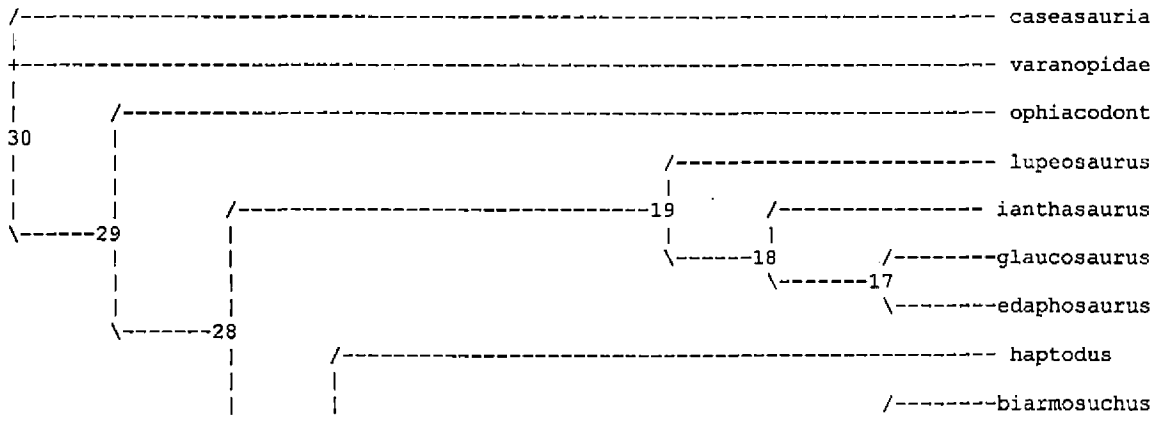
CI excluding uninformative characters = 0.7745

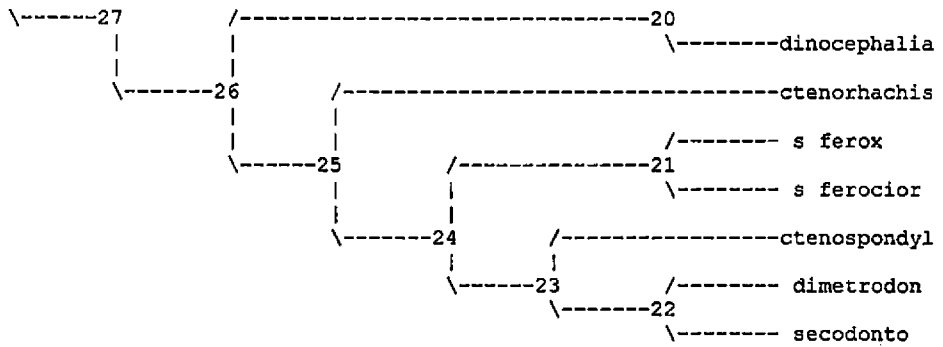
HI excluding uninformative characters = 0.2255
 Retention index (RI) = 0.8824
 Rescaled consistency index (RC) = 0.6882



Tree number 2 (rooted using user-specified outgroup)

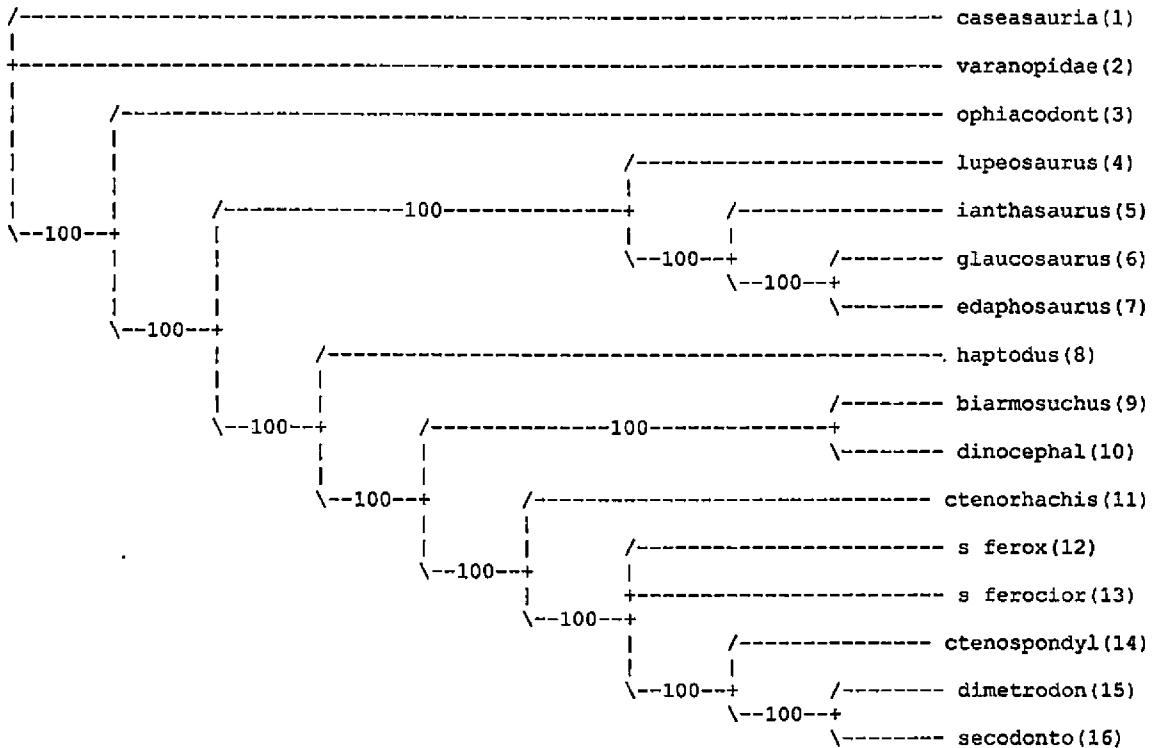
Tree length = 209
 Consistency index (CI) = 0.7799
 Homoplasy index (HI) = 0.2201
 CI excluding uninformative characters = 0.7745
 HI excluding uninformative characters = 0.2255
 Retention index (RI) = 0.8824
 Rescaled consistency index (RC) = 0.6882





2 trees saved to file "spines_Jan22_parsi_all.tre"

50% Majority-rule consensus of 2 trees



Statistics derived from consensus tree:

Component information (consensus fork) = 12 (normalized = 0.923)
 Nelson-Platnick term information = 59
 Nelson-Platnick total information = 71
 Mickevich's consensus information = 0.714
 Colless weighted consensus fork (proportion max. information) = 0.683
 Schuh-Farris levels sum = 0 (normalized = 0.000)
 Rohlf's CI(1) = 0.952
 Rohlf's -ln CI(2) = 31.896 (CI(2) = 1.41e-14)

Bipartitions found in one or more trees and frequency of occurrence:

1 1 1234567890123456	Freq	%
..*****	2	100.0%
...*****	2	100.0%
...****	2	100.0%
....***	2	100.0%
.....**	2	100.0%
.....*****	2	100.0%
.....*****	2	100.0%
.....**	2	100.0%
.....*****	2	100.0%
.....*****	2	100.0%
.....***	2	100.0%
.....**	2	100.0%
.....**...	1	50.0%

Consensus tree(s) written to treefile: spines_Jan22_parsicon.trees

Bootstrap method with heuristic search:

Number of bootstrap replicates = 100

Starting seed = 523736323

Optimality criterion = parsimony

Character-status summary:

Of 136 total characters:

All characters are of type 'unord'

All characters have equal weight

5 characters are parsimony-uninformative

Number of parsimony-informative characters = 131

Starting tree(s) obtained via stepwise addition

Addition sequence: simple (reference taxon = caseasauria)

Number of trees held at each step during stepwise addition = 1

Branch-swapping algorithm: tree-bisection-reconnection (TBR)

Steepest descent option not in effect

Initial 'MaxTrees' setting = 100

Branches collapsed (creating polytomies) if maximum branch length is zero

'MulTrees' option in effect

Topological constraints not enforced

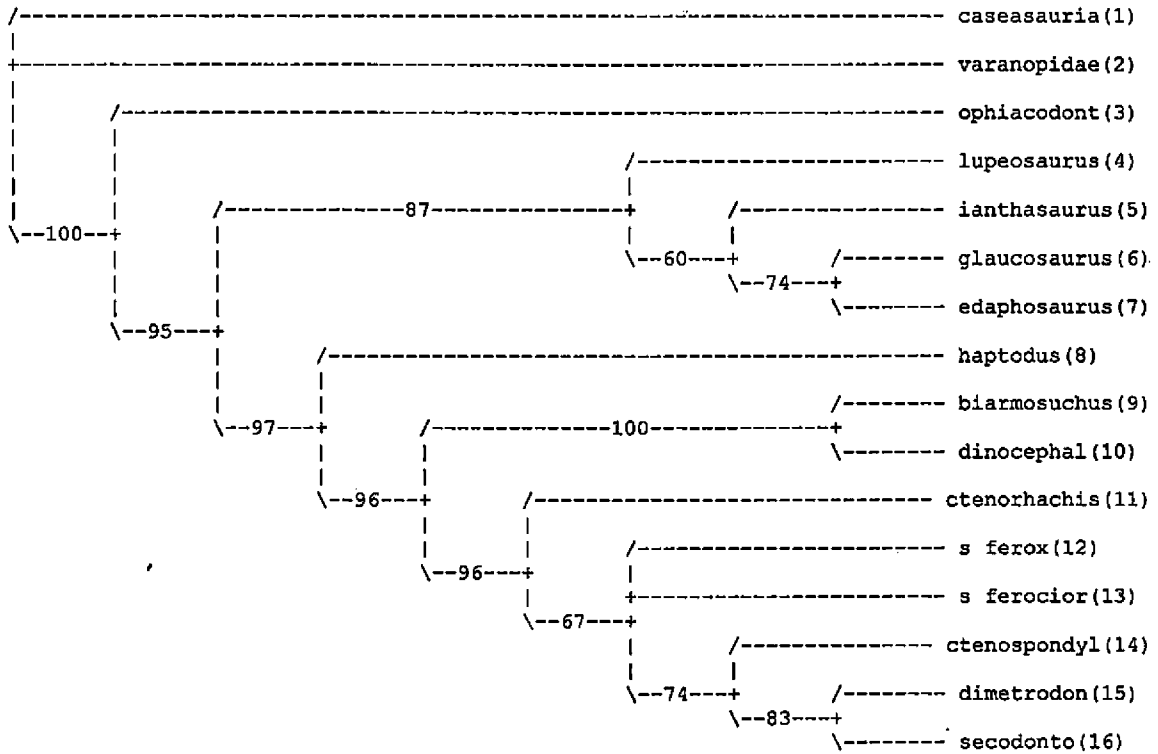
Trees are unrooted

100 bootstrap replicates completed

Note: Effectiveness of search may have been diminished due to tree-buffer overflow.

Time used = 3.00 sec

Bootstrap 50% majority-rule consensus tree



Bipartitions found in one or more trees and frequency of occurrence (bootstrap support values):

1	1	Freq
1234567890123456		
.....**.....		100.00
..*****		99.50
.....*****		96.90
.....*****		96.35
.....*****		95.94
..*****		94.82
....****		86.52
.....**		82.68
.....**		74.36
.....***		74.17
.....*****		67.03
.....***		60.21
.....**		27.82
..*..**		22.69
.....***		21.30
.....****		10.28
.....****		9.25

...*.*.*****	8.53
...**.*****	8.49
...*.*****	8.20
...**.*****	7.73
...**.*****	7.17
.....*****	7.14
...*.*****	6.30
.....**.	6.10

23 groups at (relative) frequency less than 5% not shown

APPENDIX N

PARSIMONY ANALYSIS OUTPUT FILE (WITHOUT SPINE DATA)

APPENDIX N. Parsimony analysis output file from cladistic analysis ran with characters 1-124, excluding neural spine characters.

P A U P *

Version 4.0b10 for Macintosh (PPC/Altivec)
Tuesday, January 22, 2008 2:51 PM

Outgroup status changed:

2 taxa transferred to outgroup
Total number of taxa now in outgroup = 2
Number of ingroup taxa = 14

Branch-and-bound search settings:

Optimality criterion = parsimony

Character-status summary:

Of 124 total characters:

All characters are of type 'unord'

All characters have equal weight

3 characters are parsimony-uninformative

Number of parsimony-informative characters = 121

Initial upper bound: unknown (compute heuristically)

Addition sequence: furthest

Initial 'MaxTrees' setting = 100

Branches collapsed (creating polytomies) if maximum branch length is zero

'MulTrees' option in effect

Topological constraints not enforced

Trees are unrooted

Branch-and-bound search completed:

Score of best tree found = 189

Number of trees retained = 5

Time used = 0.02 sec

Tree description:

Unrooted tree(s) rooted using outgroup method

Optimality criterion = parsimony

Character-status summary:

Of 124 total characters:

All characters are of type 'unord'

All characters have equal weight

3 characters are parsimony-uninformative

Number of parsimony-informative characters = 121

Character-state optimization: Accelerated transformation (ACCTRAN)

Tree number 1 (rooted using user-specified outgroup)

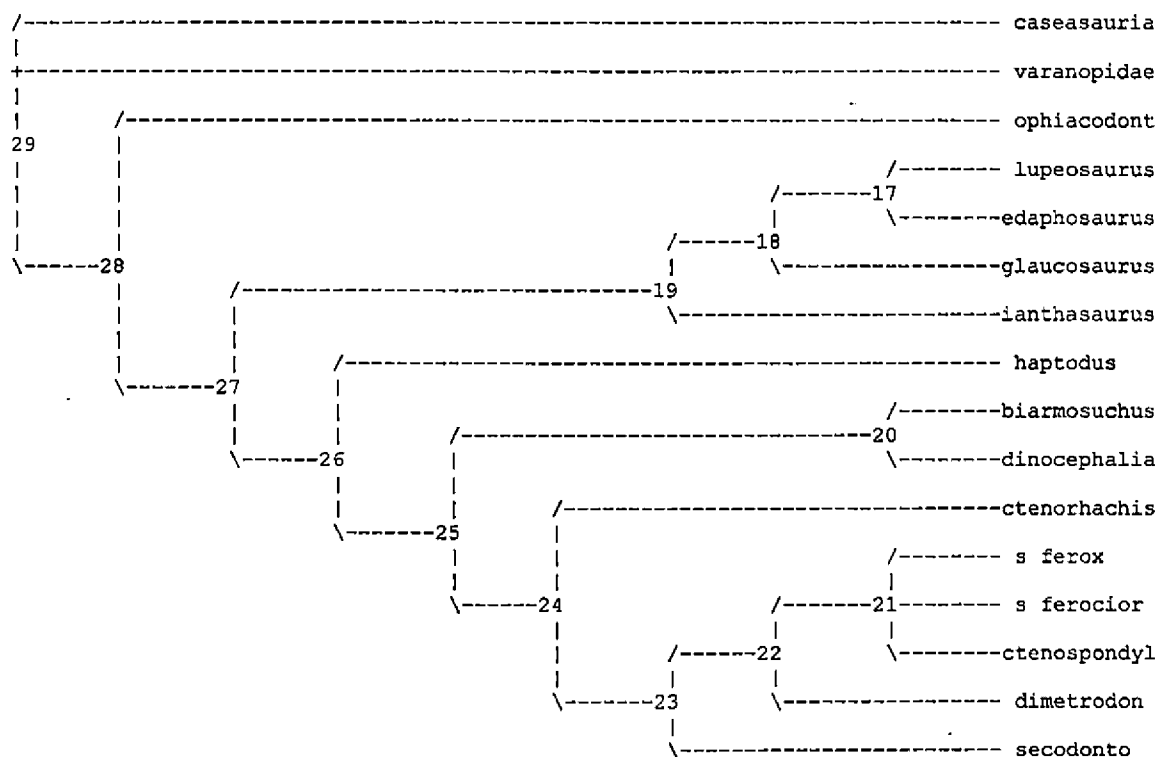
Tree length = 189

Consistency index (CI) = 0.7884

Homoplasy index (HI) = 0.2116

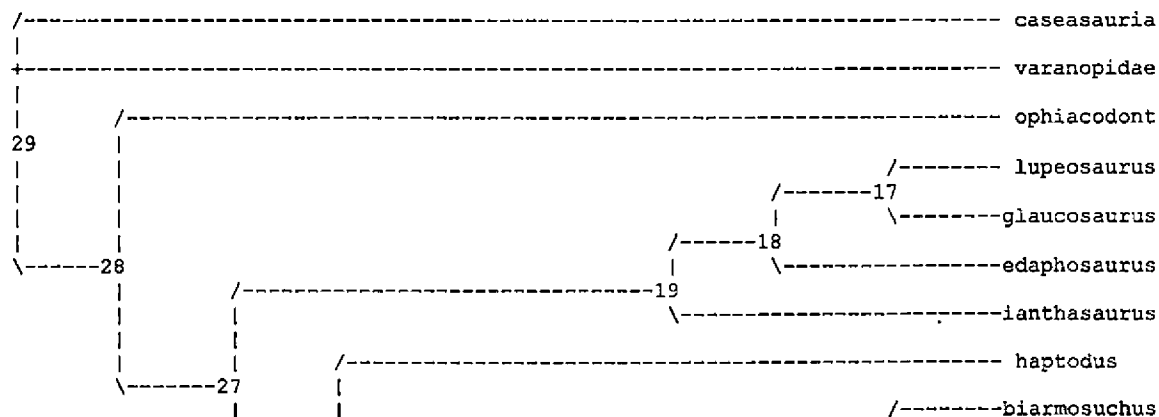
CI excluding uninformative characters = 0.7849

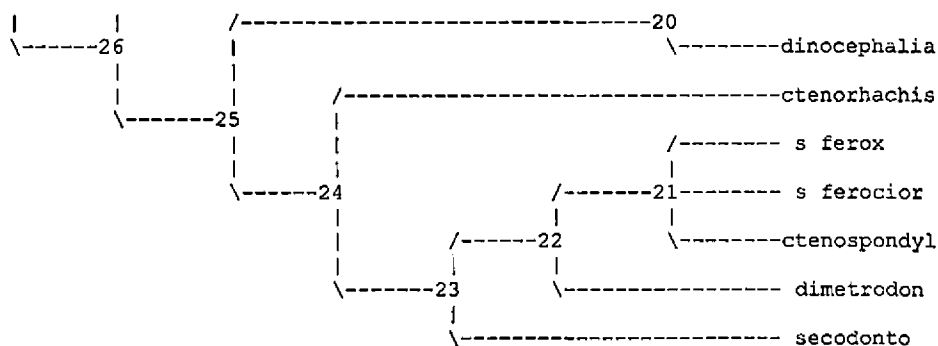
HI excluding uninformative characters = 0.2151
 Retention index (RI) = 0.8883
 Rescaled consistency index (RC) = 0.7003



Tree number 2 (rooted using user-specified outgroup)

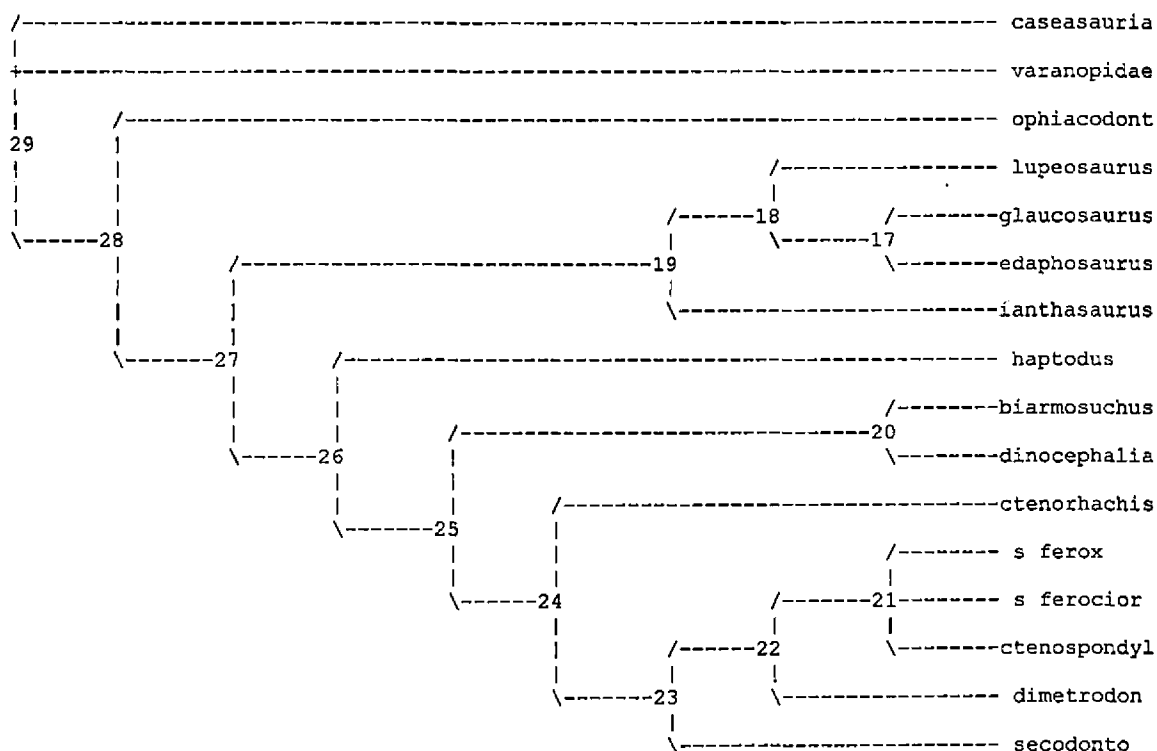
Tree length = 189
 Consistency index (CI) = 0.7884
 Homoplasy index (HI) = 0.2116
 CI excluding uninformative characters = 0.7849
 HI excluding uninformative characters = 0.2151
 Retention index (RI) = 0.8883
 Rescaled consistency index (RC) = 0.7003





Tree number 3 (rooted using user-specified outgroup)

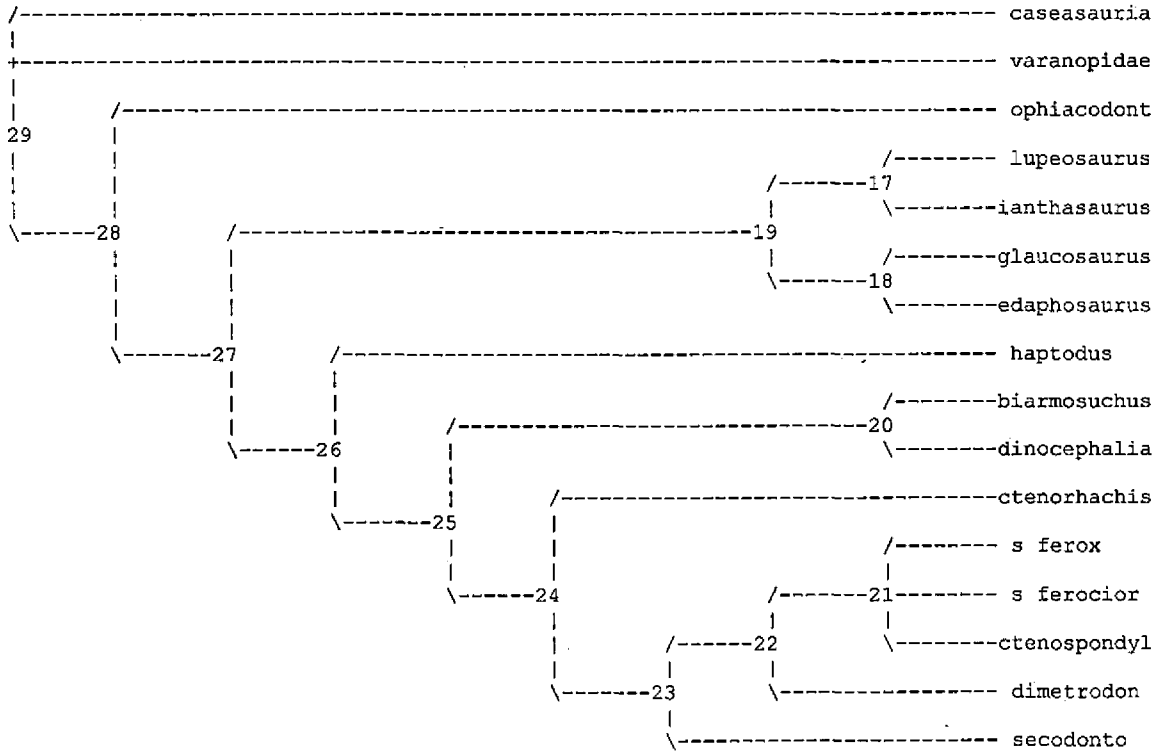
Tree length = 189
 Consistency index (CI) = 0.7884
 Homoplasy index (HI) = 0.2116
 CI excluding uninformative characters = 0.7849
 HI excluding uninformative characters = 0.2151
 Retention index (RI) = 0.8883
 Rescaled consistency index (RC) = 0.7003



Tree number 4 (rooted using user-specified outgroup)

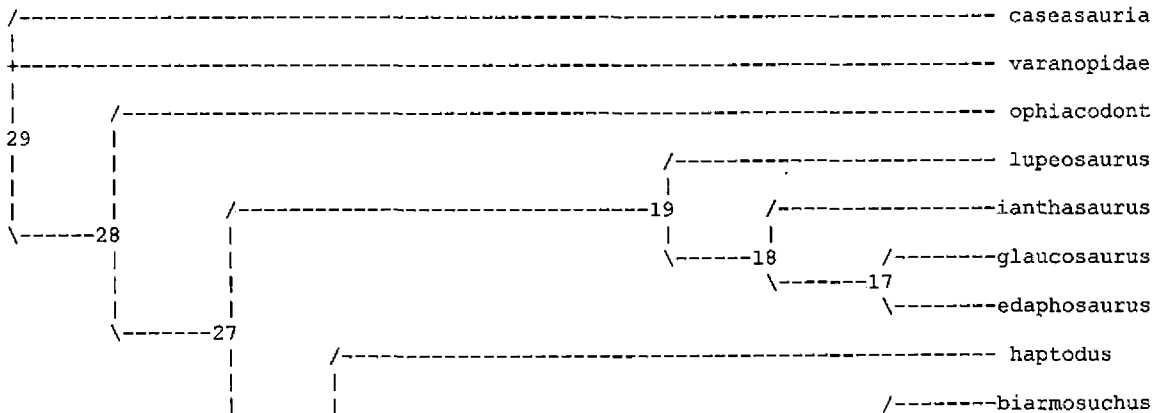
Tree length = 189
 Consistency index (CI) = 0.7884
 Homoplasy index (HI) = 0.2116
 CI excluding uninformative characters = 0.7849

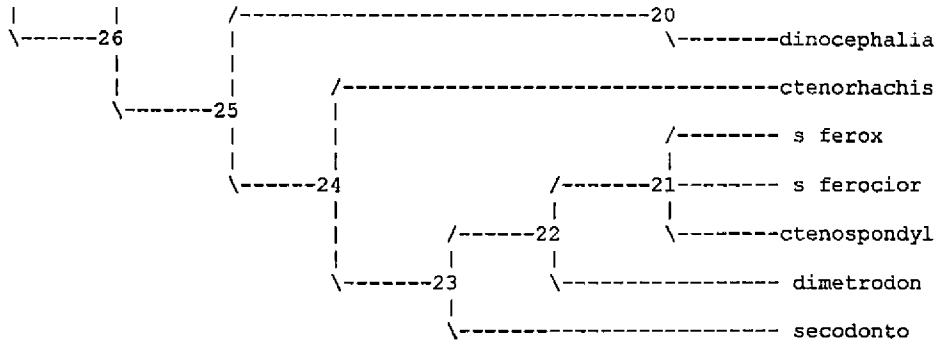
HI excluding uninformative characters = 0.2151
 Retention index (RI) = 0.8883
 Rescaled consistency index (RC) = 0.7003



Tree number 5 (rooted using user-specified outgroup)

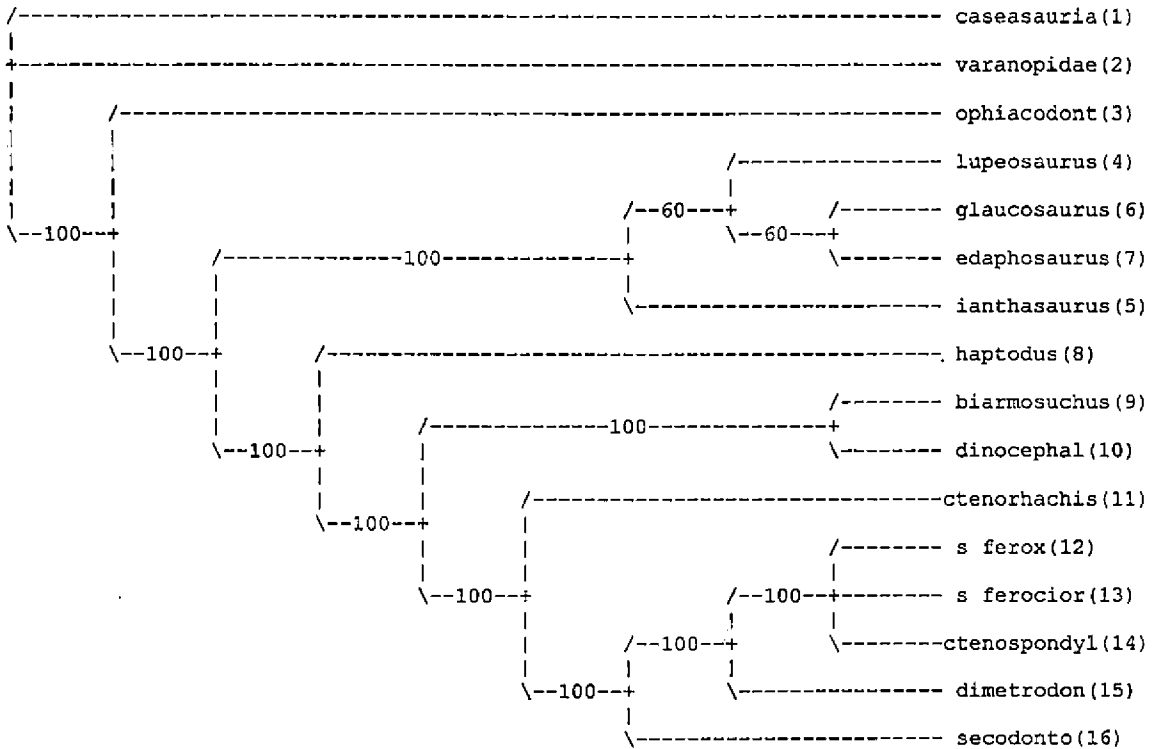
Tree length = 189
 Consistency index (CI) = 0.7884
 Homoplasy index (HI) = 0.2116
 CI excluding uninformative characters = 0.7849
 HI excluding uninformative characters = 0.2151
 Retention index (RI) = 0.8883
 Rescaled consistency index (RC) = 0.7003





5 trees saved to file "nospines_Jan22_parsi_all.tre"

50% Majority-rule consensus of 5 trees



Statistics derived from consensus tree:

Component information (consensus fork) = 12 (normalized = 0.923)
 Nelson-Platnick term information = 61
 Nelson-Platnick total information = 73
 Mickevich's consensus information = 0.755
 Colless weighted consensus fork (proportion max. information) = 0.702
 Schuh-Farris levels sum = 0 (normalized = 0.000)
 Rohlf's CI(1) = 0.984
 Rohlf's -ln CI(2) = 31.896 (CI(2) = 1.41e-14)

Bipartitions found in one or more trees and frequency of occurrence:

1	1	Freq	%
1234567890123456	123456	5	100.0%
..*****		5	100.0%
...*****		5	100.0%
....****		5	100.0%
.....**		5	100.0%
.....*****		5	100.0%
.....*****		5	100.0%
.....*****		5	100.0%
.....***		5	100.0%
.....*****		5	100.0%
.....****		5	100.0%
...*. **		3	60.0%
....**		3	60.0%
...*.*		1	20.0%
...*. *		1	20.0%
...**		1	20.0%
....***		1	20.0%

Consensus tree(s) written to treefile: nospines_Jan22_parscon.trees

Bootstrap method with heuristic search:

Number of bootstrap replicates = 100

Starting seed = 1974373299

Optimality criterion = parsimony

Character-status summary:

Of 124 total characters:

All characters are of type 'unord'

All characters have equal weight

3 characters are parsimony-uninformative

Number of parsimony-informative characters = 121

Starting tree(s) obtained via stepwise addition

Addition sequence: simple (reference taxon = caseasauria)

Number of trees held at each step during stepwise addition = 1

Branch-swapping algorithm: tree-bisection-reconnection (TBR)

Steepest descent option not in effect

Initial 'MaxTrees' setting = 100

Branches collapsed (creating polytomies) if maximum branch length is zero

'MulTrees' option in effect

Topological constraints not enforced

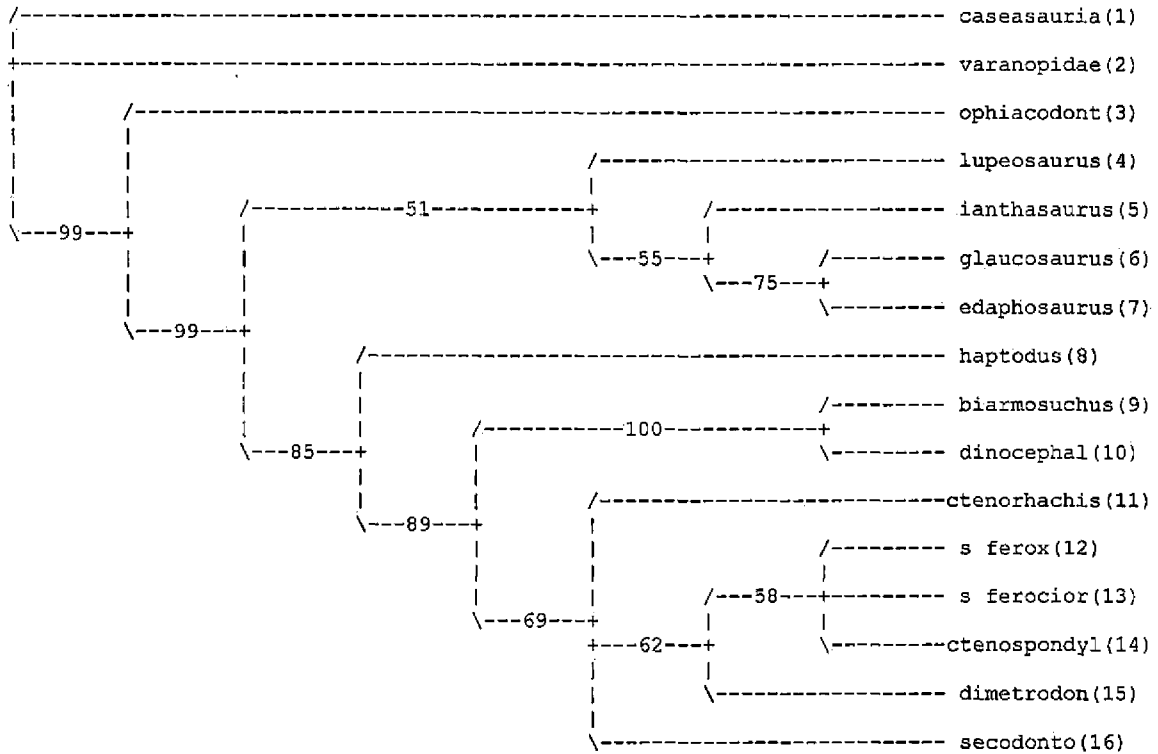
Trees are unrooted

100 bootstrap replicates completed

Note: Effectiveness of search may have been diminished due to tree-buffer overflow.

Time used = 3.90 sec

Bootstrap 50% majority-rule consensus tree



Bipartitions found in one or more trees and frequency of occurrence (bootstrap support values):

1234567890123456	1 1	Freq
.....**.....		100.00
..*****		99.45
...*****		98.66
.....*****		88.55
.....*****		84.80
.....**.....		74.63
.....*****		69.07
.....****.		61.83
.....***.		58.18
.....***		55.43
.....****		50.74
.....*****		48.02
...*.....*		33.10
...*.***		29.52
.....*****.		20.31
.....*****.		19.06
.....***		17.56
...*.....*		14.11
...*****		13.71

...*. *	10.48
.....****.	9.76
...*.....*****	9.70
...*.*.....	9.44
...**.....	8.63
.....*.*	8.37
.....**.*	5.70

26 groups at (relative) frequency less than 5% not shown

APPENDIX O
BAYESIAN ANALYSIS INPUT FILE

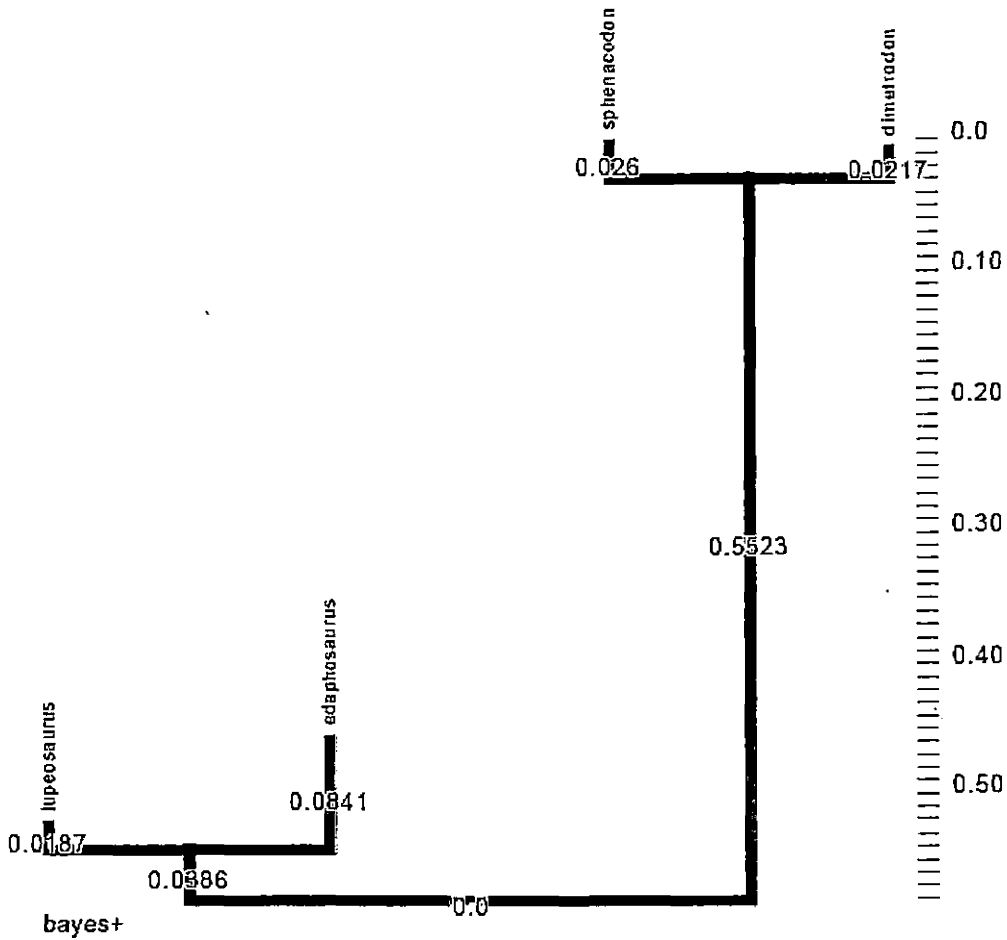

```
end;
```

```
begin mrbayes;
```

```
log start filename=spinebayes.log replace;  
lset rates = gamma;  
outgroup 1;  
constraint edaphosauridae -1 = 2 3 4;  
prset topologypr=constraints(edaphosauridae);  
mcmc ngen=5000000 printfreq=1000 samplefreq=100  
nchains=4 savebrlens=yes filename=spinebayes;  
mcmc;  
sumt filename=spinebayes burnin=12500 contype=halfcompat;  
log stop;  
end;
```

APPENDIX P
BAYESIAN ANALYSIS OUTPUT (4 TAXA)

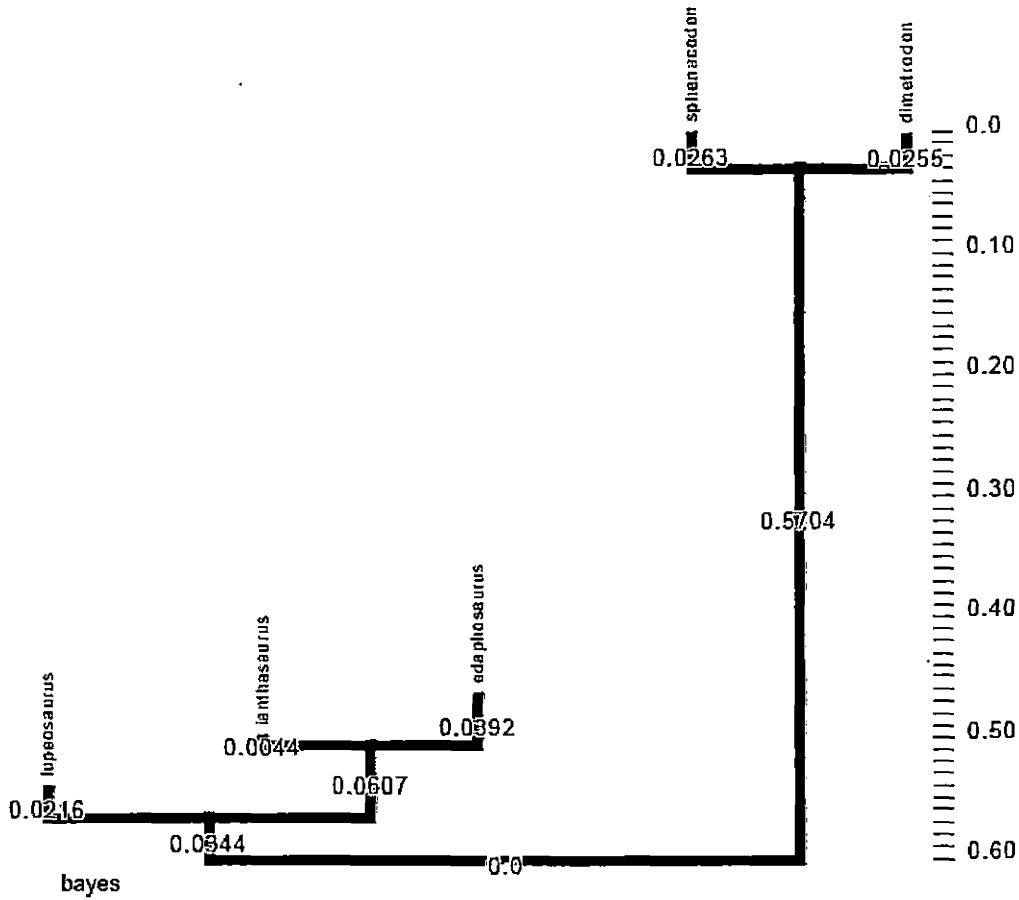
APPENDIX P. Bayesian analysis output (4 taxa). Analyzed in MrBayes (Huelsenbeck and Ronquist, 2005) for branch lengths to be used in PhySig analysis. Only *Lupeosaurus*, *Edaphosaurus*, *Sphenacodon*, and *Dimetrodon* were included in the dataset. *Ianthasaurus* was excluded due to poor preservation of the proximal neural spine and, thus, proximal comparisons of histomorphometric characters necessitated the exclusion of this taxon (see Chapter Four, Methods).



5.7300000000E-02	3.8600000000E-02	0.0000000000E+00	0.0000000000E+00
3.8600000000E-02	1.2270000000E-01	0.0000000000E+00	0.0000000000E+00
0.0000000000E+00	0.0000000000E+00	5.7830000000E-01	5.5230000000E-01
0.0000000000E+00	0.0000000000E+00	5.5230000000E-01	5.7400000000E-01

APPENDIX Q
BAYESIAN ANALYSIS OUTPUT (5 TAXA)

APPENDIX Q. Bayesian analysis output (5 taxa). Analyzed in MrBayes (Huelsenbeck and Ronquist, 2005) for branch lengths to be used in PhySig analysis. All taxa with adequate histological profiles from the distal neural spines were included in the dataset (see Chapter Four, Methods).



5.6000000000E-02	3.4400000000E-02	3.4400000000E-02	0.0000000000E+00	0.0000000000E+00
3.4400000000E-02	9.9500000000E-02	9.5100000000E-02	0.0000000000E+00	0.0000000000E+00
3.4400000000E-02	9.5100000000E-02	1.3430000000E-01	0.0000000000E+00	0.0000000000E+00
0.0000000000E+00	0.0000000000E+00	0.0000000000E+00	5.9670000000E-01	5.7040000000E-01
0.0000000000E+00	0.0000000000E+00	0.0000000000E+00	5.7040000000E-01	5.9590000000E-01

REFERENCES

- Amprino, R. 1947. La structure du tissu osseux envisage comme expression de differences dans la vitesse de l'accroissement. Archives de Biologie 58:315-330.
[in French]
- Ascenzi, A. 1976. Physiological relationship and pathological interferences between bone tissue and marrow. Pp. 403-444 in G. H. Bourne (ed.) The Biochemistry and Physiology of Bone, Volume 4. Academic Press, New York.
- Bailey, J. B. 1997. Neural spine elongation in dinosaurs: sailbacks or buffalo-backs? Journal of Paleontology 71:1124-1146.
- Benjamin, M., T. Kumai, S. Milz, B. M. Boszczyk, A. A. Boszczyk, and J. R. Ralphs. 2002. The skeletal attachment of tendons - tendon 'entheses.' Comparative Biochemistry and Physiology Part A 133:931-945.
- Bennett, A. F. and J. A. Ruben. 1986. The metabolic and thermoregulatory status of therapsids: Pp. 207-218 in N. Hotton, P. D. MacLean, J. J. Roth, and E. C. Roth (eds.) The Ecology and Biology of Mammal-like Reptiles. Smithsonian Institution Press, Washington.

- Bennett, S. C. 1996. Aerodynamics and thermoregulatory function of the dorsal sail of *Edaphosaurus*. *Paleobiology* 22:496-506.
- Berman, D. S. 1977. A new species of *Dimetrodon* (Reptilia, Pelycosauria) from a non-deltaic facies in the Lower Permian of north-central New Mexico. *Journal of Paleontology* 51:108-115.
- , 1978. *Ctenospondylus ninevehensis*, a new species (Reptilia, Pelycosauria) from the Lower Permian Dunkard Group of Ohio. *Annals of Carnegie Museum* 47:493-514.
- , 1979. *Edaphosaurus* (Reptilia, Pelycosauria) from the Lower Permian of northeastern United States, with description of a new species. *Annals of Carnegie Museum* 48:185-202.
- , A. C. Henrici, S. S. Sumida, and T. Martens. 2004. New materials of *Dimetrodon teutonis* (Synapsida: Sphenacodontidae) from the Lower Permian of Germany. *Annals of Carnegie Museum* 73:48-56.
- , R. R. Reisz, T. Martens, and A. Henrici. 2001. A new species of *Dimetrodon* (Synapsida: Sphenacodontidae) from the Lower Permian of Germany records first occurrence of genus outside North

- America. Canadian Journal of Earth Sciences 38:803-812.
- Blomberg, S. P., T. Garland, Jr., and A. R. Ives. 2003. Testing for phylogenetic signal in comparative data: behavioral traits are more labile. Evolution 57:717-745.
- Bramwell, C. D., and P. B. Fellgett. 1973. Thermal regulation in sail lizards. Nature 242:203-205.
- Buffrénil, V. de, J. O. Farlow, and A. de Ricqlès. 1986. Growth and function of *Stegosaurus* plates: evidence from bone histology. Paleobiology 12:459-473.
- Case, E. C. 1907. Revision of the Pelycosauria of North America. Carnegie Institution of Washington Publication 55. 176 pp.
- , 1909. The dorsal spines of *Chameleo cristatus*, Stuch. Science 29:979.
- , S. W. Williston, and M. G. Mehl. 1913. Permo-Carboniferous Vertebrates from New Mexico. Carnegie Institution of Washington Publication 181. 81 pp.
- Chinsamy, A. 1993. Bone histology and growth trajectory of the prosauropod dinosaur *Massospondylus carinatus* Owen. Modern Geology 18:319-329.

- and J. H. Hurum. 2006. Bone microstructure and growth patterns of early mammals. *Acta Palaeontologica Polonica* 51:325-338.
- and M. A. Raath. 1992. Preparation of fossil bone for histological examination. *Palaeontologia Africana* 29:39-44.
- Cope, E. D. 1878. Descriptions of extinct Batrachia and Reptilia from the Permian formation of Texas. *Proceedings of the American Philosophical Society* 17:505-530.
- Cubo, J., F. Ponton, M. Laurin, E. de Margerie, and J. Castanet. 2005. Phylogenetic signal in bone microstructure of sauropsids. *Systematic Biology* 54:562-574.
- , P. Legendre, A. de Ricqlès, L. Montes, E. de Margerie, J. Castanet, and Y. Desdevises. 2008. Phylogenetic, functional, and structural components of variation in bone growth rate of amniotes. *Evolution and Development* 10:217-227.
- Currey, J. 1984. *The Mechanical Adaptations of Bones*. Princeton University Press, Princeton. 294 pp.

- . 1987. The evolution of the mechanical properties of amniote bone. *Journal of Biomechanics* 20:1035-1044.
- . 2002. *Bones: Structure and Mechanics* (2nd edition). Princeton University Press, Princeton, New Jersey. 436 pp.
- . 2003. The many adaptations of bone. *Journal of Biomechanics* 36:1487-1495.
- and R. McN. Alexander. 1985. The thickness of the walls of tubular bones. *Journal of Zoology, London A* 206:453-468.
- Currie, P. J. 1997. Theropods. Pp. 216-233 in J. Farlow and M. Brett-Surman (eds.) *The Complete Dinosaur*. Indiana University Press, Bloomington and Indianapolis.
- Daly, E. 1969. A new procolophonoid reptile from the Lower Permian of Oklahoma. *Journal of Paleontology* 43:676-687.
- Daly, E. 1973. A Lower Permian vertebrate fauna from southern Oklahoma. *Journal of Paleontology* 47:562-589.
- Ebel, K. 2000. Biomechanics of the vertebral column and implications for the lifestyle of dinosaurs and

certain pelycosaurs. Freiburger Forschungshefte C
490:27-50.

-----, F. Falkenstein, F.-O. Haderer, and R. Wild. 1998.
Ctenosauriscus koeneni (v. Huene) und der Raurisuchier
von Waldshut - Biomechanische Deutung der Wirbelsäule
und Beziehungen zu *Chirotherium sickleri* Kaup.
Stuttgarter Beiträge zur Naturkunde B 261:1-18. [in
German]

Eberth, D. H. 1985. The skull of *Sphenacodon ferocior*,
and comparisons with other sphenacodontines (Reptilia,
Pelycosauria). New Mexico Bureau of Mines and Mineral
Resources Circular 190. 40 pp.

Enlow, D. H. 1963. Principles of Bone Remodeling: an
Account of Post-natal Growth and Remodeling Processes
in Long Bones and the Mandible. Charles C. Thomas,
Publisher, Springfield. 131 pp.

-----, 1969. The bone of reptiles: Pp. 45-80 in C. Gans,
A. Bellairs, and T. Parsons (eds.) Biology of the
Reptilia Volume 1: Morphology A. Academic Press,
London.

----- and S. O. Brown. 1956. A comparative histological
study of fossil and Recent bone tissues, Part I.
Texas Journal of Science 8:405-443.

- and -----. 1957. A comparative histological study of fossil and Recent bone tissues, Part II. Texas Journal of Science 9:186-214.
- and -----. 1958. A comparative histological study of fossil and Recent bone tissues, Part III. Texas Journal of Science 10:187-230.
- Etnier, S. A. 2001. Flexural and torsional stiffness in multi-jointed biological beams. Biological Bulletin 200:1-8.
- Faux, C. M., and K. Padian. 2007. The opisthotonic posture of vertebrate skeletons: postmortem contraction or death throes? Paleobiology 33:201-226.
- Florides, G. A., S. A. Kalogirou, S. A. Tassou, and L. Wrobel. 2001. Natural environment and thermal behaviour of *Dimetrodon limbatus*. Journal of Thermal Biology 26:15-20.
- Francillon-Vieillot, H., V. de Buffrénil, J. Castanet, J. Géraudie, F. J. Meunier, J. Y. Sire, L. Zylberberg, and A. de Ricqlès. 1990. Microstructure and mineralization of vertebrate skeletal tissue: Pp. 471-530 in J. G. Carter (ed.) Skeletal Biomineralization: Patterns, Processes and Evolutionary Trends, Volume I. Van Nostrand Reinhold, New York.

- Germain, D., and M. Laurin. 2005. Microanatomy of the radius and lifestyle in amniotes (Vertebrata, Tetrapoda). *Zoologica Scripta* 34:335-350.
- Haack, S. C. 1986. A thermal model of the sailback pelycosaur. *Paleobiology* 12:450-458.
- Hentz, T. F. 1988. Lithostratigraphy and paleoenvironments of Upper Paleozoic continental red beds, north-central Texas: Bowie (New) and Wichita (Revised) Groups. *Bureau of Economic Geology Report of Investigations* 170. 55 pp.
- Hieronimus, T. L. 2006. Quantitative microanatomy of jaw muscle attachment in extant diapsids. *Journal of Morphology* 267:954-967.
- Hook, R. W., and N. Hotton III. 1991. A new sphenacodontid pelycosaur (Synapsida) from the Wichita Group, Lower Permian of north-central Texas. *Journal of Vertebrate Paleontology* 11:37-44.
- Hopson, J. A. 1991. Systematics of nonmammalian Synapsida and implications for patterns of evolution in synapsids. Pp. 635-693 in H.-P. Schultze & L. Trueb (eds.) *Origins of the Higher Groups of Tetrapods: Controversy and Consensus*. Cornell University Press, Ithaca.

- Huelsenbeck, J. P., and F. Ronquist. 2001. MRBAYES: Bayesian inference of phylogeny. *Bioinformatics* 17:754-755.
- Huttenlocker, A., K. Angielczyk, and A. Lee. 2006. Osteohistology of *Sphenacodon* (Synapsida: Sphenacodontidae) and the hidden diversity of growth patterns in basal synapsids. *Journal of Vertebrate Paleontology* 26(3) supplement:79-80A.
- , E. Rega, and S. Sumida. 2007. New histological investigations of hyperelongate neural spines in eupelycosaurs (Amniota: Synapsida) and the affinities of *Lupeosaurus kayi*. *Journal of Vertebrate Paleontology* 27(3) supplement:93A.
- Kemp, T. S. 1982. *Mammal-like Reptiles and the Origin of Mammals*. Academic Press, London. 363 pp.
- . 2005. *The Origin and Evolution of Mammals*. Oxford University Press. 344 pp.
- Kishino, H., and M. Hasegawa. 1989. Evaluation of the maximum likelihood estimate of the evolutionary tree topologies from DNA sequence data, and the branching order in hominoidea. *Journal of Molecular Evolution* 29:170-179.

- Kissel, R. A., and R. R. Reisz. 2004. Synapsid fauna of the Upper Rock Lake Shale near Garnett, Kansas and the diversity pattern of early amniotes: Pp.409-428 in G. Arratia, M. V. H. Wilson, and R. Cloutier (eds.) Recent Advances in the Origin and Early Radiation of Vertebrates. Verlag Dr. Friedrich Pfeil, München.
- Laurin, M. 1993. The osteology and relationships of *Haptodus garnettensis*, a Pennsylvanian synapsid from Kansas. Journal of Vertebrate Paleontology 13:200-229.
- and R. R. Reisz, 1995. A reevaluation of early amniote phylogeny. Zoological Journal of the Linnean Society 113:165-223.
- Lee, A. H. 2004. Histological organization and its relationship to function in the femur of *Alligator mississippiensis*. Journal of Anatomy 204:197-207.
- Lewis, P. O. 2001. A likelihood approach to estimating phylogeny from discrete morphological character data. Systematic Biology 50:913-925.
- Madalena, K., S. Sumida, K. Zeigler, and E. Rega. 2007. A new record of the Early Permian pelycosaurian-grade synapsid *Dimetrodon* (Eupelycosauria: Sphenacodontidae) from the Lower Cutler Group (Early Permian) of Jemez

- Pueblo, north-central New Mexico. *Journal of Vertebrate Paleontology* 27(3) supplement:110A.
- Maddison, D., and W. Maddison. 2005. *MacClade 4: Analysis of Phylogeny and Character Evolution*. Distributed by Sinauer Associates, Inc.
- Main, R. P., A. de Ricqlès, J. R. Horner, and K. Padian. 2005. The evolution and function of thyreophoran dinosaur scutes: implications for plate function in stegosaurs. *Paleobiology* 31:291-314.
- Margerie, E. de. 2002. Laminar bone as an adaptation to torsional loads in flapping flight. *Journal of Anatomy* 201:521-526.
- , J.-P. Robin, D. Verrier, J. Cubo, R. Groscolas, and J. Castanet. 2004. Assessing a relationship between bone microstructure and growth rate: a fluorescent labeling study in the king penguin chick (*Aptenodytes patagonicus*). *Journal of Experimental Biology* 207:869-879.
- Modesto, S. P. 1994. The Lower Permian synapsid *Glaucosaurus* from Texas. *Palaeontology* 37:51-60.
- and R. R. Reisz. 1990. A new skeleton of *Ianthasaurus hardestii*, a primitive edaphosaur (Synapsida: Pelycosauria) from the Upper Pennsylvanian

- of Kansas. *Canadian Journal of Earth Sciences* 27:834-844.
- Müller, J., and R. R. Reisz. 2006. The phylogeny of early eureptiles: comparing parsimony and Bayesian approaches in the investigation of a basal fossil clade. *Systematic Biology* 55:503-511
- Nesbitt, S. 2003. *Arizonasaurus* and its implications for archosaur divergence. *Proceedings of the Royal Society London B* 270:S234-S237.
- . 2005. Osteology of the Middle Triassic pseudosuchian archosaur *Arizonasaurus babbitti*. *Historical Biology* 17:19-47.
- Olson, E. C. 1936. The dorsal axial musculature of certain primitive Permian tetrapods. *Journal of Morphology* 59:265-311.
- . 1962. Late Permian terrestrial vertebrates of USA and USSR. *Transactions of the American Philosophical Society* 52:1-224.
- Piñeiro, G., M. Verde, M. Ubilla, and J. Ferigolo. 2003. First basal synapsids ("pelycosaurs") from the Upper Permian-?Lower Triassic of Uruguay, South America. *Journal of Paleontology* 77:389-392.

- Pivorunas, A. 1970. Allometry in the limbs and sail of *Dimetrodon*. Unpublished M. S. thesis. University of Illinois, Chicago. 100 pp.
- Plochocki, J. H., J. P. Rivera, C. Zhang, and S. A. Ebba. 2008. Bone modeling response to voluntary exercise in the hindlimb of mice. *Journal of Morphology* 269:313-318.
- Ray, S., J. Botha, and A. Chinsamy. 2004. Bone histology and growth patterns of some nonmammalian therapsids. *Journal of Vertebrate Paleontology* 24:634-648.
- Rega, E., S. Sumida, K. Noriega, C. Pell, and A. Lee. 2005. Evidence-based paleopathology I: Ontogenetic and functional implications of dorsal sails in *Dimetrodon*. *Journal of Vertebrate Paleontology* 25(3) supplement:103A.
- , N. Wideman, and C. Brochu. 2002. Paleopathology of amniote specimens from the Late Paleozoic and Mesozoic of North America: comparison of gross morphological and histological analyses. *Journal of Vertebrate Paleontology* 22(3) supplement:98A.
- Reisz, R. R. 1972. Pelycosaurian reptiles from the Middle Pennsylvanian of North America. *Bulletin of the Museum of Comparative Zoology, Harvard* 144:27-62.

- . 1986. Pelycosauria. Encyclopedia of Paleoherpétology 17A. 102 pp.
- , and D. S Berman. 1986. *Ianthasaurus hardestii* n. sp., a primitive edaphosaur (Reptila, Pelycosauria) from the Upper Pennsylvanian Rock Lake Shale near Garnett, Kansas. Canadian Journal of Earth Sciences 23 :77-91.
- , -----, and D. Scott. 1992. The cranial anatomy and relationships of *Secodontosaurus*, an unusual mammal-like reptile (Synapsida: Sphenacodontidae) from the early Permian of Texas. Zoological Journal of the Linnean Society 104:127-184.
- , M. J. Heaton, and B. R. Pynn. 1982. Vertebrate fauna of Late Pennsylvanian Rock Lake Shale near Garnett, Kansas : Pelycosauria. Journal of Paleontology 56 :741-750.
- Ricqlès, A. de. 1968. Paleohistological research on the long bones of tetrapods I: Origin of the plexiform bone tissue of sauropod dinosaurians. Annales de Paléontologie 54:133-145. [in French]
- . 1969. Paleohistological research on the long bones of tetrapods III: Titanosuchians, dinocephalians, and

- dicynodonts. *Annales de Paléontologie* 55:17-60. [in French]
- . 1974a. Paleohistological research on the long bones of tetrapods IV: eotheriodonts and pelycosaur. *Annales de Paleontologie: Vertebres* 60:3-39, 8 plates. [in French]
- . 1974b. Evolution of endothermy: Histological evidence. *Evolutionary Theory* 1:51-80.
- , F. J. Meunier, J. Castanet, and H. Francillon-Vieillot. 1991. Comparative microstructure of bone: Pp. 1-78 in B. K. Hall (ed.) *Bone, Volume 3: Bone Matrix and Bone-Specific Products*. CRC Press, Boca Raton.
- Romer, A. S. 1927. Notes on the Permo-Carboniferous reptile *Dimetrodon*. *The Journal of Geology* 35:673-689.
- . 1937. New genera and species of pelycosaurian reptiles. *New England Zoological Club Proceedings* 16:89-96.
- . 1948. Relative growth in pelycosaurian reptiles. Special Publication of the Royal Society of South Africa, Robert Broom Commemorative Volume: 45-55.

- . 1961. Synapsid evolution and dentition.
International Colloquium on the Evolution of Mammals
1:9-56.
- and L. I. Price. 1940. Review of the Pelycosauria.
Geological Society of America Special Paper 28:1-538.
- Ronquist, F., and J. P. Huelsenbeck. 2003. MRBAYES 3:
Bayesian phylogenetic inference under mixed models.
Bioinformatics 19:1572-1574.
- Rubidge, B. S., and C. A. Sidor. 2001. Evolutionary
patterns among Permo-Triassic therapsids. Annual
Review of Ecology and Systematics 32:449-480.
- Rushforth, R., and B. Small. 2003. Analysis of Wichita
Group (Revised) "Series A" Dimetrodon species using
beta probability plots and Hotelling's T^2 statistic.
Journal of Vertebrate Paleontology 23(3)
supplement:91A.
- Sampson, S. 1997. Dinosaur combat and courtship. Pp.
383-393 in J. Farlow and M. Brett-Surman (eds.) The
Complete Dinosaur. Indiana University Press,
Bloomington and Indianapolis.
- Sidor, C. A., and J. A. Hopson. 1998. Ghost lineages and
'mammalness': assessing the temporal pattern of

character acquisition in the Synapsida. *Paleobiology*
24: 254-273.

Slijper, E. J. 1946. Comparative biologic-anatomical investigations on the vertebral column and spinal musculature of mammals. Koninklijke Nederlandsche Akademie Van Wetenschappen Verh. (Tweede Sectie) DI 42:1-128.

Spotila, J. R. 1980. Constraints of body size and environment on the temperature regulation of dinosaurs: Pp. 233-252 in R. D. K. Thomas and E. C. Olson (eds.) *A Cold Look at the Warm-Blooded Dinosaurs*. AAAS Selected Symposium 28, Westview Press, Boulder.

Sumida, S. S. 1989. New information on the pectoral girdle and vertebral column in *Lupeosaurus* (Reptilia, Pelycosauria). *Canadian Journal of Earth Sciences* 26:1343-1349.

----- . 1990. Vertebral morphology, alternation of neural spine height, and structure in Permo-Carboniferous tetrapods, and a reappraisal of primitive modes of terrestrial locomotion. *University of California Publications in Zoology* 122. 129 pp.

- and D. S Berman. 1993. The pelycosaurian (Amniota: Synapsida) assemblage from the Late Pennsylvanian Sangre de Cristo Formation of central Colorado. *Annals of Carnegie Museum* 62:293-310.
- , E. Rega, and K. Noriega. 2005. Evidence-based paleopathology II: Impact on phylogenetic analysis of the genus *Dimetrodon*. *Journal of Vertebrate Paleontology* 25(3) supplement:120A.
- Swofford, D. 1999. PAUP*: Phylogenetic Analysis Using Parsimony (and other methods) version 4.0 beta 10. Distributed by Sinauer Associates, Inc.
- Tracy, C. R., J. S. Turner, and R. B. Huey. 1986. A biophysical analysis of possible thermoregulatory adaptations in sailed pelycosaur: Pp. 195-206 in N. Hotton, P. D. MacLean, J. J. Roth, and E. C. Roth (eds.) *The Ecology and Biology of Mammal-like Reptiles*. Smithsonian Institution Press, Washington.
- Turner, J. S. and C. R. Tracy. 1986. Body size, homeothermy and the control of heat exchange in mammal-like reptiles: Pp. 185-194 in N. Hotton, P. D. MacLean, J. J. Roth, and E. C. Roth (eds.) *The Ecology and Biology of Mammal-like Reptiles*. Smithsonian Institution Press, Washington.

- Vaughn, P. P. 1969. Lower Permian vertebrates of the four corners and midcontinent as indices of climatic differences. Proceedings of the North American Paleontological Convention Part D:388-408.
- . 1971. A *Platyhystrix*-like amphibian with fused vertebrae, from the Upper Pennsylvanian of Ohio. Journal of Paleontology 45:464-469.
- Vogel, S. 1988. Life's Devices: the Physical World of Animals and Plants. Princeton University Press, Princeton. 367 pp.
- . 2003. Comparative Biomechanics: Life's Physical World. Princeton University Press, Princeton and Oxford. 580 pp.
- Warren, J. W. 1963. Growth zones in the skeleton of Recent and fossil vertebrates. Unpublished Ph. D. dissertation. University of California, Los Angeles: 136 pp.
- Wilson, J. W. 1994. Histological techniques. Pp. 205-234 in P. Leiggi and P. May (eds.) Vertebrate Paleontological Techniques. Cambridge University Press, NY.